TU WIEN
DEPARTMENT OF GEODESY AND GEOINFORMATION
RESEARCH GROUPS PHOTOGRAMMETRY AND REMOTE SENSING

DISSERTATION

Automating analysis and processing of high resolution point clouds for the investigation of a paleontological oyster reef

Ausgeführt zum Zwecke der Erlangung des akademischen Grades eines

Doktorin der technischen Wissenschaften
(Dr. techn.)

eingereicht von

Ana Puttonen
Matrikelnummer 01226002

Forschungsgruppen Photogrammetrie und Fernerkundung
Department für Geodäsie und Geoinformation
Fakultät für Mathematik und Geoinformation
Technische Universität Wien, TU Wien

unter der Leitung von: Univ.-Prof. Dipl.-Ing. Dr.techn. Norbert Pfeifer und Priv.-Doz. Mag. Dr. Mathias Harzhauser

Wien, Februar 2019 ....

TU WIEN
DEPARTMENT OF GEODESY AND GEOINFORMATION
RESEARCH GROUPS PHOTOGRAMMETRY AND REMOTE SENSING

DISSERTATION

Automating analysis and processing of high resolution point clouds for the investigation of a paleontological oyster reef

submitted in partial fulfillment of the requirements for the degree of

Doctor of Technical Sciences

by

Ana Puttonen

Registration Number 01226002

Research Groups Photogrammetry and Remote Sensing
Department of Geodesy and Geoinformation
Faculty of Mathematics and Geoinformation
Vienna Univesrity of Technology, TU Wien

Advisors: Univ.-Prof. Dipl.-Ing. Dr.techn. Norbert Pfeifer and Priv.-Doz. Mag. Dr. Mathias Harzhauser

Vienna, February 2019 ....

The dissertation has been reviwed by:

Supervisor: Univ.-Prof. Dr.techn. Norbert Pfeifer
Department of Geodesy and Geoinformation
TU Wien
Gusshausstrasse 27-29
1040 Vienna, Austria ....

Supervisor and reviewer: Priv.-Doz. Mag. Dr. Mathias Harzhauser
Department of Geology and Palaentology
Naturhistorisches Museum Wien, NHM
Burgring 7
1010 Vienna, Austria ....

Reviewer: Univ.-Prof. Dr. Pierre Grussenmeyer
Department of Civil Engineering and Surveying
INSA Strasbourg
24 Boulevard de la Victoire
67084 Strasbourg, France ....

Erklärung zur Verfassung der Arbeit
Author's Statement

Ana Puttonen
Hafengasse 15
1030 Wien

Hiermit erkläre ich, dass ich diese Arbeit selbstständig verfasst habe, dass ich die verwendeten Quellen und Hilfsmittel vollständig angegeben habe und dass ich die Stellen der Arbeit – einschließlich Tabellen, Karten und Abbildungen –, die anderen Werken oder dem Internet im Wortlaut oder dem Sinn nach entnommen sind, auf jeden Fall unter Angabe der Quelle als Entlehnung kenntlich gemacht habe.

I hereby declare, that I independently drafted this manuscript, that all sources and references used are correctly cited and that the respective parts of this manuscript— including tables, maps and figures—which were included from other manuscripts or the internet, are made clearly evident in the text and all respective sources are correctly cited.

(Ort, Datum) (Unterschrift Verfasser)

....

Abstract

A wide range of sensors have been developed for the acquisition of point clouds to describe the three-dimensional (3D) structure of objects. Among them, terrestrial laser scanning (TLS) is the most convenient acquisition technique for the close range and millimeter scale point cloud acquisition. High-resolution point clouds have become a powerful data to create digital, millimeter scale surfaces, and detailed 3D models. Thus, the point clouds are being applied in various disciplines. These include natural heritage, and monitoring and mapping of geological paleontological sites. Point clouds have an advantage over images in digital documentation of the current status of fossils for digital archiving and geometry extraction as they capture their three-dimensional structure. Image data alone have limitations in cases where multiple fossils overlap each other, the objects have self-similarity, or the scene has protruding objects. Thus, the complex surrounding on the oyster reef and the self-similarity of the object rendered an automatic bundle block adjustment of the reef infeasible. A fossilized oyster reef is a good example of a densely packed environment, where making geometry estimations of curved objects becomes a complex and challenging task.

This thesis presents how the point cloud processing techniques are applied on the world's largest fossilized oyster reef located in Stetten, Lower Austria. This densely packed shell bed formed about 16.5 million years ago in a tropical estuary. The original *Magallana gryphoides* oysters died exactly where they lived in their original environment, but they are not found consisting of both valves as it was in their original life structure. Instead, their single valves were scattered on a densely packed reef on the area of 459 m^2. The paleontological site was excavated during field campaigns of the Natural History Museum Vienna between 2005 and 2008. In 2014, a laser scanning and photogrammetric campaign was organized at the reef with the goal to digitize its contents. The large and complex site was digitally documented using a remotely controlled high-speed FARO Focus3D laser scanner and a Canon 60D camera with a Canon EF 20 mm f 2.8 lens. The 3D point clouds and high-resolution images from this field campaign were processed with photogrammetric methods into a digital surface model (DSM, 1 mm resolution) and an orthophoto of 0.5 mm resolution to support the paleontological interpretation of the site.

While the literature about the Early Miocene estuary is extensive, the knowledge about the fossil composition, taphonomy, size or orientation on the sites are limited. Thus, there exists an interest to test and try new techniques to document rare fossil objects to investigate such sites in effective, automatic and objective manner. Use of digital 3D point clouds provide a viable option for this and the interest towards them increased after the first published scientific contribution. Consequently, the research carried out in this thesis is of particular interest, because it aims to answer research questions which have aroused between studies of Photogrammetry and Geology. To answer these questions, the thesis proposes new methods that include developing a strategy for capturing irregular surfaces by high-resolution point clouds to detect outlines of shells, a method to count and detect the number of shells in the reef, and methods to estimate shell 3D length, to derive shell orientation, to estimate shell volumes, and to visualize and design thematic maps to improve interpretation work. The thesis also makes use of Geographic Information System (GIS) in reference data collection, and evaluation of the reliability of the automated processing results.

The thesis presents the results of research that were evaluated in six original research and conference articles. All articles were subjected to a peer-review process and published in journals

related to Earth Science topics, in an International Society of Photogrammetry and Remote Sensing (ISPRS) and AGILE GIS conference. Contributions I and II investigate research questions related to shell taphonomy, the estimation of shell number in the reef, and if the shell bed is formatted by a storm or a tsunami. Individual shell volume estimations were also considered as well as possible patterns in the distribution and composition of shells among two datasets on the reef, i.e. transects N–S and W–E. Contribution III describes the settings of data acquisition, data management and coordinate systems to digitize a large fossilized oyster reef. The study demonstrates the potential of high resolution 3D data and photographs by documenting an approach that outlines individual shells in a complex environment which is a crucial task to enumerate the shells in a paleontological site. Contribution IV examines the automatic determination of 3D orientations of fossilized oyster shells in a Cartesian coordinate system where they were represented as elongated objects whose rotation angles (roll, pitch, and yaw) were determined for an Earth Science application. The goal of the examination was to find out if the locations of strongly tilted oyster shells had a statistically significant correlation with the nearby fault lines present in the reef. The article V technically examines how to determine the 3D length of shells and demonstrates a method to automatically extract a 3D central line from various shapes of fossilized oyster shells. Certain central line properties have direct relationship with the encrustation estimates. The article VI presents the first GIS database as an interface of a digital oyster reef and managing tool for a protected natural heritage site.

The thesis contributions demonstrate that the terrestrial laser scanning point clouds are effective and convenient data sources to create millimeter scale models of paleontological sites. TLS provides accurate measurements of complex geometry objects such as fossilized oyster shells. The thesis focuses on investigating the ability and performance of laser scanning data in different modelling related tasks that include identification of fossil outlines, and determination of their size, orientation, volume, and other physical parameters which are required to make accurate paleontological interpretations. Thus, the thesis investigates photogrammetric methods that cover these requirements and provide results that can be readily visualized to support paleontological interpretations. The results considering the all evaluations ae also described. As an example of the developed methods, the thesis work contributed in preparation and publication of a comprehensive paleontological 3D dataset. The dataset documents the oyster reef with millimeter-resolution point clouds, digital surface models and orthophotos. The dataset provides an extensive testing ground for further method development in photogrammetry and computer vision communities, and it should help paleontologists in planning new data acquisition campaigns to make more accurate interpretations.

Kurzfassung

Für die Erfassung von Punktwolken wurde eine breite Palette von Sensoren zur Aufnahme der dreidimensionalen (3D) Struktur von Objekten entwickelt. Darunter ist das Terrestrische Laserscanning (TLS) eine komfortable Akquisitionsmethode für die 3D-Datenerfassung im Nahbereich. Die so erfassten Punktwolken etablierten sich als zuverlässige Grundlage für die Erstellung von digitalen, hochauflösenden und detaillierten 3D-Modellen. So werden die Punktwolken in verschiedenen Disziplinen angewendet. Dazu gehören das Naturerbe sowie die Überwachung und Kartierung geologischer paläontologischer Stätten. Punktwolken haben einen Vorteil gegenüber Bildern in der digitalen Dokumentation des aktuellen Zustands von Fossilien für die digitale Archivierung und Geometrieextraktion, da sie ihre dreidimensionale Struktur erfassen. Bilddaten haben in Fällen, in denen mehrere Fossilien einander überlappen, die Objekte Selbstähnlichkeit haben oder die Szene vorstehende Objekte aufweist, Beschränkungen. Der Komplex, der sich auf dem Austernriff befindet, und die Selbstähnlichkeit des Objekts machten eine automatische Bündelblockanpassung des Riffs unmöglich. Ein versteinertes Austernriff ist ein gutes Beispiel für eine dicht gepackte Umgebung, in der Geometrieschätzungen gekrümmter Objekte zu einer komplexen und anspruchsvollen Aufgabe werden.

In dieser Arbeit wird gezeigt, wie die Techniken der Punktwolkenverarbeitung auf dem größten fossilen Austernriff der Welt in Stetten, Niederösterreich, angewendet werden. Dieses dicht gepackte Muschelbett wurde vor etwa 16,5 Millionen Jahren in einer tropischen Flussmündung geformt. Die ursprünglichen Austern vom Typ *Magallana gryphoides* starben genau dort, wo sie in ihrer ursprünglichen Umgebung lebten, aber sie wurden nicht so gefunden, wie sie in ihrer ursprünglichen Form waren. Stattdessen waren ihre einzelnen Schalen auf der freigelegten Fläche des dicht gepackten Riffs (rund 459 m^2) verstreut. Die paläontologische Stätte wurde zwischen 2005 und 2008 im Zuge von Messkampagnen des Naturhistorischen Museums Wien ausgegraben. Im Jahr 2014 wurde am Riff eine Laserscanning- und Photogrammetriekampagne mit dem Ziel durchgeführt, dessen Inhalt zu digitalisieren. Die große und komplexe Anlage wurde mit einem ferngesteuerten High-Speed FARO Focus3D Laserscanner und einer Canon 60D Kamera mit einem Canon EF 20 mm f2.8 Objektiv digital dokumentiert. Die 3D-Punktwolken und hochauflösenden Bilder aus dieser Messkampagne wurden mit photogrammetrischen Methoden zu einem digitalen Oberflächenmodell (DSM, 1 mm Auflösung) und einem Orthophoto von 0,5 mm Auflösung verarbeitet, um die paläontologische Interpretation des Ortes zu unterstützen.

Während die Literatur über die frühe Miozän-Mündung umfangreich ist, ist das Wissen über die fossile Zusammensetzung (Taphonomie), Größe oder Orientierung an den Standorten begrenzt. Daher besteht Interesse daran, neue Techniken zu testen und zu erproben, um seltene fossile Objekte zu dokumentieren und um solche Stellen auf effektive, automatische und objektive Weise zu untersuchen. Die Verwendung von digitalen 3D-Punktwolken bietet hierfür eine praktikable Option und das Interesse daran nahm nach den ersten veröffentlichten wissenschaftlichen Beiträgen zu. Daher ist die in dieser Arbeit durchgeführte Forschung von besonderem Interesse, da sie Forschungsfragen beantworten soll, die zwischen Studien der Photogrammetrie und Geologie entstanden sind. Um diese Fragen zu beantworten, schlägt diese Dissertation neue Methoden vor, darunter die Entwicklung einer Strategie zur Erfassung unregelmäßiger Oberflächen durch hochauflösende Punktwolken, um Umrisse von Muscheln zu erkennen, eine Methode zum Zählen und Erkennen der Anzahl von Muscheln im Riff und

Methoden zur Schätzung der 3D-Länge der Schalen, um die Schalenorientierung abzuleiten, Schalenvolumina zu schätzen und thematische Karten zu visualisieren und zu entwerfen, um die Interpretationsarbeit zu verbessern. In der Arbeit wird auch ein Geographisches Informationssystem (GIS) zur Referenzdatenerfassung und die Bewertung der Zuverlässigkeit der automatisierten Verarbeitungsergebnisse genutzt.

Die Arbeit präsentiert die Forschungsergebnisse, die in sechs eigenständigen Forschungs- und Konferenzartikeln ausgewertet wurden. Alle Artikel wurden einem Peer-Review-Prozess unterzogen und in Fachzeitschriften zu Themen der Erdwissenschaften sowie auf einer Konferenz der International Society of Photogrammetry and Remote Sensing (ISPRS) veröffentlicht. In den Beiträgen I und II werden Forschungsfragen bezüglich der Schalen-Taphonomie, der Schalenzahl im Riff und der Formierung des Muschelbetts durch einen Sturm oder Tsunami untersucht. Einzelne Schalenvolumenschätzungen wurden ebenso berücksichtigt wie mögliche Muster in der Verteilung und Zusammensetzung von Schalen zwischen zwei Datensatztransekten am Riff (N-S, W-E). Beitrag III beschreibt die Einstellungen von Datenerfassung, Datenmanagement und Koordinatensystemen zur Digitalisierung eines großen versteinerten Austernriffs. Die Studie demonstriert das Potenzial hochauflösender 3D-Daten und -Fotografien, indem sie einen Ansatz dokumentiert, der einzelne Schalen in einer komplexen Umgebung erfasst. Dies ist eine entscheidende Aufgabe, um die Schalen an einer paläontologischen Stelle zu zählen. Beitrag IV untersucht die automatische Bestimmung von 3D-Orientierungen von versteinerten Austernschalen in einem kartesischen Koordinatensystem, wo sie als langgestreckte Objekte dargestellt wurden, deren Rotationswinkel (Roll, Pitch, und Yaw) für eine geowissenschaftliche Anwendung bestimmt wurden. Das Ziel der Untersuchung war herauszufinden, ob die Standorte von stark geneigten Austernschalen eine statistisch signifikante Korrelation mit den nahe gelegenen Verwerfungslinien im Riff aufweisen. Der Artikel V untersucht technisch, wie man die 3D-Länge von Muscheln bestimmen kann und demonstriert eine Methode, um automatisch eine 3D-Mittellinie aus verschiedenen Formen fossiler Austernschalen zu extrahieren. Bestimmte zentrale Linieneigenschaften stehen in direktem Zusammenhang mit den Inkrustationsschätzungen. Der Artikel VI präsentiert die erste GIS - Datenbank als Schnittstelle eines digitalen Austernriffs und eines Verwaltungswerkzeug für ein geschütztes Naturerbe.

Die Beiträge der Dissertation zeigen, dass die terrestrischen Laser-Scanning-Punktwolken effektive und bequeme Datenquellen sind, um millimetergroße Modelle paläontologischer Standorte zu erstellen. TLS bietet genaue Messungen von Objekten mit komplexer Geometrie, wie versteinerten Austernschalen. Die Arbeit konzentriert sich auf die Untersuchung der Möglichkeiten von Laserscanning-Daten in verschiedenen Modellierungsaufgaben, einschließlich der Identifizierung von fossilen Umrissen und der Bestimmung ihrer Größe, Orientierung, Volumen und anderer physikalischer Parameter, die für genaue paläontologische Interpretationen benötigt werden. Diese Arbeit untersucht dazu photogrammetrische Methoden, die diese Anforderungen erfüllen und Ergebnisse liefern, die zur Unterstützung paläontologischer Interpretationen leicht visualisiert werden können. Die Ergebnisse unter Berücksichtigung aller Bewertungen werden ebenfalls beschrieben. Als ein Beispiel für die entwickelten Methoden hat die Arbeit zur Vorbereitung und Veröffentlichung eines umfassenden paläontologischen 3D-Datensatzes beigetragen. Der Datensatz dokumentiert das Austernriff mit Millimeterpunktwolken, digitalen Oberflächenmodellen und Orthophotos. Der Datensatz bietet ein umfangreiches Testfeld für die weitere Methodenentwicklung in den Bereichen Photogrammetrie und Computer Vision und soll Paläontologen helfen, neue Datenerfassungskampagnen zu planen, um genauere Interpretationen zu ermöglichen.

Апстракт

Развијен је широк спектар сензора за прикупљање облака тачака за опис тродимензионалне (3Д) структуре објеката. Међу њима, терестричко ласерско скенирање (ТЛС) је најприкладнија техника за блископредметно скенирање објеката са циљем да се постигне милиметарска резолуција облака тачака. Облак тачака високе резолуције је адекватан скуп података за интерполацију дигиталних (3Д) модела терена. Дакле, облаци тачака се примењују у различитим дисциплинама. То укључује природне локалитете и заштићена подручја, као и праћење и мапирање геолошких и палеонтолошких налазишта.

Облаци тачака имају предност у односу на прикупљене слике у архиву дигиталне документације о тренутном стању фосила за екстракцију геометрије, јер укључују своју тродимензионалну структуру. Подаци добијени само са слика имају ограничења у случајевима када се фосили вишеструко преклапају једни преко других, или су објекти слични међусобно, или се ради о подручју које има испупчене и клизне објекте. Орто-пројекција грубих закривљених објеката је проблем, због сложеног описа аналитичког облика објекта. Чак и коришћењем детаљног дигиталног модела површине, не добија се жељени исход, јер се тешко управља видљивошћу слике и оклузијом модела, јер је ограничен на 2,5-димензионалне описе површина. Један такав пример компликоване геометрије објеката је гребен са фосилизованим остригама, густо упаковано окружење, где израда дигиталног модела терена као и оцена геометрије закривљених предмета постаје комплексан и изазован задатак.

У овом раду су представљене технике обраде тачака примењене на највећем фосилизованом гребену острига у свету који се налази у Штетену, у доњој Аустрији, некадашњој територији Панонског мора. Овај густо упаковани гребен острига креиран је пре око 16,5 милиона година у тропском ушћу. Првобитни остаци острига *Magallana griphoides* изумирали су тачно тамо где су живели у њиховом првобитном окружењу и колонији, али нису пронађени парови шкољки који се састоје од две љуштуре, леве и десне стране шкољке, као што су биле састављене у њиховој првобитној животној структури. Уместо тога, њихови појединачни делови су раштркани на гребену на површини од 459 метара квадратних. Велико палеонтолошко налазиште острига је ископано током теренских кампања организованих од стране Природњачког музеја у Бечу и њихових сарадника од 2005. до 2008. године. Ласерско скенирање и фотограметријска кампања је организована 2014. године на оригиналном налазишту са циљем да се дигитализује њен садржај. Велико налазиште са сложеном колонијом шкољки је дигитално документовано помоћу блископредметне фотограметрије, где је коришћен ласерски скенер FARO Focus 3D и Canon 60D камера са Canon EF 20 mm f 2,8 објективом. 3Д облак тачака и слике високе резолуције ове колоније шкољки су обрађени са фотограметријским методама чији су крајњи резултати следећи подаци: дигитални модел површи резолуције 1 мм (величина грида) и ортофото резолуције 0,5 мм (величина пиксела на терену). Ови подаци служе да подрже палеонтолошко тумачење налазишта и израду базе података острига.

Иако је литература о раном Миоценском ушћу велика, знања о фосилном саставу, тафономији, величини или оријентацији острига на овом јединственом локалитету су скромна. Стога постоји интересовање за тестирање и примену нових техника за документовање ретких фосилних објеката ради истраживања таквих локација на ефикасан, аутоматски и објективан начин. Коришћење 3Д облака тачака је практично за ово

истраживање, а интересовање према дигиталним подацима порасло је након првог објављеног научног рада и дељења података јавно преко платформе PANGAEA. Сходно томе, истраживање спроведено у овом раду је од посебног интереса, јер има за циљ да одговори на истраживачка питања покренута између геолошких студија и фотограметрије. Да би се одговорило на ова питања, у раду се предлажу нове методе које укључују развој стратегије за моделовање комплексних површи на основу облака тачака високе резолуције за откривање карактеристика гребена и релевантних геометријских информација. У то улази метода за детекцију тачног броја шкољки на гребену и метода за процену величине шкољки (процена 3Д дужине); затим, израчунавање оријентација, процена запремине шкољки, визуелизација и креирање тематских карата за помоћ приликом рада палеонтолога на налазишту или интерпретација**.** Рад такође користи Географски информациони систем (ГИС) при прикупљању референтних података и процени поузданости резултата на основу аутоматске обраде података.

У овој монографији се представљају резултати истраживања која су објављена у четири научна рада у часописима и два рада објављена на научним конференцијама. Сви радови су прошли процес ревизије и један од њих је нагрђен од стране Међународног удружења за фотограметрију и даљинску детекцију (ISPRS). Први и други рад истражују питања везана за тафономију шкољке, процену укупног броја шкољки на гребену и тумачење да ли је колонија шкољки обликована под утицајем олује или цунамија. Такође су разматране појединачне процене запремине шкољки, распрострањеност и састав шкољки између два скупа података на гребену (скуп север-југ и скуп запад-исток). Трећи рад описује припрему и планирање за прикупљање података, управљање подацима и координатним системима за дигитализацију великог гребена фосилизованих острига. Истраживање је показало да има потенцијала за употребу 3Д података и фотографија високе резолуције у аутоматској методи детекције појединачних шкољки у сложеном окружењу, што је кључни задатак да се евидентирају шкољке на палеонтолошкој локацији. Четврти рад испитује аутоматско одређивање 3Д оријентација шкољки у правоугаоном координатном систему, где су фосили шкољки представљени као издужени објекти. Тачни углови ротације сваке појединачне шкољке значајни су за статистичке анализе у природним наукама. Циљ испитивања је да се утврди да ли су локације јако нагнутих острига имале статистички значајну корелацију са оближњим пукотинама раседа. Ове пукотине су присутне на гребену и њихов положај је дигитализован користећи ортофото и дигитални модел површи у ГИС окружењу. Пети чланак технички испитује како одредити прецизну дужину шкољки и демонстрира методу за аутоматско израчунавање 3Д централне линије (скелетона) различитих геометријских облика фосила острига. Одређене карактеристике централне линије се користе за процену преклопа или укрштавања острига са другим шкољкама исте или различите врсте. Последњи (шести), чланак представља опис прве ГИС базе података као интерфејса дигиталног гребена шкољки и алата за управљање заштићеним природним наслеђем.

Допринос целокупне тезе показује да су ТЛС ласерски облаци тачака ефикасни и погодни извори података за креирање детаљних 3Д модела палеонтолошког налазишта. ТЛС пружа прецизна мерења објеката сложене геометрије као што су фосили шкољки. Теза се фокусира на истраживачке могућности и употребу података ласерског скенирања на различите задатке 3Д моделирања као што су индентификација фосила шкољки, њиховог облика, одређивање величине фосила, оријентације, запремине и других физичких параметара који су потребни за прецизне палеонтолошке интерпретације. Стога, теза истражује фотограметријске методе које одговарају на захтев задатка и пружају резултате који се лако могу приказати у 3Д окружењу или уз помоћ ГИС алата (тематске мапе), како би се подржале палеонтолошке интерпретације. Такође су описани у раду резултати свих евалуација фотограметријских метода који приказују колико је развијена метода примењива у палеонтологији. Палеонтолошки 3Д скуп података (облак тачака милиметарске резолуције) је доступан на захтев заинтересованих истраживача у циљу едукације и тестирања нових алгоритама, док за сада објављена јавна документација саджи дигитални модел површи и ортофото. Објављени подаци дају широки полигон за даљи развој метода у фотограметрији, а то помаже палеонтолозима у прецизнијим интерпретацијама.

Table of contents

1 Introduction

1.1. Motivation

In order to improve our understanding of events from the past, it is important to study nowadays the fossils adapted to specific local environments of former times. Consequently, fossilized shells may provide information on various physical processes that happened through a complex history of shell bed formation being shaped by more than one factor under different environmental conditions (Kidwell, 1986, 1991; Fürsich and Oschmann, 1993; Mandic et al., 2004; Zuschin et al., 2005). The shell bed in Stetten, Austria is the world's largest fossil oyster reef, which provides the rare opportunity to study the Early Miocene flora and fauna of the Paratethys Sea. This sea was part of Pannonian basin and in terms of modern state boundaries, the basin centers on the territory of Hungary, but it also covers regions of western Slovakia, southeastern Poland, western Ukraine, western Romania, northern Serbia (Vojvodina), the tip of northeast Croatia, northeastern Slovenia, and eastern Austria. Today's Black Sea, Caspian Sea, Aral Sea, Lake Urmia, Namak Lake and others are remnants of the Paratethys Sea.

The terms shell bed, reef and biostrome are used often in literature to describe related things (Trewin and Welsh, 1976, Bahr and Lanier, 1981, Harzhauser et al., 2015). The term reef appears most often in estuarine ecology (e.g.: Powell et al., 2006; Thomsen et al., 2007; Lejart and Hily, 2011; van der Zee et al., 2012; Rodriguez et al., 2014; Ridge et al., 2015, 2017). The term biostrome of Lahee (1932) is in use because many intertidal oyster bioconstructions lack a strong vertical growth component. Shell bed term refers to shell accumulation or shell-rich deposit of fossils used first time in research of Boucot et al. (1958), Walker and Bambach (1971), Roberts et al. (2008), and this term will be used often throughout our oyster research as a synonym for reef.

Geologists and paleontologist have been taking traditional measurements on the oyster reef in Stetten so far, e.g., information on orientation and length of specimen. However, that work was subjective, time consuming, limited in the number of measurements taken and not comfortable, because the reef is not easily accessible and also its protected site, so stepping or placing instruments on it is forbidden. Thus, an accidental damage or vandalism by visitors, as well as destruction by natural hazards, are constant threats to this unique site. Therefore, contactless work in the office with the digitized surface or volume data would be preferred and easier comparing to the field work. The digital models are a preeminent and unprecedented documentation of the oyster reef and may serve as a basis for restoration and maintenance.

Scientist could observe and compare fossils in the long term context, without taking them from the excavation site, for instance for research and education purposes or museum archive. Permanent availability leads to more transparent results, because it will give the possibilities for all researchers to repeat the analysis or test newly developed methods on the same data set in the future works. Finally, scientific communication in a broader community requires original data to be available for all participants, leading to more transparent results. Therefore, combined work of photogrammetry, geology and paleontology is required to document, quantify and evaluate the fossilized shells on the reef.

A major goal of this thesis is high-resolution digital documentation of the world's largest known fossil oyster reef, comprising thousands of oyster shells. This implies providing high resolution 3D data of the fossil reef in order to make easier geometrical investigations of the entire site and its specimens. That requires developing of new methods or testing already existing methods from photogrammetry and laser scanning and evaluating their suitability for this particular application. Photogrammetry provides the tools for image acquisition, projective texture information, and objective interpretation of the complex oyster reef surface. Laser scanning provides 3D point cloud data from which it will be possible to generate accurate digital surface models at the millimeter scale. This documentation can also enable international scientific community to work with the unique natural heritage data accessible via the worldwide web. The captured surface is publically accessible via the PANGAEA platform (Data Publisher for Earth & Environmental Science; Djuricic et al., 2016b). It represents a reliable and objective documentation of the excavation site, providing data for current and future paleontological and geological analyses. The 3D data can be used to reconstruct virtual fossils within a computer environment, where all essential manipulations like rotating, translating, partitioning, sectioning, measuring, scaling, magnifying, or capturing images are feasible. It will be possible to create and share virtual copies of fossil material as well as to do 3D printing of selected shells.

Although being the world's largest excavated fossil oyster reef, an interpretation and comparable analysis of the shell accumulation is missing. No quantification of the shells was performed and the taxonomic inventory was only cursorily documented during excavation. Thus, the study is aiming to identify and count individual specimen as well as to interpret their parameters such as species (taphonomy), level of overlap, abrasion, bioerosion, encrustation, fragmentation, shell side, orientation (convex side up/down), and geometrical parameters such as size, area, and rotation angles. 3D visualizations of very dense oyster data support interpretation and serve as a tool for the interactive discussion between experts from the field.

For the purpose of evaluation of our methods (to evaluate e.g. shape and size), the automatic detections need to be compared against corresponding reference data. Expert knowledge is required to detect and outline the individual shell correctly and to determine its parameters mentioned above.

The study is based on a very dense surface reconstruction of the oyster reef. It focuses on using visualization technologies from photogrammetry in geology and paleontology in order to develop new methods for automatic and objective evaluation of 3D point clouds. The method that was used to document the site as a georeferenced 3D point cloud is terrestrial laser scanning (TLS). It is an innovative method that can handle and provide large paleontological data sets. Geometric data needs support of image data to generate orthophotos of the huge paleontological excavation site. Therefore, its needed to provide high-resolution 3D surface modeling of a fossil oyster reef using TLS and close range photogrammetry, which provides millimeter-level measurement accuracy and allows rapid acquisition of huge datasets.

The expectations of the thesis is the technology transfer between the disciplines of photogrammetry, geology and paleontology. Thus, this work covers highly relevant topics of these disciplines, so it is useful to introduce the intention of each scientific discipline individually.

1.1.1. The paleontological intention and geological setting

The studied site at Stetten (48° 22’ 03.33 N, 16° 21’ 33.22 E) in eastern Austria is part of the about 20-km-long and about 7-km-wide Korneuburg Basin, which is a lower Miocene half-graben within the Alpine-Carpathian thrust-belt. The basin fill comprises the about 600-m-thick siliciclastic Korneuburg Formation of Burdigalian (= Karpatian) age, which is tilted ca. 25° in western direction.

The protected site is part of the geopark “Fossilienwelt Weinviertel” and exposes the world’s largest fossil oyster biostrome which was excavated during field campaigns of the Natural History Museum Vienna between 2005 and 2008. The shell bed is a single, about 15–25-cm-thick horizon intercalated in coarse, poorly sorted sand with scattered plant debris and mudclasts. It is interpreted to have formed in a subtropical estuary as an event layer initiated by a major storm or tsunami (Harzhauser et al., 2015, 2016). The excavated and exposed shell accumulation now covers an area of 27 x 17 m (459 m^2) comprising about 50,000 shells presented to the visitors of the geopark in the so-called “oyster hall”.

The densely packed shell bed represents an event layer that was formed ~16.5 million years ago in a tropical estuary (Sovis and Schmid, 1998, 2002; Latal et al., 2006; Harzhauser et al., 2009). It mainly comprises the giant oyster *Magallana gryphoides* (Schlotheim, 1813; Salvi and Mariottini, 2016) up to 60 cm long, which is a bivalve and calcitic shell. Each individual developed two convex, strongly elongated valves of different sizes (Fig. 1). A ligament in the hinge area, together with a single adductor muscle located posteroventrally in the interior shell cavity, kept the valves articulated during the bivalve’s lifespan. After death, the valves usually became disarticulated.

This unique fossil accumulation was formed at the onset of the last global climate maximum, known as the Middle Miocene Climate Optimum (Zachos et al., 2001). Despite the state of the art that deals with the flora and fauna of the Miocene estuary, before the research on this thesis little was known about the composition, genesis and taphonomy of the study site. A detailed analysis is required to elucidate the formation of the structure. For instance, the number of shells, the ratio between left and right valves, their orientation, and the degree of fragmentation provide bases for further interpretation. The shell bed is preliminarily interpreted to have formed during a single hydrodynamic event, such as a tsunami or a major storm (Harzhauser et al., 2009). Thus, orientation estimation of the oyster shells will be investigated in details in order to detect trends or patterns on the oyster reef.

In addition, open questions in palaeontology concern the carbonate production of the oyster reef. Therefore, a relation between shell length and volume will be generated. For that study the length will be determined by central line extraction. As the entire oyster reef is documented in the form of a digital surface model, the determination of the length of each specimen, and therefore the estimation of the carbon production for the entire reef becomes feasible. However, such data cannot be acquired on site for a larger area; it is impossible to step on the shell bed without destroying the fragile fossils. Moreover, the field measurements might be biased by subjectivity, increasing the difficulty of cross-checking the data afterwards. Finally, traditional onsite measurements consume a great deal of time. Non-destructive georeferenced data acquisition represents a major breakthrough for the analysis of such geological structures. The extent of the reef and the good condition of the fossils qualify the oyster reef for a detailed documentation for current and future scientific investigations. Thus, geospatial information needs to be acquired for modeling its objects.

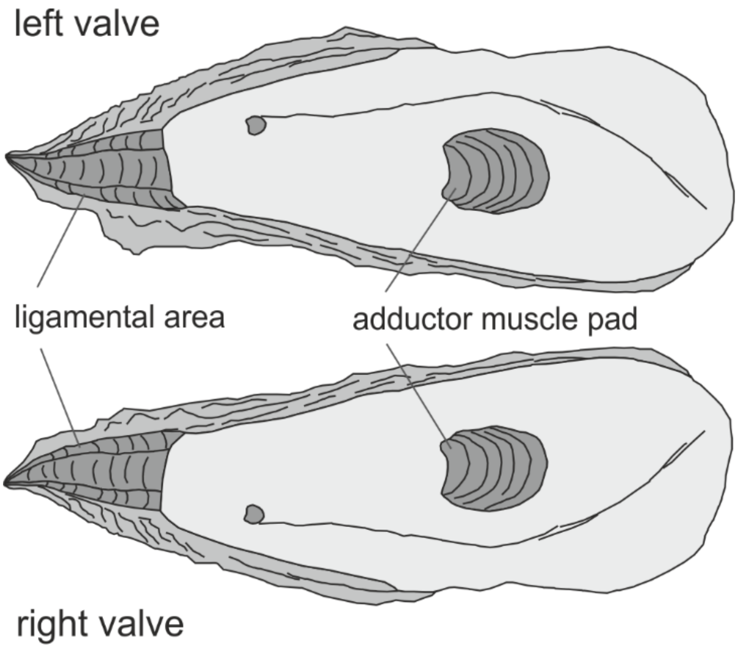

Figure 1: Technical sketch of an oyster shell (left and right valve), published in Djuricic et al., 2016a.

1.1.2. The photogrammetric intention

Progress in 3D digitizing sensor technology brings possibilities of new data collection techniques (Kraus, 2007; Buckley et al., 2008; Pfeifer et al., 2011; Goodman et al., 2013; Kurz, 2013). Therefore, it will be tested, if point clouds from close range terrestrial laser scanning can provide geometry adequate for analysis of the world's largest fossil oyster reef. In addition, images of a huge paleontological excavation site will support derivation of texture information and generation of orthophotos. Photogrammetry provides a powerful tool to digitally document protected, inaccessible, and rare fossils. This saves manpower in relation to current documentation practice and makes the fragile specimens more available for paleontological analysis and public education. The overall photogrammetric intention is development of new methods needed to protect the site and enable its analysis by using not-tactile (i.e. remote sensing) measurement techniques to study irregular objects. Irregular objects are rarely studied in photogrammetry, because typical objects are either very regular (houses, roads, etc.) or the study of an objects is replaced with the study of the surface itself or a parameter (e.g. terrain surface, vegetation density, etc.). The very irregular shell surface not only poses a problem in interpretation (manually as well as automatically) but also in aligning the orientation of the individual acquisitions relative to each other. Working on such a challenge of irregular objects is expected to advance photogrammetry in general.

Documentation, archiving, and analysis of natural and man-made objects and scenes are ongoing endeavors (Brodu and Lague, 2012; Di Salvo and Brutto, 2014; Bertin et al., 2016). If the focus is on geometrical aspects, 3D point clouds (Otepka et al., 2013) are often the primary choice for the description of objects, along with raster digital elevation models (DEMs) and triangulated models (meshes). For smaller scenes with complex geometry, terrestrial laser scanning (TLS) is a well-established method to describe objects with centimeter precision for extended areas of up to 100 m^2. However, it is challenging to achieve mm accuracy over a large site with irregular shapes. That level of accuracy requires not only one scan but, over a larger scene, coverage by several scans. The surfaces of the shells are very irregular, feature high curvature and roughness, and include overhangs. The objects range in size from a few decimeter down to a few millimeter, therefore mm resolution of their surface models is required. Respective approaches that provide very high resolution and precise 3D models are needed (Nothegger and Dorninger, 2007, 2009; Dorninger and Nothegger, 2009; Nothegger, C., 2011). In this thesis, the technique will comprise geometric, as well as photographic, documentation with a resolution of 1 mm and 0.5 mm, respectively. The automatic extraction of shells from photogrammetric data, e.g., digital surface models, is intend to be studied. Furthermore, features such as measures of concavity and convexity will be detected automatically, allowing information extraction and geological interpretation. There, the visualization of convex shell surfaces within the complex surrounding on the oyster reef will be investigated, as well as the automatic quantification of the shell number.

The oyster data set (3D point clouds, digital surface models and orthophotos) is the largest of its kind in geology and to allow a broad range of scientific analyses, including taphonomy, structural geology, tectonics, and paleoecology (e.g., Harzhauser et al., 2015). Aside from these scientific aspects, the fossil oyster reef is a protected natural heritage site and it is the main attraction of a geopark in Stetten. Accordingly, this study has aims to become a best-practice example of documentation in earth sciences.

1.2. Research questions and objectives

A number of research questions shall be answered in this thesis. Research questions are organized in photogrammetry-geology pairs. The photogrammetric question typically provides a method, with which the geological question can be answered. Additionally, the questions from 1 to 3 go more and more into detail. The Table 1 provides an overview, the questions are detailed thereafter.

Table 1: Research questions organized as photogrammetry-geology pairs.

Question	Photogrammetry	Geology
1	Can we extract individual oysters from point clouds automatically, and with which quality?	What is the specimen distribution (age, size, species, etc.)?
2	How to characterize and extract orientation of specimen?	Was it a storm or a tsunami that triggered shell bed formation?
3	How can we detect overlap and encrustation of shells?	Separate pre- and post-event patterns?

An important aspect of this thesis is to show the potential of laser scanning and photogrammetry for modeling fossil shells in complex environment and to discuss the benefits of the presented approach. Figure 2 shows the workflow diagram of the research. To scientifically evaluate the applicability of the proposed approach, the following pair-wise Photogrammetry – Geology research questions (Q) were considered:

- Q Photo – Can we extract individual oysters from point clouds automatically, and with which quality?

For answering the first photogrammetry question, an individual approach has to be developed and investigated. It is based on a geometric analysis, based on the data acquired, i.e. the point cloud. A point cloud is a set of three dimensional points in a Cartesian coordinate system (x,y,z) and has in this case a point spacing of about 1 mm, whereas the individual specimen reach in size from 14 to 60 cm. As the number of shells is high, an automatic approach for their extraction was considered necessary.

- Q Geology – What is the specimen distribution (age, size, species, etc.)?

This question was triggering the entire research. The quest for an answer leads to the measurement campaign, design of a GIS database, visualization, reference data collection, and automatic extraction approaches and evaluation of the reliability of the automated processing. It is related to integration of new technology to improve the efficiency and quality of geological/paleontological interpretation. As the reliability and accuracy of data is important, the question is how to acquire the data, and with which properties, e.g. with respect to point density. Shell identification from images requires the availability of adequate surface texture, as well as shell extraction from point cloud requires high enough density. Adequate approaches for data acquisition are either based on image processing or on direct point measurement (referred to terrestrial laser scanning).

A representative set of reference data will be initially required to learn about shells which should be detected. For this, we are gathering morphometric data on more than 10 000 left and right adult and subadult shells. Finally, automated shell detection algorithm needs to be applied to the whole data set to assess the applicability of the method to larger areas. The outcome is planned to be analyzed and compared with the manually determined shell polygons (references) within the central area of the reef. The surface matching validation method intends to use completeness, correctness, and quality assessment as defined, e.g., in Heipke et al. (1997).

- Q Photo – How to characterize and extract orientation of specimen?

Orientation presents the main direction of the elongated oysters. As oysters grow, they do not necessarily grow straight. The question thus is, how to represent the orientation of irregular, often elongated objects. Orientation will be evaluated by using shell central line, which is an imaginary curved line spanning the maximum length of the shell. A method to define automatically a central line shall be investigated. By mapping shell positions and calculating their orientations, we are aiming to discover if the storm or a tsunami waves modified the orientations, to answer the second geological question:

- Q Geology – Was it a storm or a tsunami that triggered shell bed formation?

The high-energy event, which reworked the oyster biostrome and homogenized it across the now visible area, will most probably have had a directional component, such as the run-up and backwash of a tsunami. The shells were apparently exposed on the sea bottom. During this phase, the original orientation has been strongly modified by bioturbation and the dominant hydrodynamic setting. Therefore, it is expected that the clusters of oysters with similar orientation indicate prevailing current (Nagle, 1967). Hence, the answer of this question leads to extraction of central line in 2D and 3D of specimen, since they depict very well the main direction of shells valuable for orientation calculations such as azimuth or tilt angles of the shells.

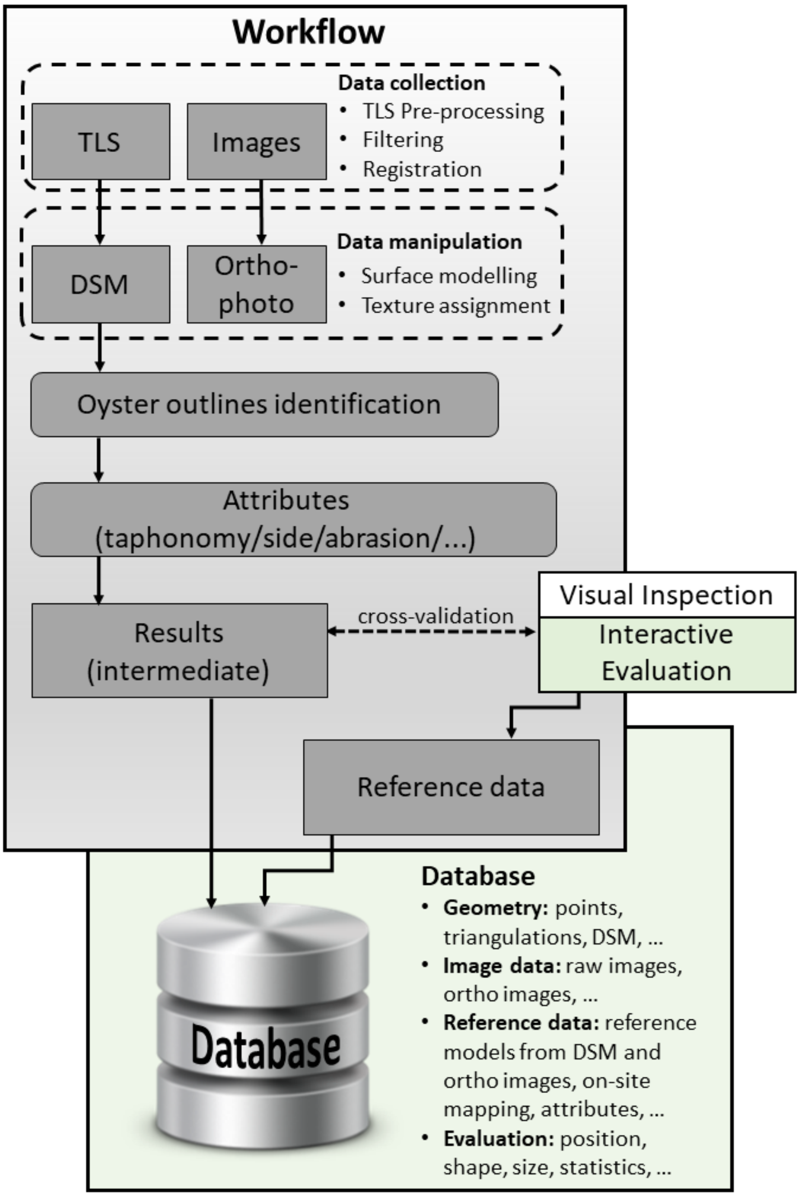

Figure 2: Workflow diagram of the research.

- Q Photo – How can we detect overlap and encrustation of shells?

For example, the species *Ostrea* lives often on the exterior part of a *Magallana* oyster. Automatic derivation of encrustation of *Magallana* by *Ostrea* would thus further support paleontological analysis providing a methodology for documenting paleontological specimens without going to the locality.

Two-dimensional and three-dimensional lengths of shells will be compared in order to visualize possible differences between 2D and 3D lengths. Differences (residuals) are expected to support automatic discovering of strongly curved shells and potential encrustation of *Magallana* by *Ostrea*, *Venerupis* or any other type of shells or even fragments. Consequently, detection of encrustation will support answering partly the third geological question:

- Q Geology – Which patterns visible in the shell bed occurred pre- and which during post-event?

A closer examination reveals that “significant” modification was also observed on the shell surface due other species settlement, predators, weathering or the strongly wave-exposed shells. Some shells have been also partly damaged during excavation. The observed settlement by barnacles and bioerosion could have occurred already while the animals were alive. In particular, bioturbation by large marine vertebrates such as rays, turtles and teleost fishes is a common phenomenon in shallow marine settings (Kidwell and Bosence, 1991; Gregory, 1991; Pearson et al., 2007; Lazar et al., 2011; Pervesler et al., 2011). The different ecological requirements of the species clearly suggest mixing of different habitats, because of many other taxa found within the shell bed beside dead *Magallana* shells. For instance, mapping features such as taphonomy, abrasion, bioerosion and encrustation, fragmentation and side of the shells will be performed. Furthermore, the statistical distribution of the features will be determined.

Research questions lead to objectives, which are given in the following. The objectives are grouped into ***3 phases***:

Objectives

(1) documenting the uniqueness of this geological site and helping to preserve it by digitizing;
(2) to test how modern photogrammetric techniques can be used in achieving (1);
(3) to develop strategy for capturing irregular surfaces by high-resolution point clouds;
(4) an analysis method to detect convex parts of shells;
(5) a method to count and detect the number of shells automatically;

Objectives (1) to (5) comprise ***Phase 1***, which includes data acquisition and shell numbering;

(6) to derive 3D shell central lines automatically and to estimate shell 3D length;

(7) to evaluate the accuracy of two-dimensional (2D) and three-dimensional (3D) shell length against manually collected reference;

(8) to apply ratio between shell area and length with the aim of identifying encrustation or strongly curved shells;

Objectives (6) to (8) build ***Phase 2***, which describes method for derivation of shell central line.

Phase 3 includes estimation of shell orientation, volume, age, and carbon production:

(9) to automatically derive the three angles of orientation of an oyster shell to better explain transport direction or presence of imbrication;

(10) to test the influence of fault lines - present in the reef - on strongly tilted oyster shells;

(11) to determine the age of shells and carbon production (based on size & volume estimation);

(12) a validation and visualization of final results.

To achieve these objectives, the methods need to be developed progressively taking in consideration that the site is protected natural heritage with the complex geometrical objects. Therefore, optimal solutions plan to be reached for capturing the whole excavation site at economically feasible costs and time. Moreover, this will present the significant automation in data processing, visualization, interpretation and derivation of geometric attributes in paleontological prospection.

Phase 1 – Digital documentation of the unique geological site will be provided by terrestrial laser scanning (TLS) at the millimeter scale. Obtaining meaningful results is not merely a matter of data acquisition with a suitable device; it requires proper planning, data management, and postprocessing (Buckley et al., 2008; Remondino and Stylianidis, 2016). Terrestrial laser scanning technology has a high potential for providing precise 3D mapping that serves as the basis for automatic object detection in different scenarios; however, it faces challenges in the presence of large amounts of data and the irregular geometry of an oyster reef. A detailed description of the techniques and strategy used for data collection and processing will be provided. An automatic analysis method for identifying and enumerating convex parts of shells intends to be investigated and evaluated. Archived accuracy in detecting the number of objects will be reported. In addition to TLS point cloud data, an orthophoto mosaic will be generated with submillimeter ground sampling distance (GSD). This high-resolution 3D information and the photographic texture will serve as the basis for ongoing and future geological and paleontological analyses. Moreover, they will provide unprecedented documentation for conservation issues at a unique natural heritage site.

Phase 2 – Method for the reliable and accurate computation of the central line of each oyster of the reef is missing. By using available digital information, 3D shell central line derivation can be investigated by adoption of existing and by developing new methods (Amenta et al., 2001; Dey and Zhao, 2004; Huang et al., 2013). High resolution orthophoto (0.5 mm) and digital surface models (1 mm) can be used to define fossil boundaries that are needed as an input to automatically extract fossil length information via central lines. In general, central lines are widely used in geosciences as they easy observe, monitor and evaluate object dimensions. The subset of 3D central lines of *Magallana gryphoides* oysters of various shapes and sizes will be computed in the study. Central line calculation will include:

i) Delaunay triangulation between the fossil shell boundary points and formation of the Voronoi diagram (Voronoi, 1908; Delaunay, 1934);
ii) extraction of Voronoi vertices and construction of a connected graph tree from them;
iii) reduction of the graph to the longest possible central line via Dijkstra's algorithm (Dijkstra, 1959);
iv) extension of longest central line to the shell boundary and smoothing by an adjustment of cubic spline curve; and
v) integration of the central line into the corresponding 3D point cloud.

The resulting longest path estimate for the 3D central line is a size parameter that can be applied in oyster shell age determination both in paleontological and biological applications. Furthermore, applying ratio between shell area and length is aiming to identify potential encrustation, because the oysters often provide habitat for other species. As the shell size has to be measured accurately, the central line method needs to be evaluated by comparing automatically extracted central lines with manually collected reference data used in paleontological analysis.

Phase 3 – Method to calculate the angles of rotation from the 3D point cloud data representing the oyster shell needs to be developed. The shell rotations are the source that can be used to reconstruct information about events and processes from the past. The rotations of objects on bedding planes is a central topic in paleontology (Lukeneder et al., 2014). However, the most analyses are characterized by the 2D-nature of the data, which focus only on the azimuth angle. This angle is interpreted as an indicator of flow or transport direction, while having two more rotation angles from the shells can be an important source of information to report in more detail about depositional condition of the specimens. Advantage of 3D data is spatial positioning of objects, parallel or tilted to the bedding plane, which might reveal imbrication or can support finding object movements due to currents, transport mechanisms, local fault lines, or encrustations (Millane et al., 2006; Milan et al., 2007, Smith et al., 2012) .

The age classes of shells plan to be established. Analysis of population structure of a fossil oyster shell bed aims to report about the growth performance of the Miocene giant oyster and to reveal its significance as part of the Miocene "carbonate factory". For this, the volume calculation of the shells is needed, for that reason the point cloud of selected shell has to be transformed into a closed mesh. Consequently, a relation between central line length (*Phase 2*) and volume data can be deduced. Thus, based on the age models of the shells, the annual carbonate production per shell can be calculated and compared with nowadays living oyster reefs.

1.3. Overview of the thesis structure

After introducing research questions and objectives in chapter 1, chapter 2 introduces laser scanning and photogrammetry applications used in previous geological and paleontological studies to map shells or in general different similar small objects (Feng and Röshoff, 2004; Heritage and Milan, 2009; Hodge et al., 2009a, 2009b; Wang C. K. et al., 2011; Wang Y. et al., 2013; Rodriguez et al., 2014; Ridge et al., 2015, 2017).

Chapter 3 contains parts of material and methods originally published in scientific articles Harzhauser et al., 2015, 2016; Djuricic et al., 2016a, 2016c, 2016d; Puttonen et al., 2018. However, parts of the articles are included in thesis with reprinting permission, under a Creative Commons Attribution 4.0 International License (https://creativecommons.org/licenses/by/4.0/). Materials and methods introduce the site and data acquisition in detail: terrestrial laser scanning (control points for registering 3D laser scans, platform, and sensor), photogrammetric imaging, coordinate systems, and management of data. This includes the strategy employed for handling the huge point clouds. Furthermore, in this chapter, digital surface model and orthophoto generation are presented as well as manual reference data collection. Moreover, the method for automatically detecting shell surfaces is presented in section 3.3. Section 3.4. describes method for 3D central line extraction and length calculation as well as a proposal for automatic encrustation detection. Section 3.5. covers the method for shell volume calculation, age class derivation as growing model of shells which is directly related with calculations of annual carbon production also described in the same section. Orientation of each shell is described by the rotation angles roll, pitch, and yaw in a Cartesian coordinate system in section 3.6., where the influence of shell orientation is investigated in order to analyze possible prevailing hydrodynamic regimes on the reef.

Chapter 4 presents the results followed by quality assessment. The links are given to corresponding supplemental materials. The sections are organized as follows: section 4.1. includes oyster reef digitizing, then, section 4.2. shows achievements regarding individual oyster extraction results, while section 4.3. is related to presentation of results about 3D orientations, and section 4.4. explains the oyster size, density, age, and carbon production estimation.

Chapter 5 presents discussion – it gives also the links to corresponding supplemental material and appendix. The sections are organized as follows: Section 5.1. includes general discussion about the reef digitizing, then, section 5.2. is related to discussion on the research questions based on oyster extraction results and evaluation.

Finally, chapter 6 – section 6.1. – outlines what worked out or what did not work out, and when it was required to focus on new developments. Section 6.2. closes the thesis with given conclusion, key findings and also suggestions for possible future research.

1.4. Contributions

In general, estimating geometric features from point clouds has many applications in computer graphics (Merigot et al., 2011); however, this technique is a novelty in geology and, more specifically, in paleontology.

Collaboration work between TU Wien, 4DIT and NHM is addressed properly in the text and made clearly evident in the chapters, and all respective sources are correctly cited. The contributions of this work are:

(1) Close-range TLS was applied for the first time for monitoring fossil oyster reefs in paleontological science;

(2) Oyster reef surface was investigated for the first time by the use of remote-sensing approach with a millimeter resolution;

(3) This study is the one which besides interpreting the overall structure of the reef, focuses on detecting single shells, by segmenting the 3D point cloud of laser scanning data into meaningful regions representing particular objects;

(4) Creating the first GIS database as an interface of a digital oyster reef and managing tool for a protected natural heritage site;

(5) Interpretations of the digital data from spatial and non-spatial aspects such as shell size, area, orientation, position, species, state of fragmentation, side, visibility of convex up and convex down shells, abrasion or bioerosion, encrustation by barnacles or another oyster, etc;

(6) The 3D central lines were used in a novel paleontological context to study fossilized oyster shells with photogrammetric and TLS-obtained 3D point cloud data (Djuricic et al., 2016d);

(7) The age classes were established based on relationship between the central line length and accurate volume calculations;

(8) The annual carbonate production per shell was calculated, reporting the fastest growing and largest species known so far, based on the age models of the shells;

(9) Developing a method to calculate the angles of rotation from the 3D point cloud data representing the oyster shell to better explain transport direction or presence of imbrication;

(10) For the first time, the influence of fault lines - present in the reef - were tested on strongly tilted oyster shells;

(11) Designing and providing various visualizations based on available DSM and orthophoto, required as thematic maps where each individual shell is linked with their descriptive attributes.

1.5. SMART – GEOLOGY Project

The PhD study was carried out during the project Smart-Geology for the world's largest fossil oyster reef, funded by The Austrian Science Fund (Der Fonds zur Förderung der wissenschaftlichen Forschung - FWF) (P-25883): https://smart-geology.geo.tuwien.ac.at/. Figure 3 presents the diagram of the "Smart – Geology" approach proposed for highly automated processing and evaluation of the results of the smart approach.

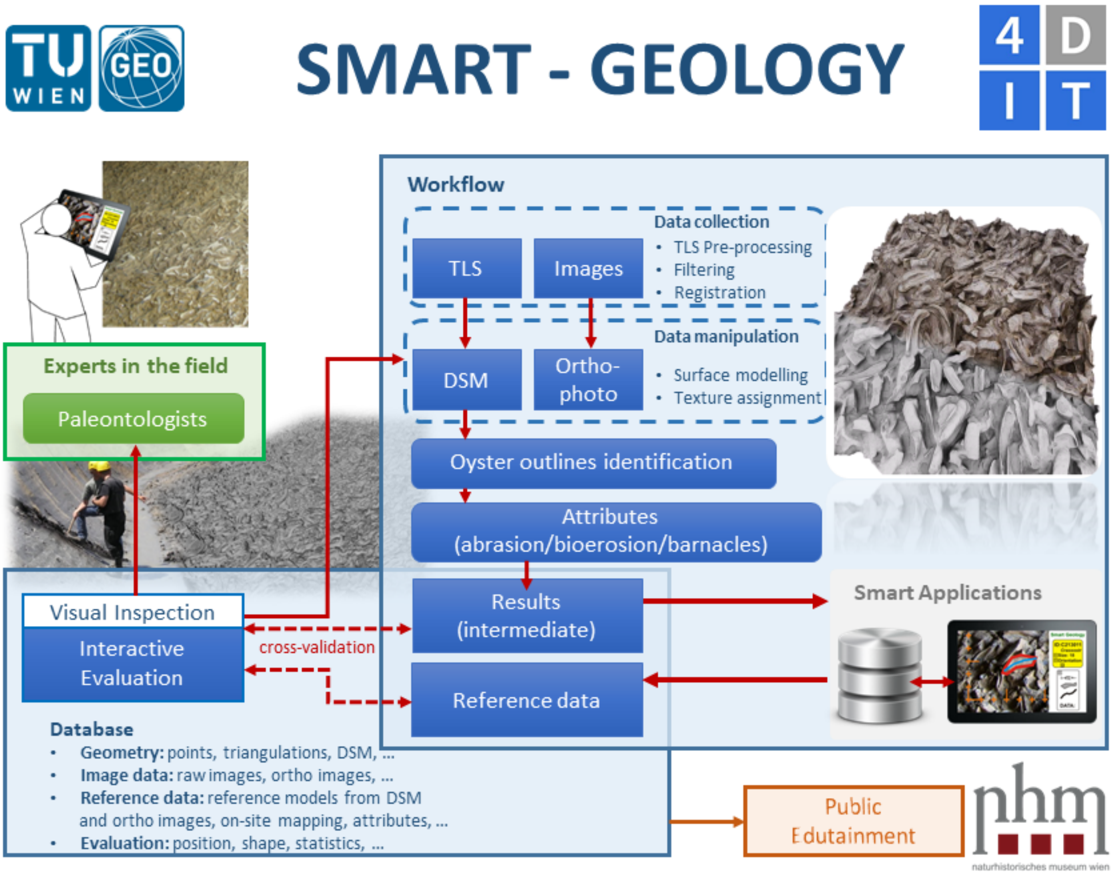

Figure 3: Workflow diagram of the project showing the "Smart – Geology" approach proposed for highly automated processing and evaluation (left) and the conventional approach (right) for evaluating and validating the results of the smart approach.

1.5.1. The following papers have been published in peer-reviewed journals

Harzhauser M., **Djuricic[1] A.**, Mandic O., Zuschin M., Dorninger P., Nothegger C., Székely B., Puttonen E., Molnar G., Pfeifer N., 2015. Disentangling the history of complex multi-phased shell beds based on the analysis of 3D point cloud data. Palaeogeography, Palaeoclimatology, Palaeoecology, 437, 165 - 180. Article I in Figure 4.

Harzhauser M., **Djuricic A.**, Mandic O., Neubauer T. A., Zuschin M., Pfeifer N., 2016. Age structure, carbonate production and shell loss rate in an Early Miocene reef of the giant oyster Crassostrea gryphoides. Biogeosciences, 13(4), 1223-1235. Article II in Figure 4.

Article I, II and III were published prior to my family name change from Djuricic to Puttonen.

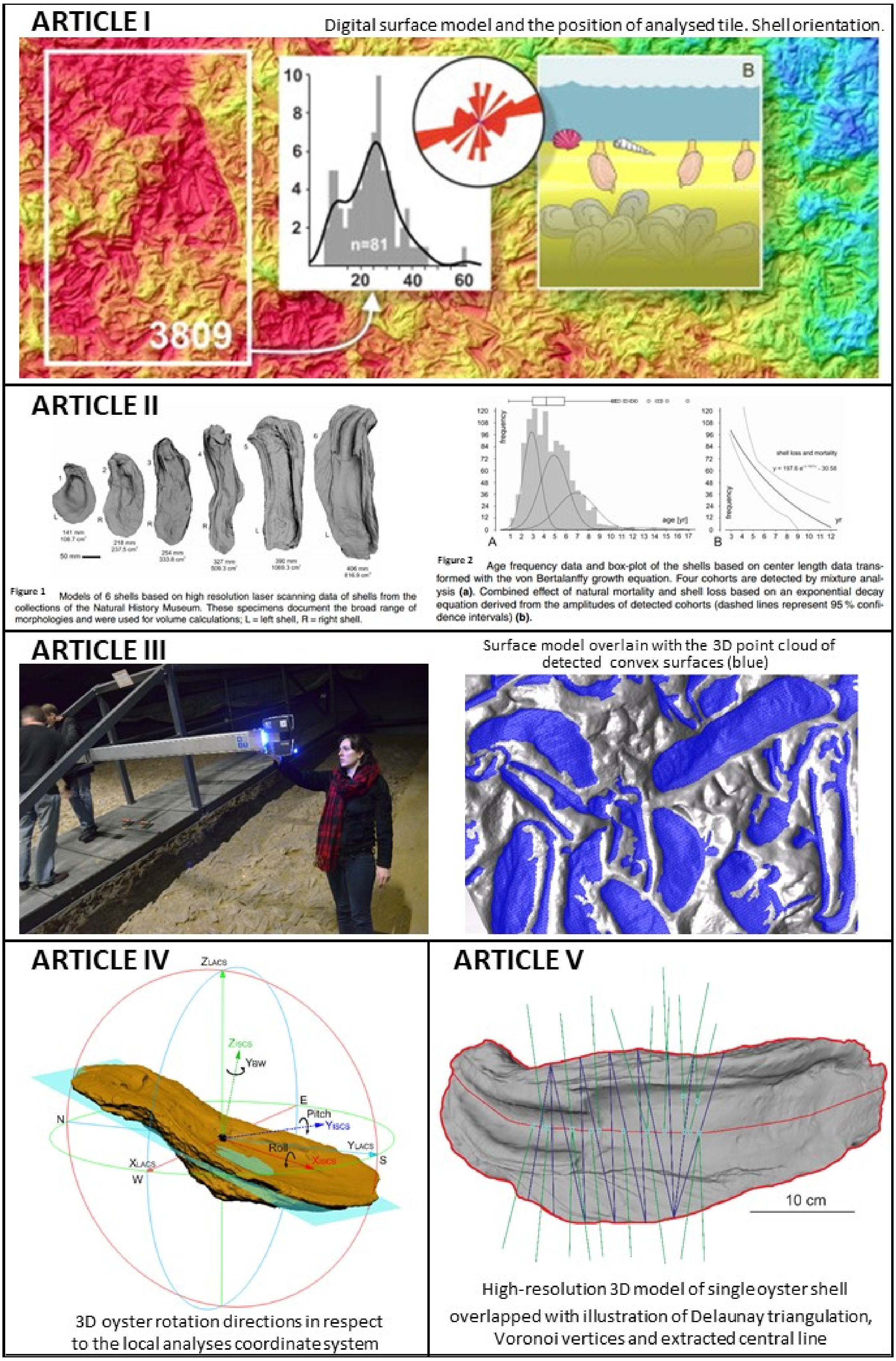

Figure 4: Graphical abstract of the scientific articles

Djuricic A., Dorninger P., Nothegger C., Harzhauser M., Székely B., Rasztovits S., Mandic O., Molnár G., Pfeifer N., 2016. High-resolution 3D surface modeling of a fossil oyster reef. Geosphere Journal, v.12, 5. Article III in Figure 4.

Puttonen A., Harzhauser M., Puttonen E., Mandic O., Székely B., Molnár G., Pfeifer N., 2018. Automatic determination of 3D orientations of fossilized oyster shells from a densely packed Miocene shell bed. International Journal of Earth Science, Springer. Article IV in Figure 4.

Molnar G., **Puttonen A.,** Székely B., Harzhauser M., Mandic O., Dorninger P., Nothegger C., Exner U., Pfeifer N. Fault system extraction of an excavated oyster reef using high-resolution laser scanned data. (in preparation)

1.5.2. Parts of the presented PhD study have been published in peer-reviewed conference proceedings

Djuricic[2] A., Puttonen E., Harzhauser M., Mandic O., Székely B., Pfeifer N., 2016. 3D central line extraction of fossil oyster shells: ISPRS Annals of the Photogrammetry, Remote Sensing and Spatial Information Sciences, v. 3, p. 121-128. Article V in Figure 4. (presentation)

Djuricic[3] A., Nothegger C., Székely B., Pfeifer N., Harzhauser M., Dorninger P., Mandic O., 2016. GIS database for the World's largest fossil oyster reef. The 19th AGILE International Conference on Geographic Information Science, 14-17th June, Helsinki, Finland. (poster)

1.5.3. Contributions to national and international conferences and research seminars, presentations and posters

Puttonen A. Investigating paleontological oyster reef using high resolution remote sensing data and GIS. Research seminar at Finnish geospatial research institute, 5th October 2018, Masala, Finland.

Djuricic A., Dorninger P., Rasztovits S., Nothegger C., Harzhauser M., Mandic O., Glira P., Pfeifer N. Pairing fossil oyster shells, CHNT - 21st International Conference on Cultural Heritage and NEW Technologies, Nov. 16-18 2016 in Vienna, Austria. (presentation)

Djuricic A., Harzhauser M., Mandic O., Pfeifer N. Surface roughness analysis of fossil oyster shells using 3D laser scanning data. Conference: 2nd Virtual Geoscience Conference (VGC), at Bergen, Norway, Sept. 21-23rd 2016. (presentation)

Djuricic, A., Puttonen, E., Harzhauser, M., Mandic, O., Székely, B., and Pfeifer, N., 2016, 3D central line extraction of fossil oyster shells: ISPRS Annals of the Photogrammetry, Remote Sensing and Spatial Information Sciences, v. 3, p. 121-128. (presentation)

Djuricic A., Puttonen E., Dorninger P., Nothegger C., Harzhauser M., Mandic O., Székely B., Pfeifer N. 3D Laser Scanning and Paleontology. Vienna young scientist symposium, June 9-10th 2016 in Vienna, Austria. (presentation)

Harzhauser M., **Djuricic A.**, Mandic O., Zuschin M., Dorninger P., Nothegger C., Székely B., Molnar G., Pfeifer N. *Limits in detecting tsunamites in the stratigraphic record –an example*

[2] Paper was selected by the Technical Commission V – Close-Range Imaging, Analysis and Applications for the ISPRS Prize for Best Papers by Young Authors in Prague (2016).

[3] Poster was selected by ESRI Committee and public audience for Best Poster Award (2016)

from the Early Miocene. Talk: Strati 2015, Graz, Austria July 19-23rd 2015, in Abstracts of 2nd International Congress on Stratigraphy. (presentation)

Molnar G., Székely B., Harzhauser M., **Djuricic A.**, Mandic O., Dorninger P., Nothegger C., Exner U., Pfeifer N. *Semi-automated fault system extraction and displacement analysis of an excavated oyster reef using high-resolution laser scanned data*. European Geosciences Union, General Assembly 2015, Vienna; in: Geophysical Research Abstracts Vol. 17, EGU2015-11417-1, 2015. (poster)

Harzhauser M., **Djuricic A.**, Mandic O., Dorninger P., Nothegger C., Székely B., Molnar G., Pfeifer N. *Disentangling the history of complex multi-phased shell beds based on the analysis of 3D point cloud data.* European Geosciences Union, General Assembly 2015, Vienna; in: Geophysical Research Abstracts Vol. 17, EGU2015-2101, 2015. (presentation)

Harzhauser M., **Djuricic A.**, Dorninger P., Nothegger C., Mandic O., Székely B., Molnár G., Pfeifer N. *New approaches in automatized recognition of geological features in 3D point cloud data*. PANGEO Austria 2014, Graz, Austria; 09/2014. (presentation)

Dorninger P., Nothegger C., **Djuricic A.**, Rasztovits S., Harzhauser M. *Smart-Geology for the World´s largest fossil oyster reef*; Poster: European Geosciences Union, General Assembly 2014, Wien; 2014-04-27 - 2014-05-02; in: "Geophysical Research Abstracts", 16 (2014), 10504-1.BibTeX. (poster)

Djuricic A., Harzhauser M., Dorninger P., Nothegger C., Mandic O., Székely B., Molnar G., Pfeifer N. *Parameter Estimation of Fossil Oysters from High Resolution 3D Point Cloud and Image Data*; Talk: European Geosciences Union, General Assembly 2014, Wien; 2014-04-27 - 2014-05-02; in: "Geophysical Research Abstracts", 16 (2014), 16040-5, BibTeX. (presentation)

1.5.4. Other related publications

Dataset is published at PANGAEA, it includes 49 tiles joined in one file (each tile is 3 × 2 m, in total 294 m²), the digital surface model (1 mm grid), the corresponding hill shade (1 mm resolution, Lambert shading, position of the light source illuminating the model: azimuth 315° and zenith angle 45°) and the orthophoto (0.5 mm resolution). The data is referenced in a local analysis coordinate system (LACS).

Djuricic A., Dorninger P., Nothegger C., Harzhauser M., Székely B., Rasztovits S., Mandic O., Molnár G., Pfeifer N., 2016. Digital surface model, hillshade and orthophoto of the world's largest fossil oyster reef, links to GeoTIFFs, https://doi.org/10.1594/PANGAEA.863615.

Oyster App[4] is published and presented at archaeological international conference:

Nothegger C., **Djuricic A.**, Harzhauser M., 2016. SMART – GEOLOGY 4 PUBLIC, 21st International Conference on Cultural Heritage and NEW Technologies, Nov. 16-18 in Vienna, Austria.

[4] Oyster App wins the 1st CHNT App Award at 21st International Conference on Cultural Heritage and NEW Technologies in Vienna (2016).

1.5.4.1. The popularisation of science through the media

The popularisation of science is the mission of NHM Wien and consequently, our project was presented through the various media. The interest arises for the newest 3D laser scanning technology, 3D digitisation, data processing and visualisation, which can contribute to gaining meaningful insights, modernisation of data collection and education. Numerous PRESS releases are the outcomes of the project as well as broadcasting in media over TV or radio. Therefore, as a PhD student, besides presenting the results at international conferences and workshops with great success by winning various scientific awards, it was important to communicate project results not only with colleagues and experts from the field, but also to public. Speaking to general audience, designing effective posters, demonstrating interactive Oyster App with elements of augmented reality or writing to catch the attention of ordinary readers about positive image of what science and technology have to offer nowadays is an effort and challenging task, but good investment for the future in rising up public interests and shaping public attitudes toward it. Therefore, few presentations are given at NHM museum in Vienna in order to communicate results of oyster research to visitors, kids, friends of museum, politicians, etc. Museum is a great place to inform wider audience about research achievements or to work on a public understanding of science. Moreover, presentations are given to teenagers at TU Wien through FIT-Programm and project was presented at events such as BeSt³, CareerFair'14 Speeddating, Langen Nacht der Forschung and also during the keynote speech at the international conference "We Build the Future", held in Zlatibor, in Serbia, where I had opportunity to talk about research, benefits as young scientist, and also in generally to advertise possibilities of studying in Austria to young and enthusiastic professionals from BSc and MSc programs.

Here is the list of newspapers, magazines, blog posts, radio and TV publications related to Smart-Geology Project: *Austrian Press Agency (APA): Measuring prehistory with "smart geology", LIVE - PR: Measuring prehistory (Evolution theory guides software development), Nachrichten aus Niederösterreich (NÖN.at): Tsunami bei Korneuburg? - Austernriff als Fenster in Vergangenheit, BE24: Im Weinviertel wird die Urzeit mit "Smart Geology" vermessen, Börse Social Network, Bussinespress: Die Vermessung der Urzeit, COMPUTERWELT: Vermessung der Urzeit mit Laserscanner, GEObranchen.de: Austernriff, Geoinformatics Newsfeed Radar: GISfeeds, Inar.de, NEWSLOCKER, OpenPR.de, Pressemitteilung Online, VDV-online, Der Standard, Wiener Zeitung, Tiroler Tageszeitung, GEO Magazine, UNIVERSUM Magazine, ORF TV, Campus & City Radio 94.4.*

2 Related Work

This chapter gives an overview about close-range remote-sensing technologies, in particular terrestrial laser scanning, including applications for the geosciences. Section 2.1 presents the latest works in geology and paleontology using photogrammery and laser scanning, which are used in modelling the geometry of complex natural surfaces in several different examples. Section 2.2 summarizes methods developed to detect the orientation of elongated objects in geosciences. Section 2.3 introduces the first time usage of laser scanning in calculating oyster shell volumes.

2.1. Photogrammetry and laser applications technology in geological and paleontological studies

The works presented herein are related to:

- geometrical shapes such as cylindrical, conical, or spiral surfaces;
- 3D surfaces in geology obtained by surveying technologies (photogrammetry and laser scanning);
- surface representations and different feature extraction techniques, primarily in geology; and
- studies focused on modeling small objects or structures similar to our fossilized objects, such as grains, river bed rocks, rough terrain, or relief with convex features;
- paleontological studies focused on parameter extraction such as length, orientation, volume, area for age structure and carbonate production calculations of the oyster reef.

Terrestrial laser scanning (TLS) applications have been used in the field of geology to map the bedding, fluvial channels, faults or rocks in order to study natural history. However, in paleontological studies its potential is still not fully utilized. TLS enables 3D geological structures to be acquired as high resolution point clouds with applications ranging from sedimentology (Brasington et al., 2012), geomorphology (Brodu and Lague, 2012, Kuhn and Prüfer, 2014), fluvial and coastal studies (Milan et al., 2007, Hodge et al., 2009, Wang et al., 2013, Abellán et al., 2013, Longoni etal., 2016; Trevisani and Cavalli, 2016), and the study of natural hazards (Barbarella et al., 2015; Telling et al., 2017, Kamintzis et al, 2018). All these studies benefit from non-contact measurements of irregular and rough surface geometry. The study areas are very often difficult to access, unpractical to measure with traditional methods due to huge areas or object number, or the individual objects located in the areas are protected. Therefore, TLS provides a powerful sensing tool that can extract valuable information remotely about Earth's surface and can be especially useful for looking at evidence of past events.

Surface modeling of oyster shells provides the tools for augmented reality and workflow automation which can possibly improve the objectivity of paleontological interpretations when compared to manual identification of natural scene elements. Accuracy of different surface representations is dependent on scale, occlusions due to acquisition geometry, point density, and roughness of the original surface (Sagy et al., 2007; Pollyea and Fairley, 2012, Soudarissanane, 2016). Surface modeling has been investigated for decades (Hoppe et al., 1992; Edelsbrunner and Mücke, 1994, Amenta et al., 2001b; Mederos et al., 2005) by taking sets of unordered 3D points as input and providing a simplified surface as output. When the target is complex natural surface and the point clouds are very dense, inhomogeneous, noisy or with present occlusions, the surface interpretation becomes difficult. The feature extraction from 3D data of natural geometrical objects is more challenging to reconstruct models and to extract information than with classic applicative data, such as urban environments or man-made objects (Huang and Menq, 2001; Rusu et al., 2008; Ioannou et al., 2012; Olsen et al., 2015; Dewez et al., 2016; Abellan et al., 2016; Cao et al., 2017; Hackel et al., 2017). These constraints arise both from the remote sensing technology and from the complexity of natural heritage environments. Therefore, reconstructing surfaces from 3D points is an important and extensively studied problem (Cazals and Giesen 2006; Boissonnat and Oudot 2005; Podolak and Rusinkiewicz 2005; Kazhdan et al. 2006, Labatut et al. 2009; Calakli and Taubin 2011). Space is often discretized using a tetrahedralization or a voxel grid, and the resulting elements are partitioned into inside and outside regions using an analysis of cells (Amenta et al. 2001b; Boissonnat and Oudot 2005; Podolak and Rusinkiewicz 2005), eigenvector computation (Kolluri et al. 2004), or graph cut (Hornung and Kobbelt 2006). Poisson surface reconstruction (Kazhdan et al. 2006) is a well-known technique for creating smooth surfaces from noisy points acquired with 3D range scanners. However, several researches have noticed that the data can be over smoothed, when the reconstructed surface is smoother than actual original surface (Alliez et al. 2007; Manson et al. 2008; Berger et al. 2011; Digne et al. 2011; Pollyea and Fairley, 2012). Therefore, the improved Poisson reconstruction algorithm incorporates the positional constraints and presents higher-quality surface reconstruction algorithm (Kazhdan and Hoppe, 2013). Surface reconstruction of datasets with unorganized point clouds, which focuses on offering complete and closed mesh models of partially sampled object surfaces is more recently introduced by Morel et al., 2018. They use a novel Poisson surface approach and their method is tested on traditional testing datasets to assess its accuracy and its ability to handle complex shapes with occlusions. The impact of scanning geometry on individual point quality is analyzed in thesis of Soudarissanane (2016), based on local planar features. The quality investigation relates random errors or precision to individual points and does not deal with systematic errors or biases. The quality of each local fit is described using a Least Squares estimation. The influence of the scanning geometry on the point quality considers the incidence angle and the range. Apart from the geometrically related research, the TLS data needs improvements when scanner intensity values are not calibrated to a physical measure of energy or target reflectivity (Pfeifer et al., 2008). Omitting the intensity calibration limits data usability significantly when considering them for automatic extraction approaches and limits the applicability of tools developed with these datasets in mind.

The bivalve oyster shell shape was approximated as a prolate spheroid to permit effective volume calculation (Alexander and Dietl, 2005). Automatic recognition of objects with simple shapes, such as planes, was described by Vosselman et al. (2004), Pottmann et al. (2004), and Schnabel et al. (2007). Recognition of a wide variety of surfaces (spiral surfaces, cones, etc.) from 3D data was studied by Pottmann et al. (2002) and Hofer et al. (2005). In addition to those studies, different sources of the geometric 3D point information have been also considered. For instance, Marshall et al. (2001) and Han et al. (2004) described methods to detect cylindrical, conical, and spherical surfaces using range images. Data sources affect properties such as noise characteristics and occlusions. Shape analysis restricted to 2D in a photographic image was studied as well, for purposes such as extracting lines and curves based on the Hough transformation (Duda and Hart, 1972). In Heijmans (1994), Boykov and Jolly (2001), and Chan and Vese (2001), the analysis of scientific images to approximate edges of objects was studied. Determined pixels of “object” or “background” provide hard constraints for segmentation. Both sources, geometry and radiometry, can be used in a combined 3D analysis. As described by Pesci and Teza (2008) and Burton et al. (2011), typical surfaces acquired in a geological survey are irregular. To identify features, or, more generally, for pattern recognition, intensity data (including spectral imaging), as in Kurz et al. (2013), can also be used as input to evaluate the reflectance and absorption properties of the material. Geological features in 3D, such as surfaces or geological bodies, are traditionally represented by polygons, polyhedrons, or voxels (Jessell, 2001). However, 3D triangulated surfaces, surface normals, and shaded relief models allow for a more precise interpretation (Samson and Mallet, 1997; Caumon et al., 2009). Detailed 3D information provides a virtual copy of the studied object and is more intuitive to interpret than traditional data from geological fields (Buckley et al., 2010). That information has demonstrated the use of laser scanning and photorealistic modeling for mapping and modeling the configuration of geological surfaces in exposed rock outcrops, as well as the ability to capture the geometry of subtle and small-scale features. Zakšek et al. (2011) present relief characteristics with hypsometric colors (graduated bands of color), elevation contours, and details by certain standard spatial analyses (e.g., slope, aspect, curvature, or local relief model), but the best visual impact is obtained with relief shading—a representation of the relief in a natural and intuitive manner. First approaches of modeling complex 3D geological surfaces were proposed by Mallet (1989) in the Paradigm GOCAD research project and by Bellian et al. (2005). Buckley et al. (2008) and Sankey et al. (2011) presented an overview of interpreting 3D data from TLS in a geological context. Measurements of surface roughness have examined elevation differences of the study site to document various surface conditions at submeter scales. Geometric documentation of natural surfaces for geological analyses with high resolution and precision, in the decimeter to centimeter range, became possible with advances in surveying technology (photogrammetry) and laser scanning (Buckley et al., 2008; Tarolli et al., 2009; Pfeifer et al., 2011). With close-range sensing technologies, with limits below 100 m, another order of magnitude in resolution and precision was reached (Hoffmeister et al., 2012; Milenković et al., 2015). Terrestrial laser scanning in complex and rough-surface terrain with millimeter-scale resolution was recently documented by Nield et al. (2013) and Arav et al. (2014). However, these studies considered only a few scan positions and a limited number of 3D points. Although surface conditions are quite different between oyster shells and grain or rock modeling applications (Feng and Röshoff, 2004; Heritage and Milan, 2009; Hodge et al., 2009b; Wang et al., 2013), there are still certain methodical similarities between our approach and theirs to evaluate shape, orientation, distribution, and size. Process analysis of a surface in geology using high-resolution TLS was described in a multi-scale approach by Brasington et al. (2012) on a river bed surface, which was comparable to the work of Baewert et al. (2014). The goal of Baewert's research was to examine the influence of the number of scan positions and grid cell size on roughness calculations during postprocessing. In addition to data acquisition and surface representation from full-waveform TLS data, Di Salvo and Brutto (2014) extracted individual objects. The extraction of a number of geometric primitives, such as rock blocks, served to calculate the volumes of individual elements and to measure distance between them. In order to improve automatization of object extraction, Brodu and Lague (2012), Otepka et al. (2013), and Dittrich et al. (2017) suggested deriving features for each point and classifying the point cloud with respect to those features. They described extracting optimized 3D or 2D features from the derived optimal neighborhood size to optimally describe the local structure for each 3D point. Eigen features from a covariance matrix of a point set with the sample mean are commonly used geometric features that can describe the local geometric characteristics of a point cloud and indicate whether the local geometry is linear, planar, or spherical (Lin et al., 2014). In general, estimating geometric features from point clouds has many applications in computer graphics (Merigot et al., 2011); however, this technique is a novelty in geology and, more specifically, in paleontology.

Recently, close-range TLS was applied for the first time for monitoring intertidal and subtidal oyster reefs in estuarine science (Rodriguez et al., 2014, Ridge et al., 2017) due to their economic importance and sea level tracking. Acoustic techniques are state of the art for these purposes (Allen et al., 2005; Grizzle et al., 2005). Similarly, coral reef surfaces were investigated by the use of remote-sensing approaches with a resolution below 1 m by Goodman et al. (2013) and Hamylton et al. (2014). All these studies tend to focus on the overall structure of the reef and do not aim to detect single shells. Consequently, millimeter resolution has not, to my knowledge, been achieved to date.

Beside TLS studies introduced related to current living oyster and coral reefs, in paleontology, TLS and photogrammetry have been incorporated to capture high-resolution data from remote localities and sites with large concentrations of dinosaur footprints (Breithaupt et al. 2004, Bates et al. 2008). Dinosaur tracks and other trace fossils are geologic features and as such are subject to the same natural processes as other rock formations. Those studies focused on parameter extraction such as length, orientation or area. Falkingham et al. (2014) mapped the dinosaurs' fossil footprints and trackways preserved in the Glen Rose Formation along the Paluxy River, Texas (USA) using a Riegl LMS-Z420i LiDAR laser scanner and following works of Farlow et al. (2012) and Bates et al. (2009). The same site was interesting to Platt et al. (2018) for collecting LIDAR data with a Z+F IMAGER® 5006i laser scanner and a Leica ScanStation C10. Unfortunately, many tracks were full of water; this precluded photogrammetry because water levels would have provided false track bottom surfaces. Therefore, the Leica ScanStation C10 was chosen because its green laser was able to penetrate the water to record actual track floors. Beside the dinosaurs' footprints, 3D models of dinosaurs and elephant skeleton were constructed in several recent paleontological studies from laser scanning data (Bates et al., 2009a, 2009b, 2010). The purpose of these studies was to estimate the volume, i.e. the body mass of dinosaurs. A long-range laser scanner was used to digitize several mounted skeletons, allowing the reconstruction of body volumes and respiratory structures as a 3D model. Lallensack et al. (2015) reconstructed dinosaur tracks from historical or archival analog photographs. Work of Adams et al. (2010) demonstrates the feasibility of using portable 3D laser scanner - NextEngine 3D Scanner HD to capture field data - vertebrate track, original fossil morphology and texture and create high-resolution, interactive 3D models (approximately 0.3 mm) of at-risk natural history resources. An optical handheld scanner OptiNum RE was recently used during the fossil excavation in a study by Harmand et al. (2015) to map the World's oldest stone tools discovered in Kenya. However, all those studies present techniques for small selected area or individual specimen handling, with photogrammetry software that are specially adapted to typical use cases in paleontology, in order to prepare virtual visits on the web or as a virtual tool in museum exhibitions, but they are not easily applicable for huge paleontological site with complex surface geometry, including more than 50 000 specimens, and with limited access and illumination.

2.2. Orientation of elongated objects

Bivalve shells are adapted to specific local environments (Dunca et al. 2009; Versteegh et al. 2011) as a consequence of hydrodynamic events from the past. The shell orientation is one of the sources that can be used to reconstruct information about events and processes from the past. Many shell beds pass through a complex history of formation being shaped by more than one factor under different environmental conditions (Kidwell, 1986, 1991; Fürsich and Oschmann, 1993; Mandic et al., 2004a; Zuschin et al., 2005). Consequently, shell beds may provide information on various physical processes that caused the accumulation. The orientation of objects on bedding planes is a central topic in paleontology. The pioneering paper by Nagle (1967) experimentally tested the influence of waves and currents on shell orientation. The position of elongated objects, such as mollusc shells, was investigated in numerous papers, where the measurements aim at deciphering past depositional environments and hydrodynamic regimes, such as prevalent currents, wave action, storm directions and turbidite flows (e.g. Grant et al., 1992; Hladil et al., 1996; Newell et al., 2007; Roberts et al., 2008; Harzhauser et al., 2015). In most cases, information on fossil orientations is only available from traditional field measurements, which are difficult to resample and sensitive to subjective interpretations. Manual measurements are also time-consuming, which limits the number of measurements taken, thus leading to spatially limited sampling. Whilst direct field-measurements are still common practice, already Brenchley & Newall (1970) improved the level of objectivity and reproducibility by deriving measurements from field-photographs. A further drawback of most analyses is the 2D-nature of the data, which focus only on the azimuth angle of the orientation. This angle is interpreted as an indicator of flow or transport direction, while having two more orientation angles from the shells can be an important source of information to report in more detail about depositional condition of the specimens. Advantage of 3D data is spatial positioning of objects, parallel or tilted to the bedding plane, which might reveal imbrication or can support finding object movements due currents, transport mechanisms, local fault lines, or encrustations. Lukeneder et al. (2014) and Mayrhofer et al. (2016) developed a 3D approach to capture the orientations of ammonite shells in a sediment-block by virtual shell reconstructions, derived from serial grinding techniques. The resulting 3D visualizations allowed measuring the azimuth angle and two more angles. The obvious disadvantage of this approach is its destructive nature, resulting in the complete loss of the studied objects.

A major advantage and potential is offered by the application of the newest technology, terrestrial laser scanning and close range photogrammetry, which provides millimeter-level measurement accuracy and allows rapid acquisition of huge datasets (Stylianidis & Remondino, 2016). However, only few studies so far have tried to take advantage from TLS for paleontological studies. Millane et al. (2006) used laser scan derived digital elevation models to quantify imbrication of pebbles and to reconstruct flow directions in alluvial deposits. Sediment transport processes were also the focus of Hodge et al. (2009), who used TLS to identify grain-scale topographic data from gravel bed surfaces. Heritage et al. (2009) and Smith et al. (2012) applied

TLS to determine the shape, orientation and grain roughness in gravel-bed rivers. A TLS-derived topographic model of a fluvial system was the base for Brasington et al. (2012) to test hydrodynamic simulations and quantify erosion and transport rates. Similarly, Milan et al. (2007) used 3D laser scanning to quantify small-scale changes in river channels to assess erosion and deposition volumes. Thus, most applications focused on fluvial sedimentation, whereas the advantages of TLS were rarely exploited for paleontological data sets.

2.2.1. Generalization of objects by central line

Elongated objects, sea shells, are in this thesis generalized using the central line primarily to derive their orientations. In general, generalization of object central line is investigated using images, mesh surfaces, or point clouds. The state of the art presents works in a wide variety of applications of 2D and 3D approaches in computer graphics, mobile mapping and GIS, medical image analysis, etc. However, 3D central lines on surfaces in paleontological context, especially for fossil oysters using photogrammetric technology, are not yet reported in the literature. Our algorithm is similar to the algorithms that use Delaunay (1934) triangulation and Voronoi (1908) diagrams as intermediate steps to generate the vertices of the polygonal representation.

The terms central line, skeleton and medial axis are used often in literature to describe related concepts (Greenspan et al., 2001; Palagyi et al., 2001). The terms central line and medial axis appear most often concerning thinning of the object on the surface such as road (Doucette et al., 2004). The term skeleton is more associated to volumetric data such as 3D trees, sculptures, body (Tagliasacchi et al., 2009; Livny et al., 2010; Bucksch and Fleck, 2011; Kasap and Magnenat-Thalmann, 2011).

The review paper from Cornea et al. (2005a) categorizes many of the existing skeleton algorithms for 3D shapes into classes based upon implementation and discusses how these classes achieve the various properties. The popular approaches use: i) distance field (Gagvani and Silver, 2001), where they derive three-dimensional sampled volumes and the distance field is the minimum distance from any boundary voxel; ii) thinning method as a linear process also in the number of object voxels (Palágyi and Kuba, 1998); iii) geometric method based on medial axis transform (Amenta et al., 2001) using a finite union of balls and their relationship with surfaces where the set of centers of the balls form the medial axis of the observed surface; iv) potential field such as vector field (Cornea, 2005b), i.e. a 3D array where each voxel contains a vector value (magnitude and direction) and its topological characteristics are used such as critical points and critical curves, to extract the curve-skeleton.

Moreover, pixel based methods were studied by Lam et al. (1992) when thinning methodologies based on pixel deletion or erosion criteria were needed to preserve the linear connectivity of patterns. Niblack et al. (1992) described also an algorithm for generating connected skeletons of objects in a binary image. The most dominant applications nowadays for central line extraction based on images are road mapping and medical purposes. Reconstruction of road central lines from mobile mapping image sequences which can be used to update a Geographic Information System (GIS) database is introduced in (Mayer et al., 1998; Tao et al., 1998; Doucette et al., 2004; Miao et al., 2013). Approach for vascular medical imaging (Krissian et al., 2000) uses gradient information at a given distance of the vessel central lines tested on real X-ray images of brain vessels. An overview on medical central line extraction is given in (Schaap et al., 2009).

Furthermore, a geometric-based framework for extracting curve-skeletons is applied directly on the mesh domain and does not require voxelization (Au et al., 2008). The method extracts a 1D skeletal shape by performing geometry contraction using constrained Laplacian smoothing and it is demonstrated through various bone-skeletons examples.

Raumonen et al. (2013) analyzed laser scanning data with standard fitting procedures to obtain the orientation and size of tree structures. The method presents the reconstruction of a trunk–branch skeleton based on 3D point cloud information. Dey and Zhao (2004) show a scale and density independent algorithm that approximates the medial axis from the Voronoi diagram of a set of sample points. Gorte and Pfeifer (2004) addressed in their work 3D modelling and reconstruction of a tree in terms of stem and branches, where an algorithm has been designed in 3D voxel space. The CAMPINO method is introduced by Bucksch and Lindenbergh (2008), see also (Bucksch et al., 2009), where their skeleton is represented as a graph, which can be embedded into the point clouds based on cycle elimination in a graph as derived from an octree based space division procedure.

As application, Cai and Rasdorf (2008) predicted 3D lengths using LIDAR point cloud and planimetric road central line data. Tagliasacchi et al. (2009) based their approach on the notion of a generalized rotational symmetry axis for curve skeleton extraction. With proper joint handling, this leads to complete, characteristic curve skeletons even with significant missing data. Cao et al. (2010) present an algorithm based on Laplacian contraction. The method is robust to noise and sample distribution, and can handle a moderate amount of missing data. Also Huang et al. (2013) demonstrated L1-medial skeletons extraction from unorganized, unoriented, and incomplete 3D raw point clouds.

2.3. State of the art – fossil oyster volume calculations

Terrestrial laser scanning (TLS) technology is not broadly used in paleontological studies to date. Although some in situ preserved fossil reefs are known (e.g., Hosgör, 2008; Ragaini and Di Celma, 2009; Chinzei, 2013), no laser scanning data from them exist, which would allow a direct spatial comparison between the oyster reefs. The previous studies are based on collection material using different methods, such as images from a scanning electron microscope (SEM), manual in situ measurements or oblique photographs.

This thesis presents the first results of a full survey of a fossil oyster reef with TLS. The survey produced 3D point cloud data of the reef in millimeter resolution which is used for accurate shell volume calculations. Beside the static laser scanning of the reef, individual oyster shells were digitized and measured with higher resolution point clouds using a ScanArm scanner (3D METRIS MCA, 3600 M7 - range of 7-axis articulated measuring arms). The data of individual excavated oyster shells is collected with sub-millimeter resolution. This data supported detailed 3D modeling of the shells and was used for volume derivation. Apart from this research, very little is known about the shell volume estimation when taking in consideration the complex geometry of the shell inner and outer surface. Literature reports about a few attempts to approximate the volume of oyster shells and discussions that biomass scales near the square of the shell length rather than the cube (Powell and Stanton, 1985; Powell et al., 2015). Thus, previous volume related studies used approach which helped to understand the occupancy of space of the object similar to a form of minimum bounding box, but they had difficulties in finding the geometry of the object shapes close to oyster model in reality. No previous study, to our knowledge, tried to compute volume of fossil shell beds using their 3D models derived from point cloud data. Lack of reef level volume estimations is due to complexity. 3D laser scanning and photogrammetric surveys make such modelling feasible for the first time. Once parameters such as length, volume, area, fossil shell density are calculated, they can be used for different ratio calculations and correlated to the age structure estimates. Hence, we present the first analysis of volume based research using data sample of 1121 shells of the giant oyster *Magallana gryphoides.*

3 Materials and Methods

3.1. Site, data acquisition and data set

High-resolution dataset consists of images and 3D point cloud data. Data collection at original oyster reef site Fossilienwelt included two survey methods: close range photogrammetry and terrestrial laser scanning (TLS), which provided images with a nominal ground resolution of approximately 0.6 mm per pixel and 3D point clouds with the distance between the laser scanning points ranging from 0.7 mm (center) to 1 mm (outer edges) per scan. The data collection was carried out in January 2014. In addition, second data collection was organized in the photo studio of the Institute of Art and Design (TU Wien) for nine selected oyster shells for even higher resolution modelling. Their scanning was individual, each shell was captured separately using measuring arm which contains a triangulation laser scanner and a camera. It provided sub-mm resolution point clouds (~25 points per mm^2).

Nothegger (2011) proposed to use phase-shift scanners for the application of high-resolution and highly accurate scanning of large sites, and among them was the oyster reef. Such a laser scanner measures a cloud of 3D points. An analysis of the point cloud to improve precision (e.g., filtering) was described by Dorninger and Nothegger (2009). Therefore, the entire site of ~459 m^2 is presented with 3D data set of approximately one billion points. This was achieved by the ability to acquire many more scanning positions with a better configuration. Image data were acquired as well. The photos were used to generate high-resolution orthophotos, which were primarily used for the interactive verification of the automatically generated results and also for the generation of textured 3D models for visualization purposes (Harzhauser et al., 2015, 2016; Djuricic et al., 2016a).

3.1.1. Study site

The excavated shell bed (27 m × 17 m) is protected by an indoor hall as part of the geo-edutainment park, “Fossilienwelt Weinviertel.” The hall comprises the oyster reef, surrounded by two natural walls of sand, two construction walls, a mobile bridge, a lower visitors’ platform with reflectors below, an upper platform with stairs and projectors, and reflectors on the ceiling. The man–made objects within the oyster hall are later on excluded from the final data set. In August 2012, the oyster reef was declared a protected site under the nature conservation laws of Lower Austria (§12 NÖ Naturschutzgesetz) due to its exceptional scientific importance.

3.1.2. Control points

The control points were distributed regularly (Figure 5A), and they served the purpose of registering 3D laser scans, as well as being a link to an external coordinate system, as discussed in the Coordinate Systems section. Control points were placed on the pillars around the oyster reef (15 points in Figure 5B), to provide the reference point network. In addition, 18 control points (from point number 23 to 40) were placed directly on the oyster reef from a mobile bridge spanning across the oyster reef (Figure 5A and 5C), and seven more points were placed on the visitors' platform around the reef (points 16, 17, 18, 19, 20, 21 and 22). Control points on the reef were distributed in a grid of 6 m × 3 m (Figure 5A) as paper marks. All 40 points were measured by means of a total station (Leica 1200 series) from two different positions from the platform and from one position at the opposite corner; their precision is better than 2 mm.

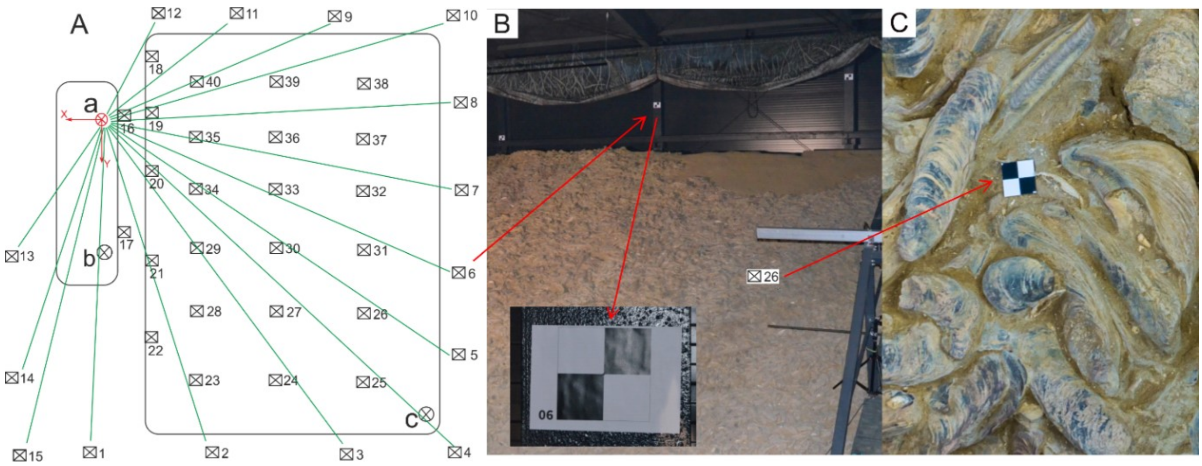

Figure 5: (A) Determining the control points by polar surveying in the reference point network. The red circle represents the first position of the total station. Circles with crosses are prisms. Squares with crosses are paper marks. (B) Examples of control points on the pillars. (C) Control points on the reef. Figure is originally published in Djuricic et al. (2016b).

Points 1, 2, 4, 6, and 10 (see Figures 5A and 6) of the reference network were permanently marked by holes embossed in the steel pillars of the construction walls (see Table 2). The data collection was carried out in January 2014 and might be repeated in the future with new technology such as hyperspectral laser scanning (Hakala et al., 2012; Kurz et al., 2013; Puttonen et al., 2015) or imaging.

Table 2: Coordinates of permanently marked control points in the indoor hall of the covering the oyster reef (see also Figure 5A). The ACS (acquisition coordinate system) is levelled, i.e. the Z-axis follows the plumb line. The LACS (local analysis coordinate system) is oriented to follow the strike and dip directions of the oyster reef. UTM is in Zone 33N. Additionally, the orthometric height is given to provide easting, northing and height above sea level, considering the geoid undulation of 44.58 m. All coordinates are given in meters. Table is originally published in Djuricic et al. (2016b).

	ACS			**LACS**			**UTM**			
Point ID	X	Y	Z	X	Y	Z	E	N	U	H
1	−2.974	17.710	−1.884	44.646	26.750	13.603	600662.374	5358036.460	226.223	181.643
2	−7.026	17.504	−1.600	40.751	26.467	12.468	600666.376	5358037.118	226.508	181.928
4	−16.923	18.503	2.094	30.171	27.277	12.501	600676.318	5358037.229	230.203	185.623
6	−17.417	7.761	1.146	30.228	16.527	11.511	600675.607	5358047.957	229.268	184.688
10	−18.168	−8.339	0.987	29.866	0.416	11.209	600674.550	5358064.034	229.127	184.547

Table 3: Transformation between coordinate systems (CS). Generally, the transformations follow the definition of $\mathrm{P}' = \mathrm{T} + s\mathrm{RP}$, where P is the point in the source coordinate system, P' the point in the target coordinate system, T a translation, s the scale factor, and R a rotation matrix (orthogonal matrix). Table is originally published in Djuricic et al. (2016b).

Source CS	**Target CS**	$\boldsymbol{T}$	$\boldsymbol{s}$	$\boldsymbol{R}$
ACS	UTM (ENU)	$\begin{pmatrix} 600657.436 \\ 5358053.718 \\ 228.125 \end{pmatrix}$	0.999677	$\begin{pmatrix} -0.9937099 & 0.1119843 & -0.0002257 \\ -0.1119840 & -0.9937093 & -0.0011630 \\ -0.0003545 & -0.0011304 & 0.9999993 \end{pmatrix}$
ACS	LACS	$\begin{pmatrix} 47.100 \\ 9.100 \\ 16.517 \end{pmatrix}$	1	$\begin{pmatrix} 0.9379668 & -0.0178940 & -0.346263 \\ 0.0190740 & 0.9998181 & 0 \\ 0.3462001 & -0.0066046 & 0.9381374 \end{pmatrix}$
UTM (ENU)	UTM E, UTM N, ortho H	$\begin{pmatrix} 0 \\ 0 \\ -44.58 \end{pmatrix}$	1	$\boldsymbol{I}_{3,3}$

Figure 6: Transformation between UTM and ACS was performed with 4 identical points (red circles numbered 1-4 in the figure). The orthophoto also illustrates how the hall is rotated approximately 3° w.r.t. the north direction. The rms of coordinate differences between UTM and transformed ACS coordinates at those 4 identical points is 5.3 mm.

3.1.3. Data acquisition and platform

There is no possibility of positioning an instrument or a tripod on the oyster reef because of conservational concerns. It is not possible to walk over the oyster reef, hence to overcome this limitation, a long mobile bridge was constructed, which can be moved in a south/north direction (Figures 7 and 8). Most data were acquired from it including central part of the reef, but the remaining part, which covers the reef borders, was measured from the visitors' platform. To provide an unobstructed view, a long, stiff (and heavy) metal structure was built to carry the scanner (Figure 7A) and the camera on the top (Figure 7B), under a 3.1 m × 2.1 m tent.

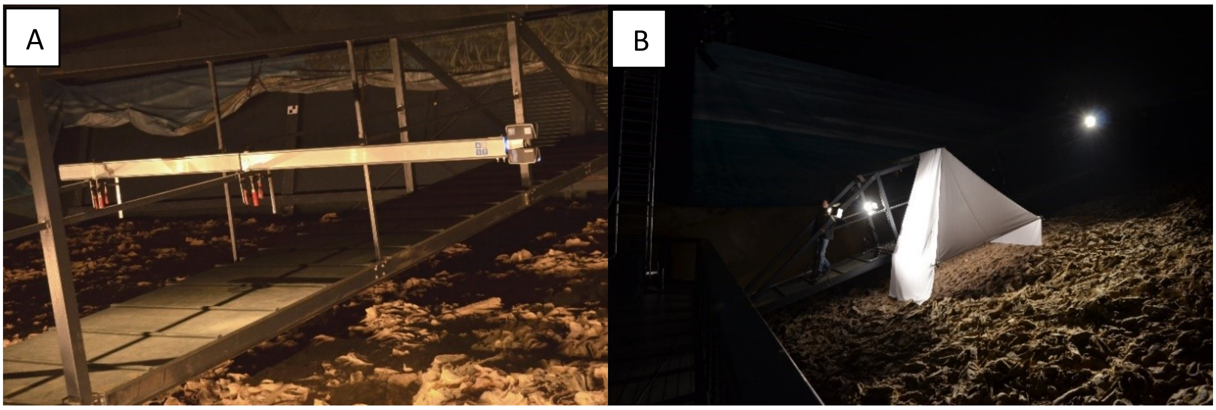

Figure 7: (A) The mobile bridge; 3D capturing of the exposed oyster reef surface using stable terrestrial laser scanning (TLS) positions. The movable bridge enabled contactless access across the reef and detection of the surface from a height of ~2.5 m. (B) A special light tent was constructed and illuminated simultaneously from several sides with studio spots to achieve a homogeneous illumination over the entire reef.

Figure 8: The local analysis coordinate system (LACS) adjusted to the oyster field. Note that the origin is shifted even farther to the back than shown in this figure.

3.1.4. Sensors

We used a FARO Focus3D laser scanner that was controlled remotely from the stable visitors' platform. This is a high-speed 3D laser scanner for detailed measurement and documentation that collects 3D points with a rate of up to 1 MHz and a range of up to 100 m with a 3.8-mm-diameter laser beam (FARO, 2018). Experimental analysis has shown that, over short distances, the single- point measurement precision of FARO TLS data is actually ~2 mm up to 10 m range (FARO, 2018). The surface of the exposed oyster reef was surveyed by TLS, and texture capturing was done by photographic imaging. The precision of the individual measurement is defined by the scanner specification. To increase the precision of the result, we applied point-based filtering (i.e., averaging). Hence, we are able to achieve 1 mm precision. Occlusions were minimized by the constellation of the scanner during scanning (high overlap and various incidence angles). For photogrammetric data acquisition, a uniform illumination was necessary to enable an image acquisition that was almost shadow-free. A Canon 60D camera with a Canon EF 20 mm f/2.8 lens was used to capture images (each 5184 × 3456 pixels). On average, the ground sampling distance (GSD) was 0.6 mm, and the footprint of the image was ~3.1 m × 2.1 m on the reef. Images were taken with 80% overlap over the longer image edge and 50% overlap over the shorter side. The camera was mounted approximately orthogonal to the oyster reef plane. Due to the low ambient light, artificial lighting (close to studio conditions) was necessary for image acquisition. Particular emphasis was taken to ensure homogeneous, diffuse lighting conditions to minimize shadows. Therefore, the structure for image acquisition was surrounded by reflectors and a tent (Fig. 7B).

3.1.5. Acquisition strategy

Scanning the fossil shell bed required multiple viewpoints to ensure minimization of scan shadows and to provide homogeneous point coverage. The scanning height of 1.5 m above the reef also led to the capturing of overhangs. Thus, scans were acquired in a regular grid of 2 m × 2 m, with the distance between the laser scanning points ranging from 0.7 mm (center) to 1 mm (outer edges) per scan. In total, 83 scan positions were sufficient to collect data covering the entire reef. From all those positions, approximately one billion points were acquired at the site, corresponding to ~150 points per square centimeter. The high number of nearly orthogonal scanning positions enabled a homogenous point density on the surface of the oyster reef. Regarding investigation of the quality of measurements obtained with laser scanners (Pfeifer et al., 2007; Kaasalainen et al., 2011; Soudarissanane et al., 2011; Milenković et al., 2015), it is recognized that not all points measured by the laser scanner can serve for modeling of the irregular surface. Hence, the most reliably scanned area of each scan is taken into consideration by restricting the distances to less than 15 m. The scans were oriented in the acquisition coordinate system (ACS) (introduced in more detail below in the Coordinate Systems section) with the control points on the reef, the walls, and the visitors' platform by means of the scanner software FARO Scene. In each scan, 15 or more control points (i.e., planar photogrammetric targets; Figure 5B and 5C) were identified, covering the entire field of view. A global accuracy of better than 3 mm was achieved, but local discrepancies between overlapping scans are smaller, in the region of 1–2 mm.

3.1.5.1. Bundle block adjustment

Photogrammetric images were oriented in the ACS by means of a bundle block adjustment (BBA) with control points (photogrammetric targets and distinct points in the TLS data) on the reef. We used Agisoft PhotoScan (PhotoScan software, http:// www .agisoft .com/) for automatic feature extraction, matching, and relative orientation of all images. Measurements of photogrammetric targets and distinct points were added manually. Subsequently, a datum transformation was applied with the control points. All observations were exported (image coordinates of feature points and control points and control-point coordinates in ACS) and used as input for a BBA in software developed in-house, thus allowing better control over camera calibration and control-point consideration. The distinct points in the TLS data were necessary to counteract distortions in areas without targets (i.e., the lower part of the reef, which was less accessible). The distinct points were measured directly in the TLS data and were necessary for automatic detection of wrong tie-point correspondences. To avoid tensions between different coordinate systems (Luhmann et al., 2014) and realizations of coordinates, all existing stochastic quantities (accessible from the total station campaign and the registration of the TLS data) of the control points were introduced into the BBA. The camera calibration was performed by self-calibration (also in the BBA). The mean error of tie-point coordinates close to the reef center was ~1.5 mm (in X and Y directions) and 2.4 mm (in Z direction); and close to the edge of the reef, it was 2 mm (X and Y) and 4 mm (Z).

3.1.6. Coordinate systems

During its formation in Early Miocene time, the living oyster reef as well as the shell bed were horizontal. During the Middle Miocene, the entire basin fill, including the shell bed, was tilted tectonically by ~25° to the west (Zuschin et al., 2014). We thus established the following coordinate systems to reconstruct the original situation during shell bed formation for subsequent geological and paleontological analyses:

(1) Acquisition Coordinate System (ACS);

(2) Local Analysis Coordinate System (LACS); and

(3) Universal Transverse Mercator (UTM) system.

The ACS is a local coordinate system used during the measurements with a total station and a TLS (Figure 5A). Polar measurements (angles and distances) were used to determine the 3D positions of points on the object relative to a well-defined point where the total station was placed, which was the origin of the acquisition coordinate system (point “a” in Figures 5A and 6). A second well-defined point on the visitors’ platform was selected for purposes of orientation (point “b” in Figure 5A). The horizontal direction from the first to the second point was set to zero. The LACS (Figure 8) is a coordinate system defined by a Euclidean transformation from the Acquisition Coordinate System. It represents the “horizontal geological” coordinate system. The axes follow the dip and strike directions, and the third axis, Z, is orthogonal to the adjusting plane through the field. Axis X extends downward in the field, and Y is horizontal. Thus, the Y axis is basically parallel to the length axis of the hall. The origin of the local analysis coordinate system was placed behind the corner of the oyster field, which is diagonally opposite the entrance of the hall.

3.1.6.1. Transformation from the ACS to the LACS and from the ACS to the UTM

The oyster reef is situated on a plane with small deviations relative to the total extent of the reef. An orthogonal regression plane was determined from a subset of the TLS point cloud. This subset was a sub-sampled point cloud that ensured the global approach (working on the entire reef at once) was successful by avoiding numerical problems (covariance matrix of one billion points). The plane was determined by a principal component analysis (PCA) of the point cloud. From this, the rotation matrix to transform the points from the acquisition coordinate system into the local analysis coordinate system was determined. The entire area of interest was rotated by 20.26° to define a locally horizontal geological coordinate system, the LACS. The transformation from the ACS into the LACS is described by a transformation comprising rotation, translation, and scale identical to 1.0. The local analysis coordinate system has the same scale as the range measurements of the total station (Table 3). Finally, a transformation to the UTM System was also performed to ensure compatibility with future campaigns and to allow for comparison with other geological data from the region. The transformation parameters are given in Table 3). The registration method used control points (only the reference points on the pillars obtained from the total station measurements) to transform multiple scans into the local analysis coordinate system. These control points are transformed to UTM33N coordinates on the basis of four east, north, up (ENU) control points observed by GPS measurements outside the oyster hall (Figure 6). When the parameters obtained from the spatial similarity transformation are applied, the points fit with a root mean square (rms) coordinate difference of 5 mm. Height is obtained from GPS measurements based on ellipsoidal height above WGS84 per the GRS80 ellipsoid (Hofmann-Wellenhof et al., 2011).

3.1.7. Point cloud manipulation

3.1.7.1. A high- resolution and dense TLS point cloud

To improve the point cloud, outliers were removed, and noise was filtered (Nothegger and Dorninger, 2009). The improved point cloud was input into the meshing process, where a polyhedral mesh was created. The consistency of the point cloud was aided by exploiting overlapping scans—up to five, depending upon the location within the reef, thus minimizing errors caused by auto correlated noise in the distance sensor of the FARO scanner. These errors are not reduced by filtering a single scan only. Due to the complex surface structure, it often occurs that the emitted laser beam hits two or more distinct surfaces simultaneously. It is impossible for scanners utilizing the phase-shift measurement technique to discriminate between those signals solely on the basis of the integral signal received by the scanner (Nothegger and Dorninger, 2007). Considering the scanning position for each individual scan, locally estimated surface normals can be analyzed to eliminate those points being characterized by normals facing almost orthogonal to the direction of the scanning beam. Additionally, single outlying points were eliminated as outliers after multiple scans were merged, thus identifying apparent (not actual) surfaces that were not facing the scanner viewpoint but lay inside the beam direction. Registration of the individual scans must be sufficiently accurate to avoid additional errors. That goal was realized by using at least 15 control points per scan, with a precision of better than 2 mm. The 3D model based on the TLS data was generated using the Poisson surface reconstruction method (Kazhdan et al., 2006). The result is a triangulated surface with an approximately homogeneous edge length of 0.7 mm on average. The method also reduced the number of points to ~40% of the original TLS points on the reef. The Poisson surface reconstruction algorithm is especially suitable for merging point clouds or meshes because of its implicit averaging, resulting in a surface that appears smooth even in the presence of noise in the individual point clouds. The reason for this is that, internally, the surface is reconstructed as a twice-differentiable scalar field, and the triangulation—the output of the algorithm—is an approximation of that smooth scalar field. Due to this averaging of up to five individual point clouds, the localized upper limit of the standard deviation between the triangulated mesh and the generated surface mesh is up to 2 mm, given that the surface is sufficiently flat. In areas with high local curvatures, the area of the laser beam footprint (3 mm) limits the achievable accuracy. By using the nodes of the triangulated model, a homogeneous, high resolution 3D point cloud is generated for further analysis. A high-resolution and dense 3D point cloud of a small part of the oyster reef is shown in Figure 9.

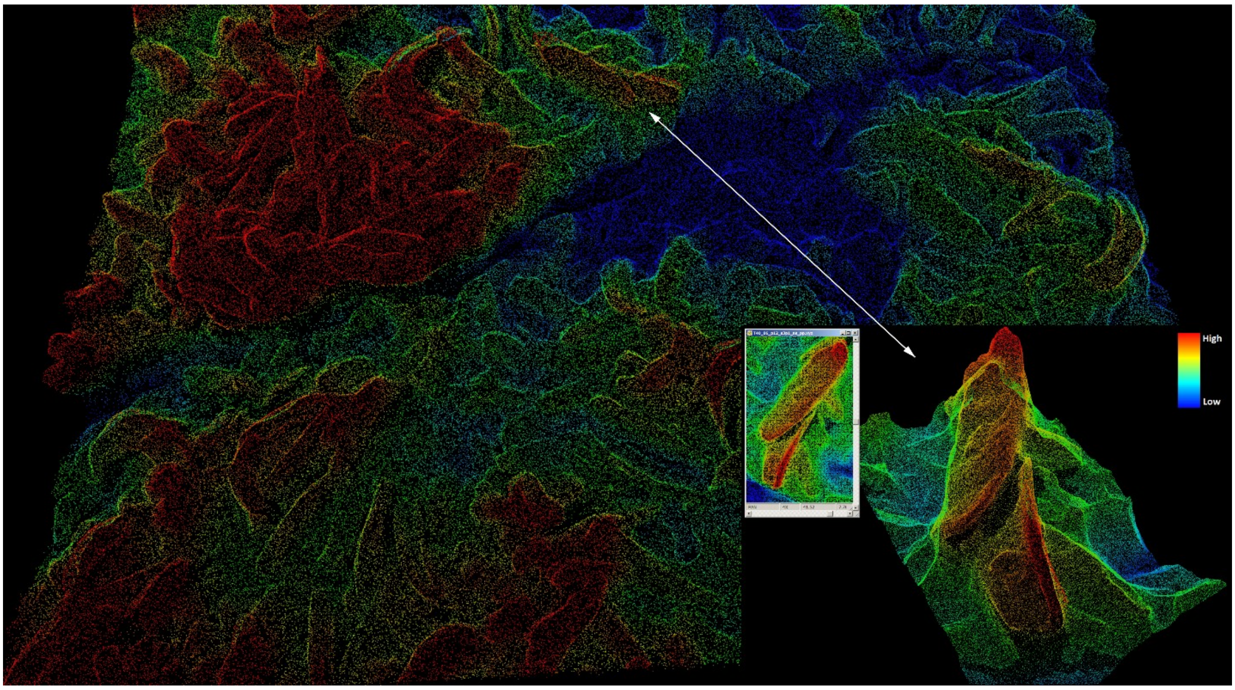

Figure 9: High-resolution 3D point cloud of an area of 3 m × 2 m showing the faults (blue region) crossing the shell bed and two shells (insert). Figure is originally published in Djuricic et al. (2016a).

3.1.7.2. The sub-mm resolution point clouds

The sub-mm resolution point clouds were provided for nine selected specimens from the collections of the Natural History Museum using close-range laser scanning technology. They vary in size and four of these shells represent left–right shell pairs of an individual (Figure 42). The data were captured with a measuring arm (METRIS MCA, 3600 M7: Metrology 7-axis) at operational range up to 1 m (Figure 10). A hand-help triangulation laser scanner (a laser plane and a camera) was mounted at the end of two arms of fixed length with flexible joints. The laser scanner takes measurements with a maximum scan rate of 80 stripes per second with a strip-width of about 200 mm; the camera has a resolution of 1000 dots per strip. The scanning strategy was to scan the single shell part wise and then to combine parts into the final shell model. In the first step, more than half of each shell was scanned and in the second step the other half. The overlap between both parts was more than 70%, which was sufficient for successful registration of the scanned parts. During this registration process, the geometric transformation is determined, which puts the two 3D laser point clouds together based on the points in the overlapping part. This procedure is done using the iterative closest point (ICP) algorithm. The resulting point cloud is analyzed in order to reduce noise and thus improve the surface description. Outliers (wrongly determined points not on the surface) were manually eliminated. Additionally, the raw point cloud (over 1.5 million points per shell) was uniformly sub-sampled to allow interactive handling. The final resolution is better than 0.18 mm (i.e., around 25 points per mm^2).

The point clouds from each shell have been processed individually in order to create the closed mesh model of oyster shell (Figures 10 and 42), and if there were areas with small holes, then they were closed by interpolating a surface in those parts. On the closed mesh models of oyster shells used for volume computation, quality computation and topology measures are performed. Approximating the volumes of oyster shells in automatic way is supported by algorithm for fast and accurate computation of polyhedral mass properties (Mirtich, B., 1996). It uses volume integrals based on triangulation method to efficiently an accurately compute the needed volume data. Since the oyster shell mesh model is given as union of triangles, the center of mesh was found (centroid). Connecting each triangle to the centroid, the object is simplified to tetrahedrons. Sum of the volume of tetrahedrons gave the polyhedron volume.

Figure 10: 3D capturing of the individual oyster shells using ScanArm laser scanner (METRIS MCA, 3600 M7).

3.1.8. DSM Generation

Surface models may be derived in the form of a regular grid. The digital surface model (DSM) describes the top surface of the terrain (Figure 11). The regular DSMs of the oyster field, rather than the unstructured point clouds, are appropriate in this stage of the work to obtain the relief of the reef surface—estimating concavity, convexity, or flatness of the locally selected neighborhood region. Detailed high-resolution (millimeter) surface estimation allows analysis of the surface model for features at the centimeter to decimeter scale (Hodge et al., 2009a; Bertin et al., 2016). However, concerning our application, work with point clouds will be used in future research. Because the oyster reef surface includes overhangs, not all details can be maintained when converting from the point cloud to a scalar-valued function (2.5D representation) parameterized over the reference plane. In areas of overlap, the uppermost surfaces were chosen to be represented in the height model, as they were always scanned, whereas the lower surfaces were not necessarily scanned due to occlusions. The points below overhangs were excluded by using point-cloud processing on a cell basis. In cells of 1 mm × 1 mm, the point with the maximum height value was included in the interpolation process. The interpolation method was moving least squares (Lancaster and Salkauskas, 1981), with a tilted plane used as the surface model and interpolating the eight nearest points at the grid post. Grid spacing was 1 mm. The maximum radius from the grid post to the points was 6 mm, but, with the exception of border areas, the radius was rarely reached by the eight nearest points. Computation was performed using scientific software for orientation and processing of airborne laser scanning data (OPALS; Pfeifer et al., 2014). The number of points for the tiles to be interpolated was 14 million points on average, and this was reduced to 6 million grid posts, excluding the overlapping area. The digital surface model and corresponding hill shade data are publicly available at PANGAEA (Djuricic et al., 2016b).

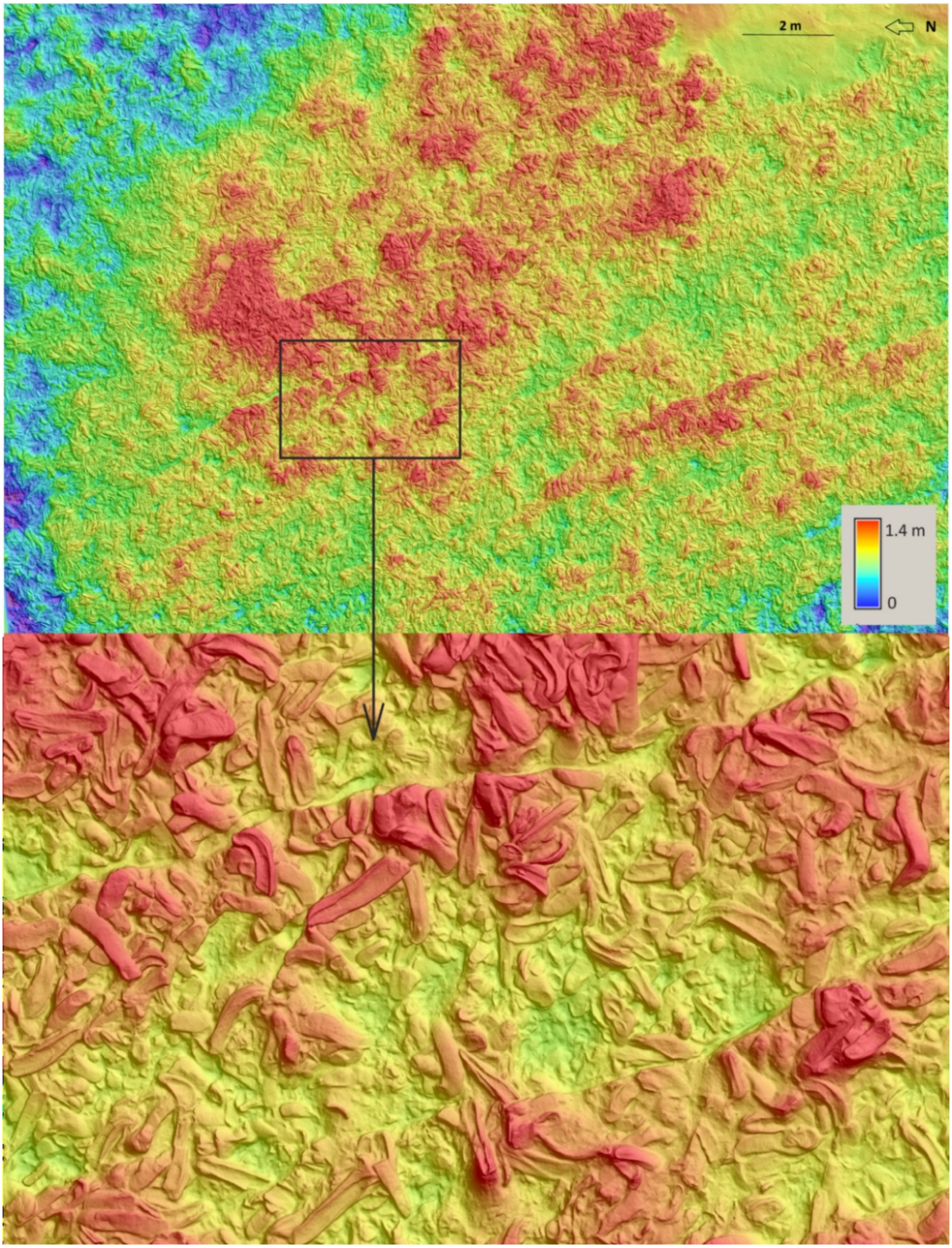

Figure 11: Digital surface model (DSM) hillshaded and color-coded model by height in the local analysis coordinate system (LACS) (red colored pixels representing high areas to dark blue pixels as low areas). Figure is originally published in Djuricic et al. (2016a).

3.1.9. Orthophoto

Texture is assigned to the DSM for more realistic visualization of the oyster reef. With the knowledge of exterior and interior orientation of the recorded images that have been computed by the bundle block adjustment, it was possible to project the RGB information onto the DSM surface, resulting in an orthophoto (OP). In total, 300 individual images with a nominal ground resolution of ~0.6 mm per pixel were used in the OP generation process. The high-resolution OP has a pixel size of 0.5 mm. A radiometric correction (contrast and brightness adjustment) was applied on the images to minimize the remaining influences of artificial lighting, while enhancing contrast by histogram stretching. Thus, the image colors do not appear natural, but they are optimized for visual interpretation in the context of scientific paleontological analysis (Figure 12). The 3D distance between any single DSM point and the camera projection center (depth) was in the range of 2.4–3.6 m, due to reef topography. The orthophoto data are publicly available at PANGAEA (Djuricic et al., 2016b).

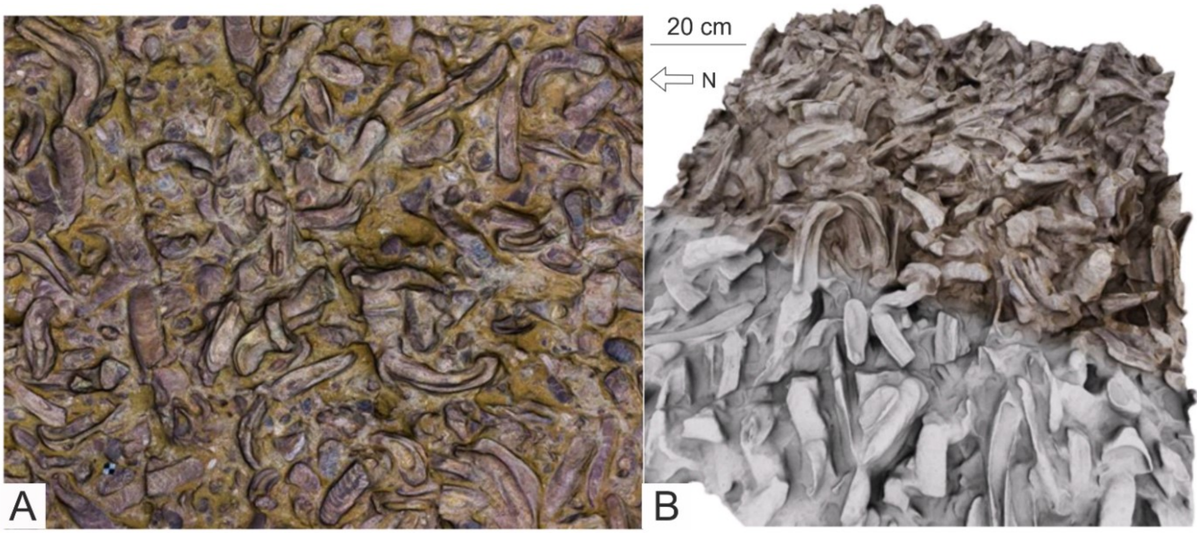

Figure 12: (A) Orthophoto of a contrast- enhanced photo mosaic, overlain with a shaded relief derived from the 3D model (2 m × 1.6 m). (B) Oblique view of the high-resolution 3D model (lower: shaded digital surface model; upper: texture). Figure is originally published in Djuricic et al. (2016a).

3.1.10. Data management

The large data volume, 50.3 GB, required piece-wise processing of the data. Therefore, the data were organized into 81 rectangular tiles, with 2–17 million points per tile (110 MB to 1 GB). In total, 29 tiles are in a range from 110 MB to 500 MB; 21 tiles are in a range from 500 to 900 MB; and 32 tiles are in a range from 900 MB to 1GB. Not all of the 81 tiles are covered entirely with shells; some also contain plain sand areas. The area covered by shells and visible from the scan positions is 367 m^2. The tiles were defined with an extension of 2.1 m (east-west) by 3.1 m (north-south). An overlap of 5 cm (i.e., 10 cm in total) was chosen to avoid border effects during processing, thus resulting in 81 tiles in a grid structure, with a starting point xo = 30 m, yo = 0 m, and the grid offset 3 m in Y and 2 m in X.

3.2. Reference data

For automated analysis of the oysters in the reef, the detection of individual objects is necessary. For the purpose of evaluation of our method, the automatic detections need to be compared against corresponding reference data. Therefore, reference data section presents collection of the object outlines and design of database based on object attributes.

Reference data for object delineation was obtained manually for 10,284 objects. The majority of objects represent *Magallana gryphoides*, which is also the largest species found on the oyster reef. It is up to 60 cm long, according to data analysis by Harzhauser et al. (2015). The brownish and massive calcitic oyster shells are represented exclusively by disarticulated single valves. Expert knowledge is required to detect and outline the individual shell correctly and to determine its parameters—species; level of overlap; shell side (left, right, unknown); orientation (convex side up/down, not known); fragmentation (complete, low, moderate, high); and tile number, see Table 4. Digitization of the validation data was performed manually in ArcGIS, producing vector data stored as shape files. The fastest digitization was achieved with the shaded relief of the DSM as the bottom layer, a semi-transparent orthophoto superimposed onto it, and the previously digitized outlines on the topmost layer. One row and one column of tiles were digitized manually (Figure 13); these 13 tiles form a cross in the center of the oyster reef and allow computing gradients based only on reference data.

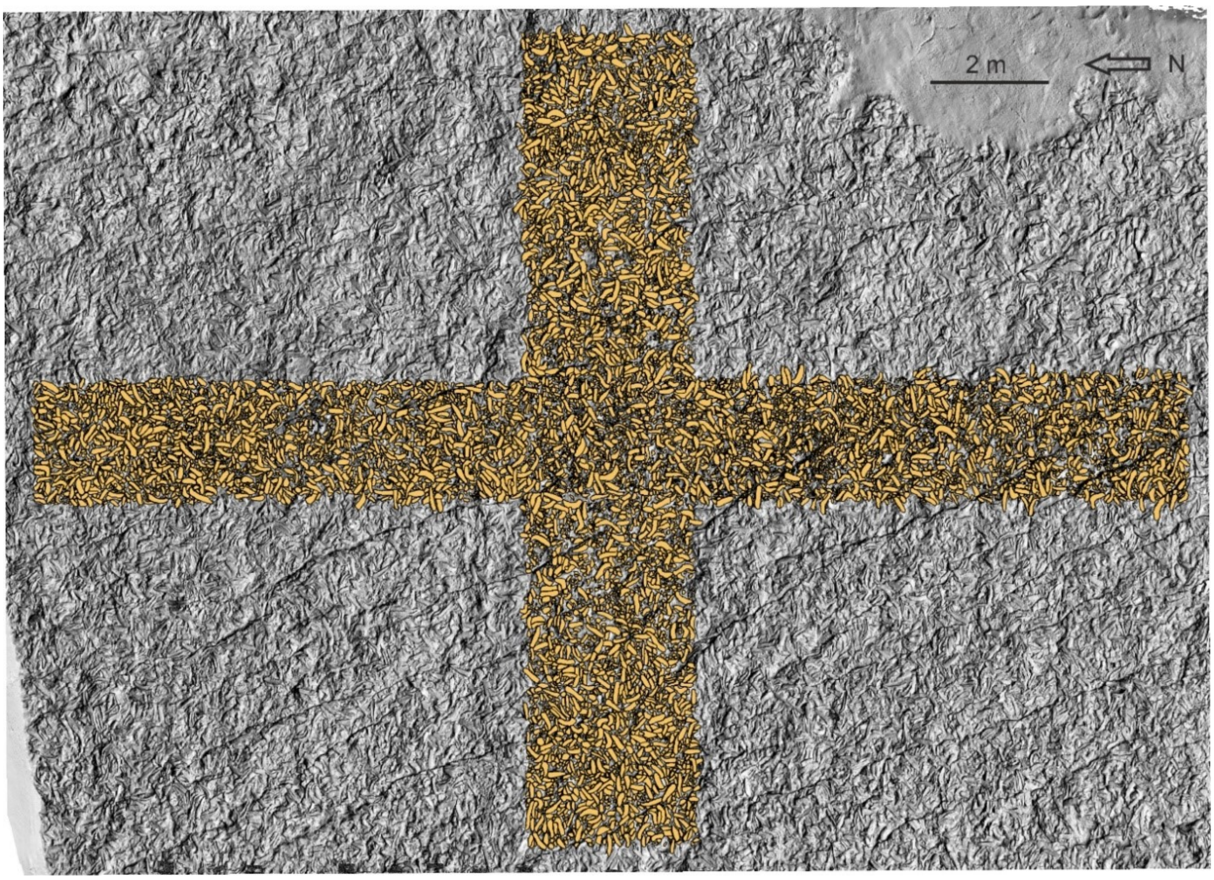

Figure 13: Overview of manually defined outlines (dark yellow) of 10,284 individual objects for the selected reference areas (covering the central, upper, and lower parts and left and right sides of the reef). Figure is originally published in Djuricic et al. (2016a).

Table 4: The list of database attributes, their data type, range of values and unit. Table is originally published in Djuricic et al. (2016d).

Name of attribute	Data type	Range of values	Unit	Additional explanation
ID	integer	2 bytes, positive numbers	/	Number of fragments expected to reach: 2^16~65536
Level	integer	3 bit, positive numbers	/	Number of overlaps that can occur on the reef 1, 2, 3, 4, etc.
ID secondary (IDs)	integer	2 bytes, positive numbers	/	IDs contains a possible pair of broken shell.
Taxon	text (length 30)	Key list: i) Magallana gryphoides ii) Ostrea digitalina iii) Pecten. iv) Venerupis v) Perna vi) Gastropod vii) Fragment - unknown	/	Presents the name of a species, mostly oysters (i and ii), but database contains other species as well (iii-vii).
Position	text	Key list: i) interior – convex down ii) exterior – convex up iii) unknown	/	Applies only to oysters.
Side	text	Key list: i) left ii) right iii) unknown	/	It does not apply to all specimen but only to oysters.
State of specimen	text	Key list: i) high fragmented ii) moderate iii) low iv) complete shell	/	Presents the stage of fragmentation.
Length 2D	decimal number, precision 4, scale 2	Positive numbers	cm	The 2D length is measured along the specimen based on projected shell outline.
Length 3D	decimal number, precision 4, scale 2	Positive numbers	cm	The 3D length is measured along the specimen including surface curves and roughness.
Area	decimal number, precision 4, scale 2	Positive numbers	cm^2	Area is calculated based on shell polygon defined by shell boundary.
Yaw angle *(normal axis)*	decimal number, precision 4, scale 2	Range from 0-180 clockwise from north (0) to south (180)	°	Yaw axis presents an axis drawn vertically in respect to shell top surface, and it is perpendicular to the other two axes.
Pitch angle *(lateral axis)*	decimal number, precision 4, scale 2	Range from -90 to +90 where 0 = horizon, +90 = straight up and –90 = straight down	°	Pitch axis is an axis running from the left to right side of commissure plane, and goes along the shell width.
Roll angle *(longitudinal axis)*	decimal number, precision 4, scale 2	Range from -90 to +90 where 0 = horizon, +90 = full roll right and –90 = full roll left	°	Roll axis is defined as an axis drawn through the body of the shell from oyster hinge to the distal shell margin.

3.3. Individual shell detection

A major goal of this study is developing a method for the automatized detecting and counting of individual shells. Mature *Magallana* valves have a surface area ranging between 2000 mm^2 and 60,000 mm^2 in this geological exposure, while juvenile or fragmented specimens can be smaller. Specimens with the convex side facing upward have a rough surface and are distributed over the entire reef. A single *Magallana* valve typically has a thickness of ~25 mm, often elevating the top surface of the shell entirely from the reef. To detect those specimens, a measure of convexity was targeted; specifically, openness was computed for each grid point (Figures 14, 15).

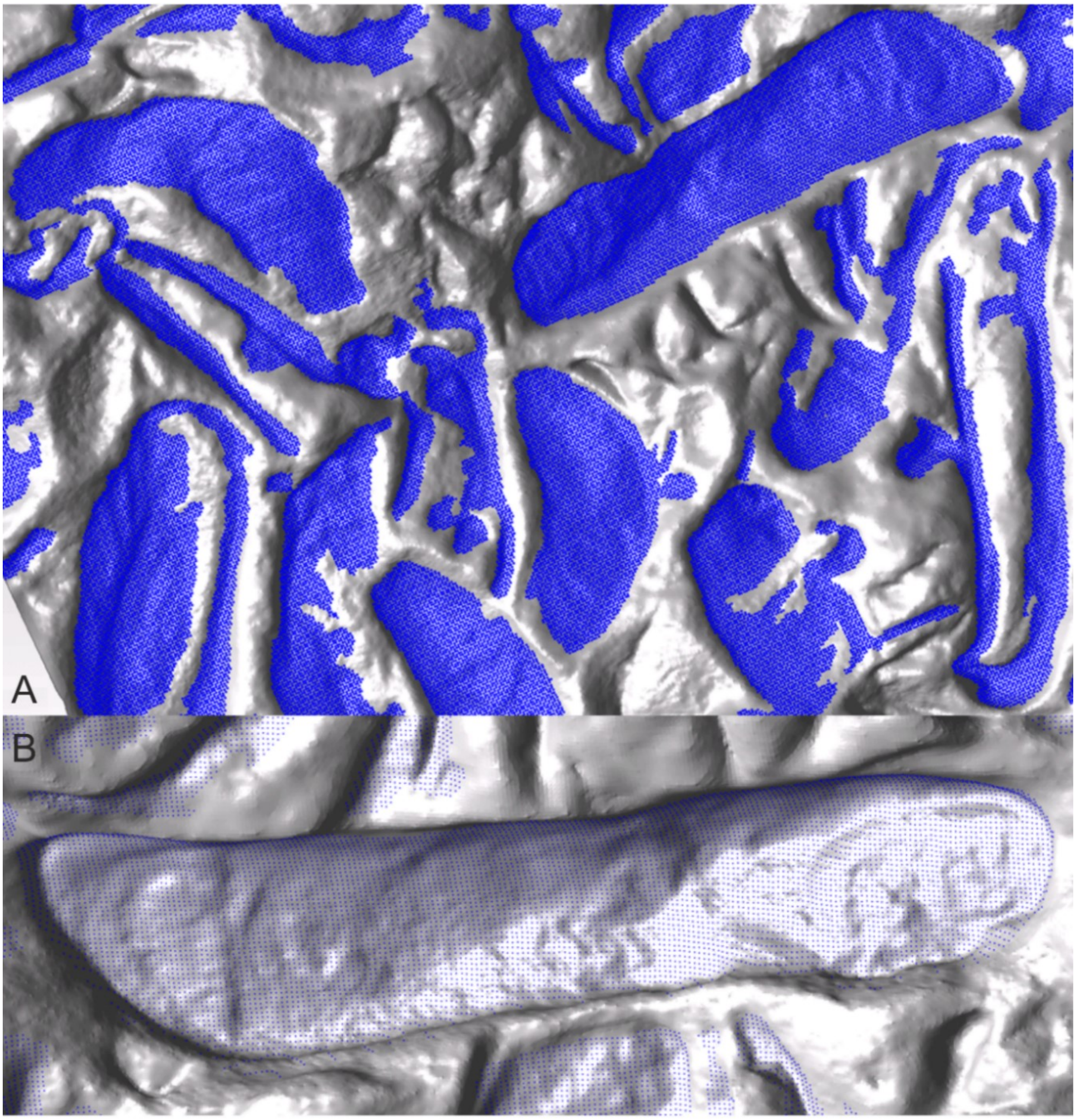

Figure 14: (A) Surface model overlain with the 3D point cloud of detected convex surfaces (blue); (B) detail of one complete convex-up oyster valve. Figure is originally published in Djuricic et al. (2016b).

The aim of the openness feature is to provide a measure of visibility of the neighborhood from the viewing point. It includes all surrounding points that are in line of sight with that viewing point and excludes points that are blocked by local terrain or any obstacles. It was introduced by Yokoyama et al. (2002) as a cone-fitting approach to measure the opening angle of a cone centered at a grid point and constrained by the neighboring elevations within a specified radial distance (Figure 15). It is basically a convexity/concavity measure calculated from local terrain profiles in principal compass directions (Mandlburger et al., 2009). In most cases, that measure works well in distinguishing convex surfaces from the rest of the terrain. There was a further investigation to find which size of neighborhood is optimal for analysis of the variation in the rougher surfaces. Thus, the feature provides an angle of the fitted cone, which is derived for each point, with a preset kernel (k) radius (e.g., neighborhood size is: 2k + 1; k = 1 mm, 3 mm, 5 mm, . . . , 27 mm). Openness is expressed in two models—positive for concave features and negative for convex features.

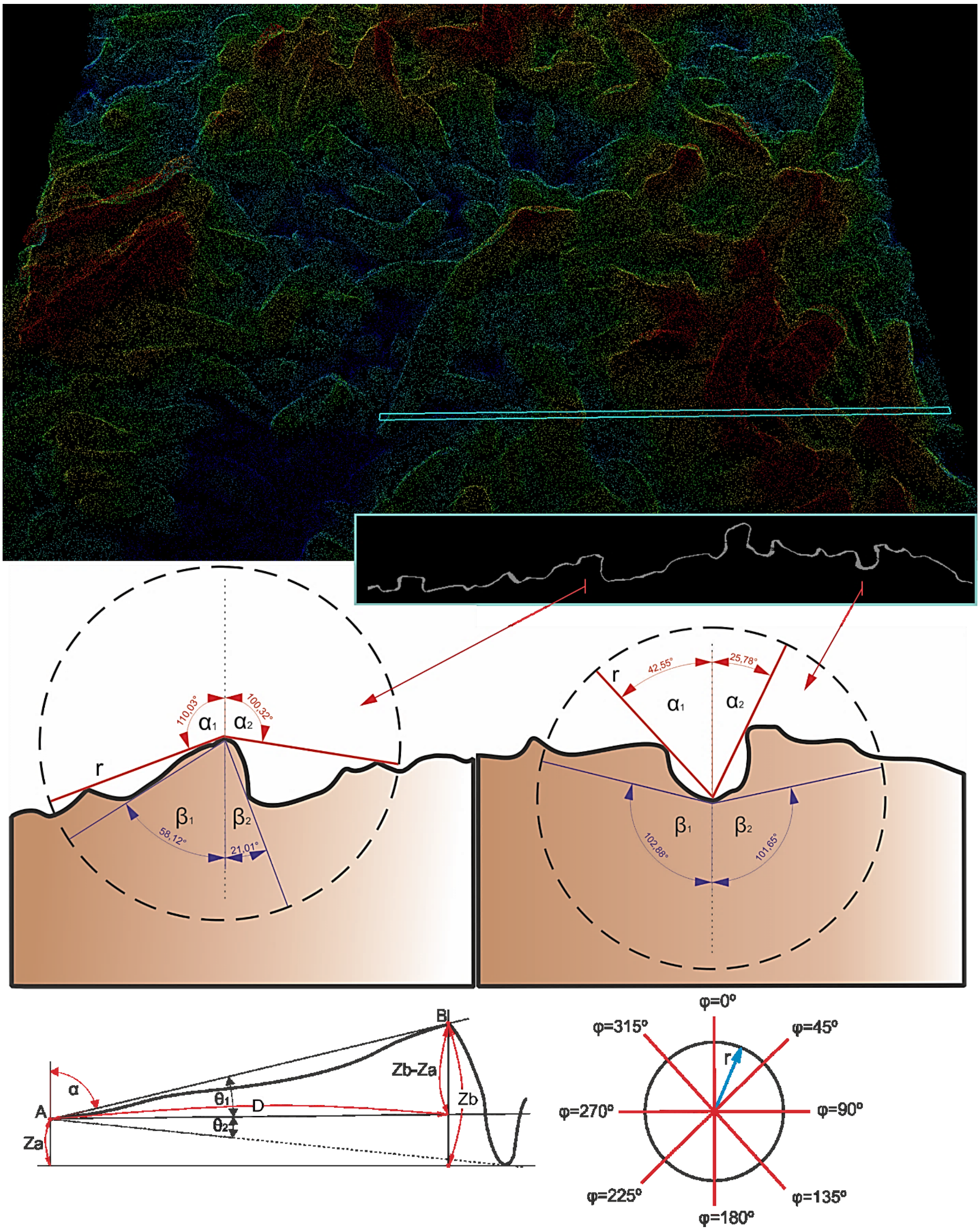

Figure 15: Profile example of the oyster reef 3D point cloud, where openness features are illustrated (left: convex = negative openness; right: concave = positive openness). Figure is originally published in Djuricic et al. (2016b).

The following quantities are introduced to compute openness (see also Figure 15):

A (Xa, Ya, Za)—reef view point;

B (Xb, Yb, Zb)—point restricting the view in the neighborhood of A due to topography;

C (Xc, Yc, Zc)—any point in the neighborhood of A;

D — horizontal distance between A and B;

φ — azimuth angle (0°, 45°, 90°, . . . , 315°);

r = 2k + 1 — kernel radius (i.e., neighborhood size) in pixels;

θ — elevation angle between reef view point (A) and each grid point (B) located along four sections (axis parallel and diagonal; see Figure 15) with specified azimuth angle j and kernel radius k;

α — zenith angle at a reef DSM grid point calculated along one of eight azimuths j and specified kernel radius k;

$\widehat{\boldsymbol{\alpha}}$ — mean of angles along r;

n — number of section points dependent on k;

point B is the point that has the minimum a for each section.

$$\mathbf{D} = \sqrt{(\mathbf{Xa} - \mathbf{Xb})^2 + (\mathbf{Ya} - \mathbf{Yb})^2}\ .\ (1)$$

$$\boldsymbol{\theta} = \boldsymbol{arctan}\frac{(\mathbf{Zb} - \mathbf{Za})}{\mathbf{D}}\ .\ (2)$$

$$\boldsymbol{\alpha} = \mathbf{90}^{\circ} - \boldsymbol{\theta}_{\mathbf{1}},\ \text{if Za < Zb. (3) or}$$

$$\boldsymbol{\alpha} = \mathbf{90}^{\circ} + \boldsymbol{\theta}_{\mathbf{2}},\ \text{if Zb < Za. (4)}$$

$$\widehat{\boldsymbol{\alpha}} = \frac{\sum \boldsymbol{\alpha}}{\mathbf{n}}\ .\ (5)$$

$$\overline{\boldsymbol{\alpha}} = \frac{\sum_{i=1}^{8} \widehat{\alpha}_{r}^{\varphi}}{\mathbf{8}} = \frac{(\widehat{\alpha}_{r}^{0} + \widehat{\alpha}_{r}^{45} + \cdots + \widehat{\alpha}_{r}^{315})}{\mathbf{8}}\ .\ (6)$$

The applied workflow is based on a raster of negative openness, i.e., a raster f(x,y). The threshold t is set to zero, and values are converted into binary values (blue and white in Figure 16D), where value 1 is assigned to foreground and 0 refers to background, i.e., g(x,y).

$$g(x,y) = \begin{cases} 1,\ \text{if } f(x,y) < t \\ 0,\ \text{if } f(x,y) \geq t \end{cases}\ .\ (7)$$

Single pixels and small areas are excluded for further analysis based on a minimum area threshold (Figure 16E). Mathematical morphology is applied to obtain smoother outlines and to fill in small gaps (few pixels). A majority filter replaces the neighboring pixel values, depending on the size of the kernel (Figure 16F); for example, m = 1 (3 × 3 mm), m = 2 (5 × 5 mm), up to m = 6 (13 × 13 mm). Further processing includes connected-components analysis on the basis of the 8-neighborhood array. Pixels in the neighborhood are connected in regions. Each component obtains a unique ID.

Figure 14A shows automatically detected convex surfaces overlapping the mesh model of the oyster reef. In the first step, the area of connected components is incompletely filled due to the diversity of concavity and convexity. To achieve higher completeness detection, a flood-fill operation is performed (Figure 16G). This operation changes connected background pixels (0s) to foreground pixels (1s) and stops when it reaches object boundaries. Correspondingly, the method is applied to the whole data set to assess the applicability of the method to larger areas, and the results are analyzed.

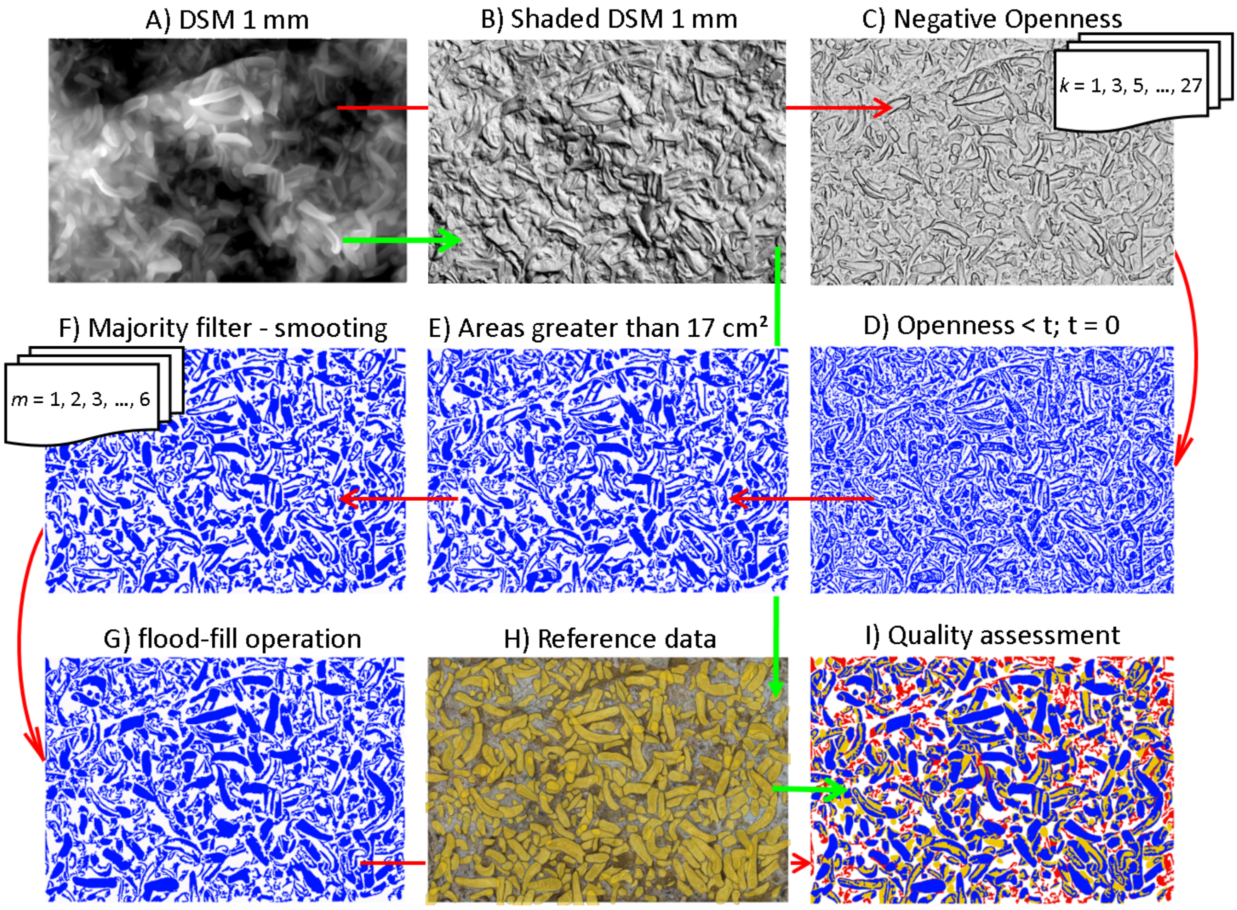

Figure 16: Automated method for individual shell detection shown on portion of data 2 m × 3 m. (A) Generated DSM from 3D point cloud data ranging from black (0) to white (19 cm); (B) Lambert shading of DSM used for interpreting reference data (green path); (C) negative openness derived from DSM for different kernel sizes (red path); (D) binary raster where value 0 is white background and 1 is blue detected object; (E) binary raster after eliminating min. areas; (F) majority filter size m = 6 (13 mm × 13 mm); (G) flood-fill operation; (H) manually digitized individuals overlie orthophoto; (I) quality of detection, see Figure 22A (in Results). Figure is originally published in Djuricic et al. (2016b).

3.4. Oyster shell central line extraction

The linear approximation of real objects can be simplified representation of complex object forms such as a large fossil oyster shells. We used closed boundaries of complete (not fragmented) shells as input for the method for automatic central line determination. Oyster shell boundaries in 2D were extracted manually from digital surface models and from orthophotos. *Magallana gryphoides* shows a very broad range of morphologies, ranging from elongate shells to strongly curved and sigmoidal shapes (Figure 35). Therefore, measuring shell length as a straight line, as done in other extant and fossil shell species, is inadequate. To overcome this problem, we evaluated shell length based on the 3D center line, which aims for capturing the real shell length as far as possible. Here it is an imaginary curved line spanning the maximum length of the shell. The advantage of this method is that the center line will approximate the “real” lengths of the curved and irregularly shaped shells much better than any manual attempt in the field. For the automatic determination of the center line we used the shell boundary, which comprise about 1000 points on average. For easier calculation the outline point number was reduced to 100 and then filtered to points with close to even spacing. The 3D central line extraction algorithm includes following workflow of seven steps:

1: Constrained Delaunay triangulation between the fossil shell boundary points and formation of Voronoi diagram;

2: Extraction of Voronoi vertices within the oyster shell boundary and construction of a connected graph from them;

3: Reduction of the graph to the longest path via Dijkstra's algorithm;

4: Central line extension to the shell boundary. End nodes are inspected if this fulfils continuity conditions (see below: as a condition for accepting an elongation or not is given further below);

4a: If a node fills the conditions, then the central line is extended from the node to the oyster shell boundary by fitting a line.

4b: If a node does not fulfil the conditions, then travel the central line to the nearest junction point and check for continuity. After a junction point is found, extend the central line from that node to the oyster shell boundary with line fitting.

5: The extended longest path is smoothed by an adjusting cubic spline curve;

6: 3D clipping of the point cloud using oyster boundaries and assigning corresponding attributes;

7: Forming of 3D central line by imputing the height value of the nearest clipped point to every central line node.

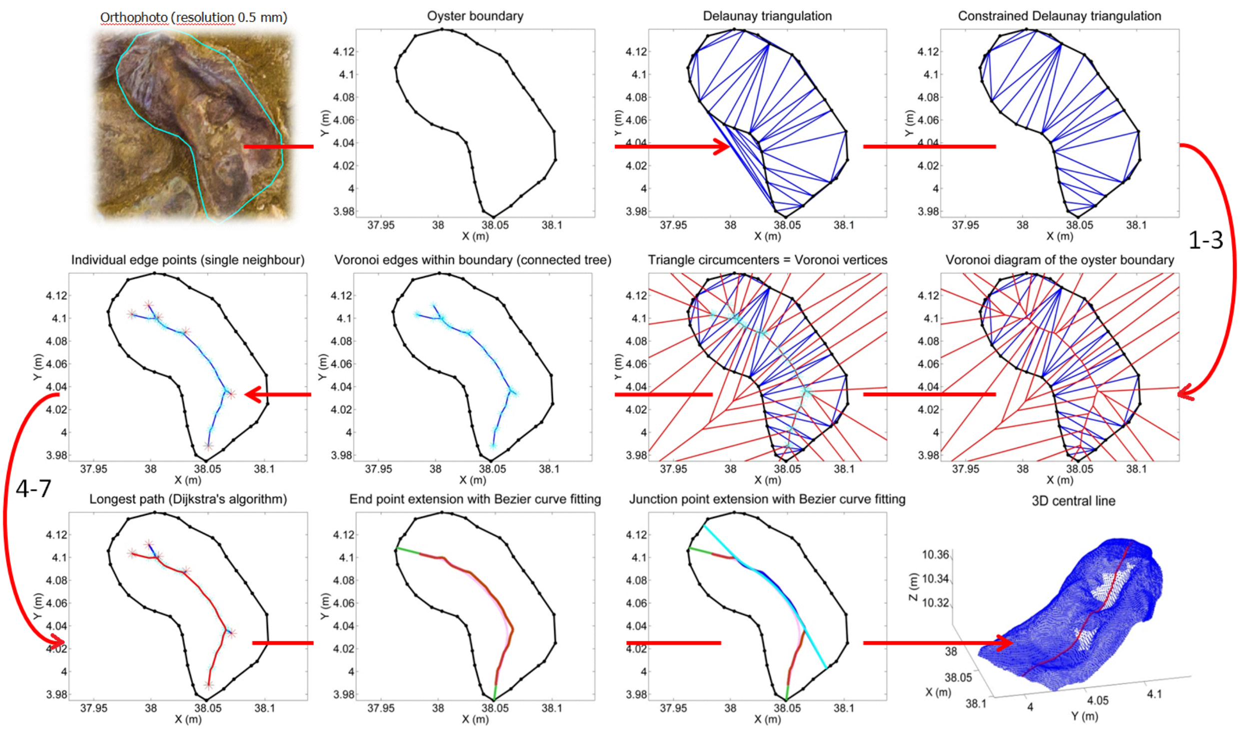

Figure 17: The automatic process of the central line detection. Top row: step 1; Middle row: steps 1-3; Bottom row: steps 4-7. Figure is originally published in Djuricic et al. (2016d).

The mathematical definition of the 2D shell central line (steps 1-3) is the longest line which connects neighbouring Voronoi vertices inside the oyster shell boundary. The vertices were obtained from the constrained Delaunay triangulation (DT) of the boundary points (outline segments as constraining edges). To find the medial axis transform for the oyster outline, the Voronoi diagram (VD) was formed. Here, the Voronoi vertices within the oyster boundary are shown with cyan colour. By taking the edges between the Voronoi vertices within the boundary, we get a medial axis transform (MAT) for the oyster (Blum, 1967). The MAT is also a connection map between the Voronoi vertices. To determine the longest path in the connected tree (Figure 17), the edge points (red) in it were selected, i.e. points with only a single neighbor. The longest path and its length were determined by applying Dijkstra's algorithm (Dijkstra, 1959) between all edge points in the connected tree. Furthermore, we looked for the potential intersections between the longest path end points and the border outlines by checking conditions: if beginning/end ratio threshold for the central line (of total length) and opening angle threshold were satisfied, the line is extended to boundary intersection. The junction points need to be far away from the oyster beginning/end point less than 30% (or more than 70%) of the total length of the central line; the opening angle of the junction point and two neighbourhoods surrounding points (previous and further) has to be less than 155 degrees. If both conditions are satisfied the path is extended to the outline by intersection. Otherwise, the end point was replaced with a junction point on the smallest opening angle and the line was then extended to boundary. Moreover, cubic Bézier curve is fitted to the points of the longest path. The curve is used to smooth the path model and to remove wiggling effect (Figure 17).

In our implementation it is assumed that the central line represents the largest dimension between the oyster beginning (part with hinge) and end (part with muscle), and that it is always in the middle between the shell borders independently of convex up or convex down shell positions (see Figures 35 and 40). The next operation includes embedding of the 2D central line into the corresponding 3D point cloud. That requires a relevant area of the original 3D point cloud for 3D central line extraction. Therefore, clipping of original point cloud is performed by excluding points that are outside of the shell boundary. Subsequently, assigning the third component Z to the 2D central line points is achieved by running an N-D nearest point search for every point using Quickhull algorithm (Barber et al., 1996). Finally, the closest 3D point is adopted as the most appropriate for 3D Euclidian distance calculation. The 3D central line implies tilt of the shells and curves along the top shell surface. The curves are caused by local slope change on the shell surface or by change of boundary shape which the central line follows.

3.4.1. Evaluation of automatic central line extraction based on reference data

The shell central line has its biological, but also mathematical definition. The biological definition of the shell central line is an imaginary curve of the commissure plane, connecting oyster hinge with the distal shell margin, striking parallel to the maximum concavity zone, through the soft parts of the bivalve. It is roughly equidistant to the lateral shell margin, which may be distorted by the laterally projecting growth lamellae developing occasionally on the exterior shell surface. The mathematical definition of the shell central line is dependent on the 2D geometry of shell outlines, and it is not affected from surface topology. It is the longest line which connects neighbouring Voronoi vertices inside the oyster shell boundary, obtained from the constrained Delaunay triangulation (DT) of the boundary points (outline segments as constraining edges).

The reference central line follows the biological definition and the automatic central line extraction follows the mathematical definition, being therefore not completely congruent with each other. Therefore, a method for evaluation of an estimated central line is implemented based on defined criteria:

i) The length differences;

ii) Centering of the line – exactly or approximately to within a specified error;

iii) Visual appearance.

Oyster shell central line extraction may be used for various biological or paleontological applications and interpretations, and thus different evaluation measures may apply. We describe two measures. With these measures we differentiate between extraction capability and extraction accuracy. The first level of evaluation has to satisfy criteria of extraction capability and then extraction accuracy may be relevant for final evaluation. Therefore, we give priority to the length and compare the automatically extracted line with corresponding reference length.

3.5. Oyster age class derivation

This section presents the method for oyster age class derivation through the tasks given in the following sub-sections. In section 3.5.1 the volume computation method for individual fossilized shells is summarized. It uses algorithm of Mirtich (1996) to derive volumes of sub-mm resolution mesh shells models. Section 3.5.2 presents the extension of volume computation to the larger data set of the reef. Section 3.5.3 proposes a growth model for purposes of oyster age class derivation. Section 3.5.4 presents improvement in shell density estimation based on layer analyses of left and right shell cross sections. Ana Puttonen conducted a research in Section 3.5.1 and research in sections 3.5.2 – 3.5.4 is led by Mathias Harzhauser.

3.5.1. The volume of individual shells

The volume of nine individual shells was determined using close-range laser scanning technology, which provides high resolution models with sub-mm resolution. For volume calculation the point cloud has to be transformed into a closed mesh. Remaining holes, non-manifold surfaces and additional not connected components were identified and removed. Finally, the surface area of the mesh and its volume were computed using the algorithm of Mirtich (1996).

3.5.2. The volume of shells on the reef

Beside the nine measured shells from the collections of the Natural History Museum, the volume of shells which can not be removed from the site and scanned from both sides in order to generate the closed mesh model, it is computed as approximation based on empirical volume data (3.1.7.1. and 3.5.1.). A relation between central line length and volume was deduced. The largest shell measured was 406 mm long but no empirical volume data are available for larger shells, because these cannot be removed from the site. Therefore, the von Bertalanffy equation would not be applicable for shells larger than ∼40 cm. Consequently, we chose a logistic function to approximate the inverse von Bertalanffy equation:

$$\vartheta = \frac{3.2439E06}{1 + 118.86e^{-0.0099889\,SL}}, (8)$$

where v is the volume in mm^3 and SL the central line length in mm (Figure 18). The equation was applied to data set of 1121 shells laying on the oyster reef.

3.5.3. Growth model

The growth model derivation includes the growth curves calculation of extant *Magallana* species. They are routinely calculated with the von Bertalanffy equation (von Bertalanffy, 1934). The equation is

$$SL_t = SL_{max}(1-e^{-k(t-t0)}), \quad (9)$$

where SL_t is shell length at time t, SL_{max} is the asymptotic shell length, t_0 is the size at time 0, and k is a rate constant. Herein, we used the length of the central line of each shell as SL_t as this measure captures the real growth length of the partly strongly curved or sigmoid specimens. For SL_{max} we used the size-to-age data of the 78 cm long shell, which is the largest individual known so far.

3.5.4. Shell density

Shell density is estimated by taking in consideration the ratio between chalky and foliate layers. The calcitic *Magallana*[5] shells consist of two structures: thin but densely spaced foliate layers separated by thick layers of light-weight chalky material (Stenzel, 1971; Higuera-Ruiz and Elorza, 2009). This fast growing structure is interpreted to be a major adaptive advantage of *Magallana* to impede drilling predation and to prevent from sinking in the soft bottom (Seilacher, 1984; Chinzei, 1995; Kirby, 2001; Vermeij, 2014). In fossil shells the chalky layer is completely recrystallized and has the same density as the foliate layer. Nevertheless, it is optically easily recognized by its lighter color and the nearly opaque appearance. A polished longitudinal section of an articulated *Magallana gryphoides* shell (providing data for left and right shells) was scanned and the ratio between both shell structures was quantified by image analysis (Figure 47). This method is only an approximation to the true value, as the ratio may vary locally (Durve and Bal, 1960; Chinzei, 1995), but it is clearly an improvement compared to former studies that used only linear transects or sectors within the shell (Durve and Bal, 1960; Chinzei, 1995; Kirby, 2001).

3.6. Oyster shell orientation

A new approach is developed to assess data on 3D-orientation of elongated objects in geoscience by applying non-destructive, high-resolution TLS. Hence, this study automatically derives the three angles of orientation of an oyster shell to better explain transport direction or presence of imbrication. For this, developed method calculates the angles of rotation from the 3D point cloud data representing the oyster shell. The reference boundary of each specimen (= shell margin) are used to assign the respective 3D points to the object. The high number of data points describing each specimen is a major advantage compared to 2D approaches or the "three points per specimen"—approach as used by Mayrhofer et al. (2016).

The shells of *Magallana gryphoides* have an unusual big size (compared to present species). The largest specimen on the shell bed attains 602 mm in lengths (with a mean of 237 mm). Herein, we focus exclusively on 1904 shells of the oyster *Magallana gryphoides* defined in the

[5] *Crassostrea gryphoides* (Schlotheim 1813) has been moved to the genus *Magallana*.

database with attribute "complete" or "low fragmented", i.e., having only minor damages that do not obscure natural shell shape. Moderately fragmented to strongly fragmented shells, representing less than half of the original length, are excluded as well as shells of other mollusc species. The reason for this selection is the elongate shape of the well preserved oysters, whereas most other objects lack a distinct main axis.

For analyses, the oyster shells are treated as elongated flat elements in 3D space with predictable axes in all three spatial directions: shell length is larger than its width, which is larger than the height. Thus, the length, width, and height axes can be considered as pairwise orthogonal. These three axes are the base to measure rotation angles, following the principles originally used in aerial photogrammetry (Bäumker and Heimes 2002): rotation around yaw (= γ) (normal axis, Z), pitch (= ϕ) (lateral axis, Y), and roll (= ρ) (longitudinal axis, X). The yaw axis represents an axis drawn vertically in respect to the shell top surface, and it is perpendicular to the other two axes. The pitch axis is an axis running from the left to the right lateral sides of the shells (Figure 18), corresponding to the width of the shell. The roll axis is defined as an axis drawn through the body of the shell from the anterior part (= hinge area) to the posterior shell margin, coinciding with the length of the shell (Figures 18 and 19). These axes are represented by the letters X_{ISCS}, Y_{ISCS}, and Z_{ISCS} and the reference frame of the entire oyster reef is defined by the LACS, i.e., X_{LACS}, Y_{LACS}, and Z_{LACS} axes.

We assume that the shells are evenly captured by data points on the exposed shell surface, which exhibits the extension in length and width, thus representing the two larger axes. Note that we define the direction of the axes here. In such a case, the direction of those two axes can be computed automatically, as well as the extent along each of those axes. The third axis is determined by augmenting the first two vectors to a right handed three-dimensional Cartesian coordinate system. We are, furthermore, assuming that the third axis is pointing upwards. With other words, the oyster shells are "lying" and not "standing". This approach does not provide information if the length axis points from hinge to posterior margin or vice versa and does not distinguish between convex-side up and convex-side down positions (= if interior or exterior side of the shell is visible). However, such contextual attributes can be added to the point cloud of each shell and its axes.

Based on empiric data and direct observation, we can postulate that the objects studied are generally lying, approximately flat on the underlying surface, i.e., the shell bed. No chaotic orientation was observed. This means that the length axis coincides approximately with this plane. As start (hinge side) and end (muscle side) of the shell can be provided by paleontological experts, the direction of the length axis can be given in the range of 0°–360°. This introduces additionally to axis direction also axis orientation. The positive X_{ISCS} axis points from the hinge to the muscle (Figure 19). This angle represents the yaw, heading, or azimuth. An azimuth is an angle measured clockwise. The 0° direction is pointing North, the 90° is pointing East, and the 180° direction is pointing South. The rotation around the lateral axis for a flat lying object is 0°. It can be positive and negative (see below). This angle represents the pitch. If it is positive, it means that the positive length axis is pointing upwards. Finally, the rotation along the length axis represents the roll. It can be positive or negative as well. It is positive if the Y-axis is rotated into the direction of the Z-axis (Figure 19). The superior coordinate system is the LACS. It is attached to the shell bed, with the X-axis pointing downwards along the fall line, the Y-axis approximately to south (with a deviation of 3°), and Z-axis upwards (Figure 8).

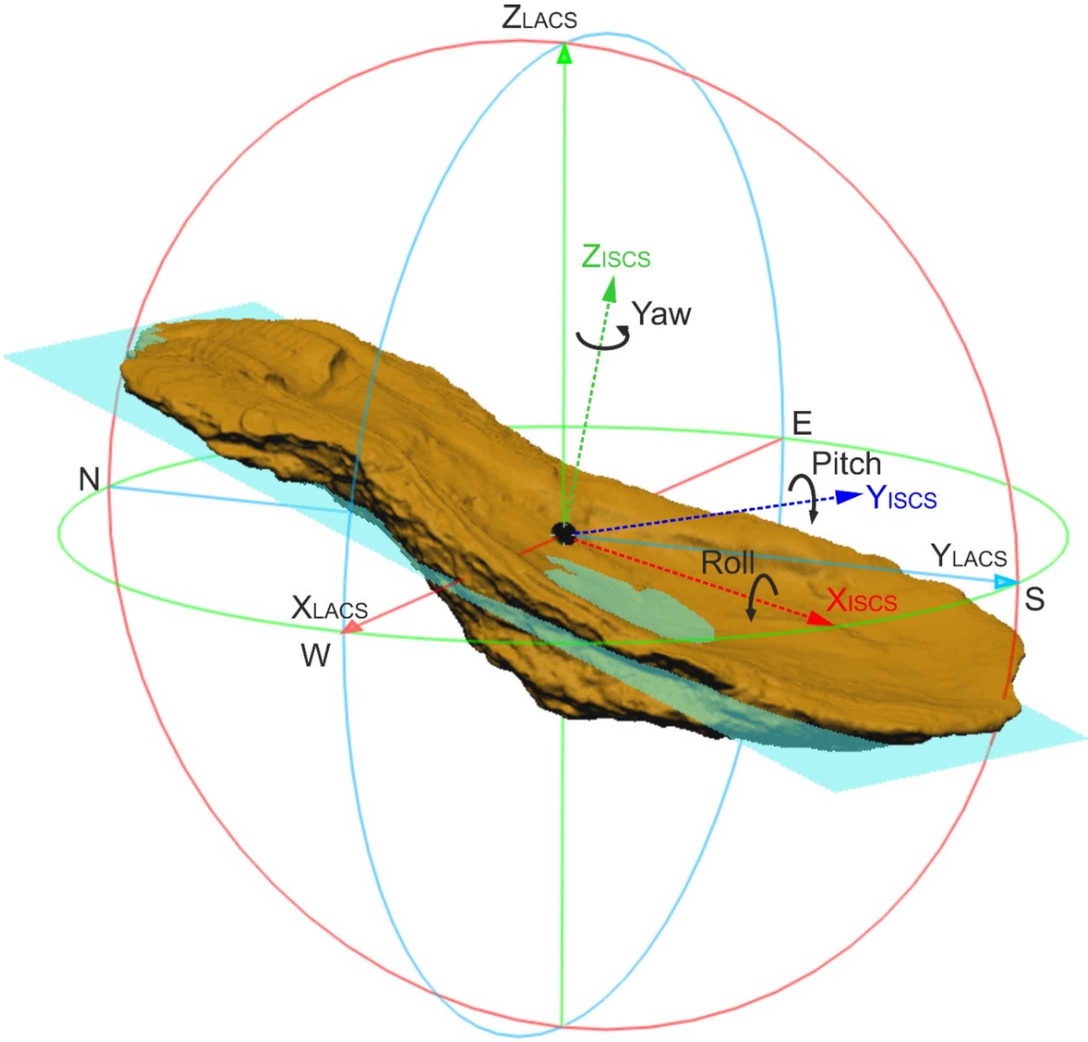

Figure 18: 3D visualization of an elongated and tilted fossil oyster shell with the corresponding individual shell coordinate system (ISCS) and determined rotation directions in respect to the local analyses coordinate system (LACS). Note that positive direction of the X_{ISCS}-axis is pointing from the position, where the hinge was located to the muscle position. Figure is originally published in Puttonen et al. (2018).

The predefined order of rotations around the axes is necessary to define unique rotation angles. The rotation of a shell is described by the sequential rotation around the three axes in the sequence Z_{ISCS}-axis (height axis of the object with the yaw angle γ), Y_{ISCS}-axis (width axis with pitch angle ϕ), and X_{ISCS}-axis (length angle with roll ρ[6]):

$$\begin{pmatrix} \cos(-(90°+\gamma)) & -\sin(-(90°+\gamma)) & 0 \\ \sin(-(90°+\gamma)) & \cos(-(90°+\gamma)) & 0 \\ 0 & 0 & 1 \end{pmatrix} \begin{pmatrix} \cos(-\varphi) & 0 & \sin(-\varphi) \\ 0 & 1 & 0 \\ -\sin(-\varphi) & 0 & \cos(-\varphi) \end{pmatrix} \begin{pmatrix} 1 & 0 & 0 \\ 0 & cos\rho & -sin\rho \\ 0 & sin\rho & cos\rho \end{pmatrix}. \quad (10)$$

[6] Note that ρ is counted mathematically positive, contrary to γ and ϕ.

The point coordinates of the object are formulated as $P_i = (x_i, y_i, z_i)$, i = 1,… n, where the points $p_1 \ldots p_n$ belong to the oyster. The structure tensor T has the second central moments of the point coordinates. It is decomposed into the eigenvalues λ with associated eigenvector υ:

$$T\upsilon_j = \lambda_j \upsilon_j. \quad (11)$$

With sorted eigenvalues λ1 > λ2 > λ3 and associated eigenvalues, matrix A = ($\upsilon_1, \upsilon_2, \upsilon_3$) can be constructed (see below), where the eigenvectors and the individual shell axes are related as $\upsilon_1 = X_{ISCS}$, $\upsilon_2 = Y_{ISCS}$, and $\upsilon_3 = Z_{ISCS}$. The direction of the axes may have to be inverted to follow the orientation as described above (also for the computation of the angles from matrix A).

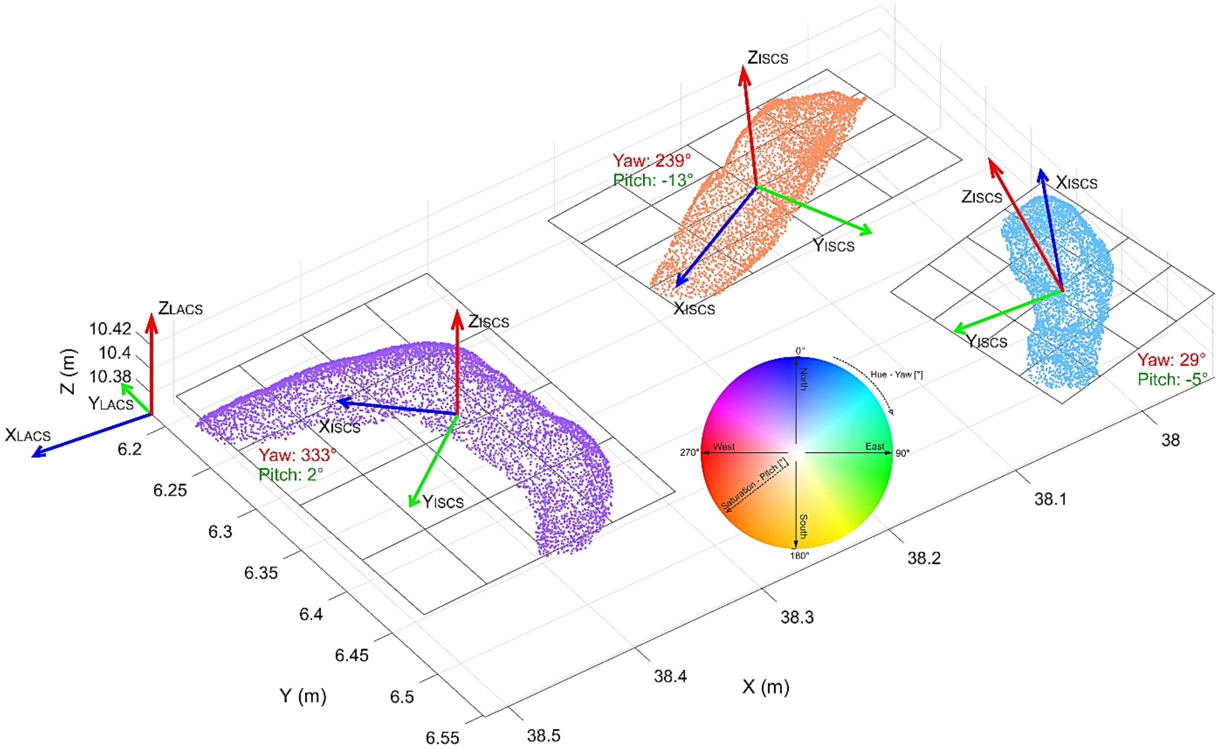

Figure 19: 3D-point clouds of three individual shell examples and their rotations around Z and Y axes. Color wheel coding depends on the angles. Hue encodes orientation angle yaw and saturation encodes pitch angle, while roll angle is not visualized. The color is darker on the places, where the pitch (tilt) is larger or lighter if the shell is approximately horizontal. Figure is originally published in Puttonen et al. (2018).

The matrix (A) of the axes X_{ISCS}, Y_{ISCS}, and Z_{ISCS} is:

$$A = (\upsilon_1, \upsilon_2, \upsilon_3). \quad (12)$$

Here $\upsilon_1, \upsilon_2, \upsilon_3$ are the eigenvectors for the sorted eigenvalues $\lambda_1 > \lambda_2 > \lambda_3$ of the second centralized moments of the 3D points on one shell. In order to uniquely determine angles from the rotation matrix A the orientation of the eigenvectors have to be checked by the following criteria:

i) The determinant of A must be positive, i.e. det(A) = +1. If determinant of A is negative, i.e. det(A) = -1, then A is redefined as A: = -A.

ii) If υ_3 is pointing downwards, i.e. $\upsilon_{3,z} < 0$, then redefine A accordingly:

$$A = (\upsilon_1, -\upsilon_2, -\upsilon_3). \quad (13)$$

iii) Without further context, the orientation of υ_1 cannot be determined and it should be set to point always (e.g.) eastwards. The yaw angle γ is then restricted to [0°,180°]. If, on the other hand, context knowledge allows determining the orientation of υ_1, then γ can be determined in [0°,360°]. This introduces two paths in the method:

iii-a) No orientation, υ_1 points eastwards: Should $\upsilon_{1,x} < 0$, then A is redefined to:

$$A = (-\upsilon_1, -\upsilon_2, \upsilon_3). \text{ (14)}$$

iii-b) Orientation given by context knowledge: Here, the hinge position (start of the shell) or muscle position (approximately the end of the shell) can be added to the data as a descriptive attribute, using, e.g., the oyster central line (Djuricic et al., 2016d). Therefore, the direction of the length axis can be given in a range of 0°–360°. Then verify:

$$\upsilon_{1,2D}^T \cdot \left(\binom{x}{y}_{muscle} - \binom{x}{y}_{hinge} \right) > 0. \text{ (15)}$$

The index *2D* refers to the vector composed only of the *x* and *y* coordinate. If the verification provided a value below 0, then redefine

$$A = (-\upsilon_1, -\upsilon_2, \upsilon_3). \text{ (16)}$$

The matrix of the axes (A) is after these transformations a right handed coordinate system, named the individual shell coordinate system (ISCS, Figure 18). The first axis, i.e. the first column vector, is pointing from hinge to muscle, the third axis, i.e. the third column vector, is pointing upwards.

The rotation matrix

$$\begin{pmatrix} \cos(-(90°+\gamma)) & -\sin(-(90°+\gamma)) & 0 \\ \sin(-(90°+\gamma)) & \cos(-(90°+\gamma)) & 0 \\ 0 & 0 & 1 \end{pmatrix} \begin{pmatrix} \cos(-\varphi) & 0 & \sin(-\varphi) \\ 0 & 1 & 0 \\ -\sin(-\varphi) & 0 & \cos(-\varphi) \end{pmatrix} \begin{pmatrix} 1 & 0 & 0 \\ 0 & cos\rho & -sin\rho \\ 0 & sin\rho & cos\rho \end{pmatrix} \text{ (17)}$$

is simplified to:

$$\begin{pmatrix} cos(90°+\gamma) & sin(90°+\gamma) & 0 \\ -sin(90°+\gamma) & cos(90°+\gamma) & 0 \\ 0 & 0 & 1 \end{pmatrix} \begin{pmatrix} cos\varphi & 0 & -sin\varphi \\ 0 & 1 & 0 \\ sin\varphi & 0 & cos\varphi \end{pmatrix} \begin{pmatrix} 1 & 0 & 0 \\ 0 & cos\rho & -sin\rho \\ 0 & sin\rho & cos\rho \end{pmatrix} =$$

$$\begin{pmatrix} -sin\gamma & cos\gamma & 0 \\ -cos\gamma & -sin\gamma & 0 \\ 0 & 0 & 1 \end{pmatrix} \begin{pmatrix} cos\varphi & -sin\varphi sin\rho & -sin\varphi cos\rho \\ 0 & cos\rho & -sin\rho \\ sin\varphi & cos\varphi sin\rho & cos\varphi cos\rho \end{pmatrix} =$$

$$\begin{pmatrix} -sin\gamma cos\varphi & \sin\gamma\sin\varphi\sin\rho + \cos\gamma\cos\rho & \sin\gamma\sin\varphi\cos\rho - \cos\gamma\sin\rho \\ -cos\gamma cos\varphi & \cos\gamma\sin\varphi\sin\rho - \sin\gamma\cos\rho & \cos\gamma\sin\varphi\cos\rho + \sin\gamma\sin\rho \\ sin\varphi & \cos\varphi\sin\rho & \cos\varphi\cos\rho \end{pmatrix} = \begin{pmatrix} r_{1,1} & r_{1,2} & r_{1,3} \\ r_{2,1} & r_{2,2} & r_{2,3} \\ r_{3,1} & r_{3,2} & r_{3,3} \end{pmatrix}. \text{ (18)}$$

Using the matrix elements $r_{1,1}$, $r_{2,1}$ and $r_{3,1}$ in further computation, the angles yaw - γ, pitch - φ and roll - ρ can be computed.

$$\tan\gamma = \frac{r_{1,1}}{r_{2,1}} \text{ (19)}$$

When γ is in a range of 0°-180° (path iii-a), if the inverse function of tan provides a value below 0°, then 180° is added to γ.

When γ is in a range of 0°-360°(path iii-b), the function "tan2", i.e. the function considering the quadrants and the signs of counter and nominator, has to be used.

$$\sin \varphi = r_{3,1} \quad (20)$$

The inverse sin function provides pitch angle ϕ values between -90° and +90°.

$$\sin\rho = \frac{r_{3,2}}{cos\varphi} \quad (21)$$

Roll angle ρ is in the range between -90° to +90°.

The method for oyster shell orientation presents an efficient measurement and analysis of the orientation of thousands of specimens and is a valuable progress compared to the traditional 2D approach, which measures only the azimuth (yaw) angles.

4 Results

4.1. Oyster reef digitizing

Oyster reef digitizing work uses TLS-derived data and orthophotos that are visualized with GIS tools to develop a database. The database is further used to quantify and assess taxonomic composition, size distribution, degree of fragmentation and 2D orientation of individual oyster shells in the digitized Miocene shell bed. A digital surface model with 1 mm grid resolution was derived using the highest point in each grid cell in TLS data. The photos were combined with an orthophoto mosaic with 0.5 mm pixel size. Both the high-resolution surface model and its texture are important components for further geological interpretation and paleontological reconstruction of different shell species whose length may vary from a few centimetres up to 60 cm.

4.1.1. 3D models of the reef

3D point clouds and 3D geometric models are established as the foundation for the representation and analysis of the oyster reef surface in this multidisciplinary research combining palaeontology and photogrammetry. The achieved point density of about 150 points/cm² resulted in a sufficient resolution for model creation as shown in Figures 9 and 11. Each part of the reef was covered with at least five overlapping scans. For model generation, a triangulated irregular network (TIN) was calculated that provides models commonly used for visualization and interpretation. The quality of triangulation model, influences directly the shell detection accuracy and quality from the oyster reef (Figure 14A). A digital documentation preserves the current status of the whole reef in the form of highly detailed digital models such as:

- 3D triangulation model (TIN, 0.7 mm average edge length)
- 2.5D grid (Digital Surface Model – DSM of 81 tiles, 1 mm resolution)
- Mesh models (nine shells scanned separately with scan arm, 0.18 mm resolution; see Figures 18 and 42).

4.1.2. Oyster outline database

The reasons to create a reference database of the oyster reef came during the research on this thesis because there were no earlier publications on reference samples of shells openly available. A reference data set was created by digitizing shell polygons interactively in the digital orthophoto as a transparent layer overlapping the digital surface model. We chose to digitize all specimens and fragments recognizable as shells independent of their size. The reference data include oysters *Magallana gryphoides* (Schlotheim, 1813), *Perna aquitanica* (Mayer, 1858), *Ostrea digitalina* (Dubois de Montpereux, 1831), Venerupis basteroti (Mayer, 1857), Pecten styriacus (Hilber, 1879), gastropod shells, and not known fragments that are sometimes smaller than 5 cm (Figure 21). Regarding the close neighborhood setting on the reef certain fragments were joined, touching or overlapping each other. But since they are obviously separate entities for the experts from the field, they were also digitized as separate polygons. In total, 10,284 polygons were digitized. They present independently determined reference data of very inhomogeneous shell shapes. The amount of a shell reference sample is determined by the coverage area spanning from the center of the reef in four directions (N-S, W-E). The DSM and the orthophoto as well as a label layer with polygons (red) created from the reference data set are shown in Figure 20.

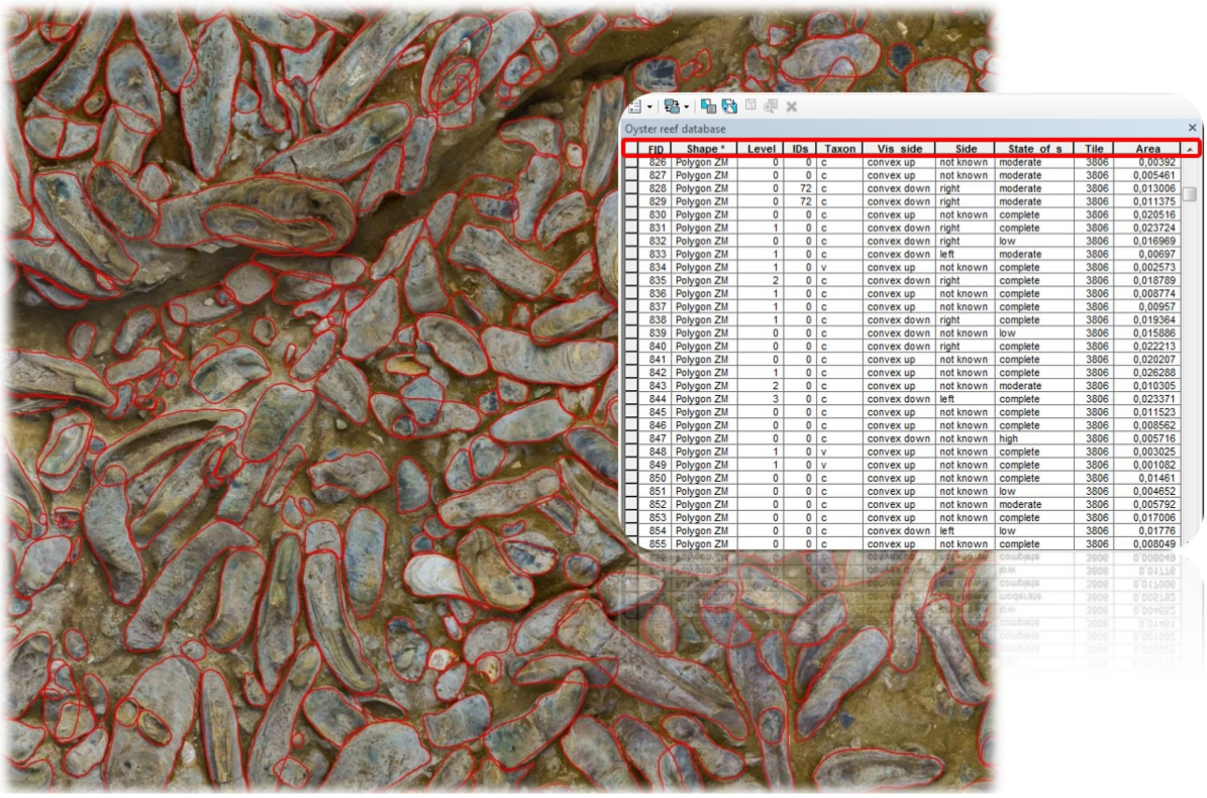

Figure 20: (Left) Example of individual fossil outlines; (Right) Overview of the oyster reef database attributes.

The shell detection depends on several factors. These include the size, shape, position, visible side, and remaining colour of the specimen, partly buried sides or low visible appearance caused by sand deposition. The outline preferences digitized by an operator were evaluated by a paleontology expert, and hence this part of the process took long time. Several iterations and consultations were necessary in order to learn what are the most important distinguishable parts between species and their shapes. Concentration on specific details on the shells improved the final interpretation.

Interpretations, in form of shell outlines, are stored in a GIS database with a data structure enabling fast access despite the large data volume and ensuring a consistent repository for the researchers involved. The GIS database has numerical and descriptive elements. Numerical attributes are identity (ID), level of overlap, length (2D and 3D), orientation (yaw, pitch, and roll angle), and descriptive attributes are taxon (7 different species), side of the shell (left, right, unknown), state of specimen (complete, fragmented, not determined), shell position (convex up, convex down), area, etc. An example of data structure is illustrated in Figures 20 and 21, and the list of database attributes, their data type, range of values, unit and more detail explanation are presented in Table 4.

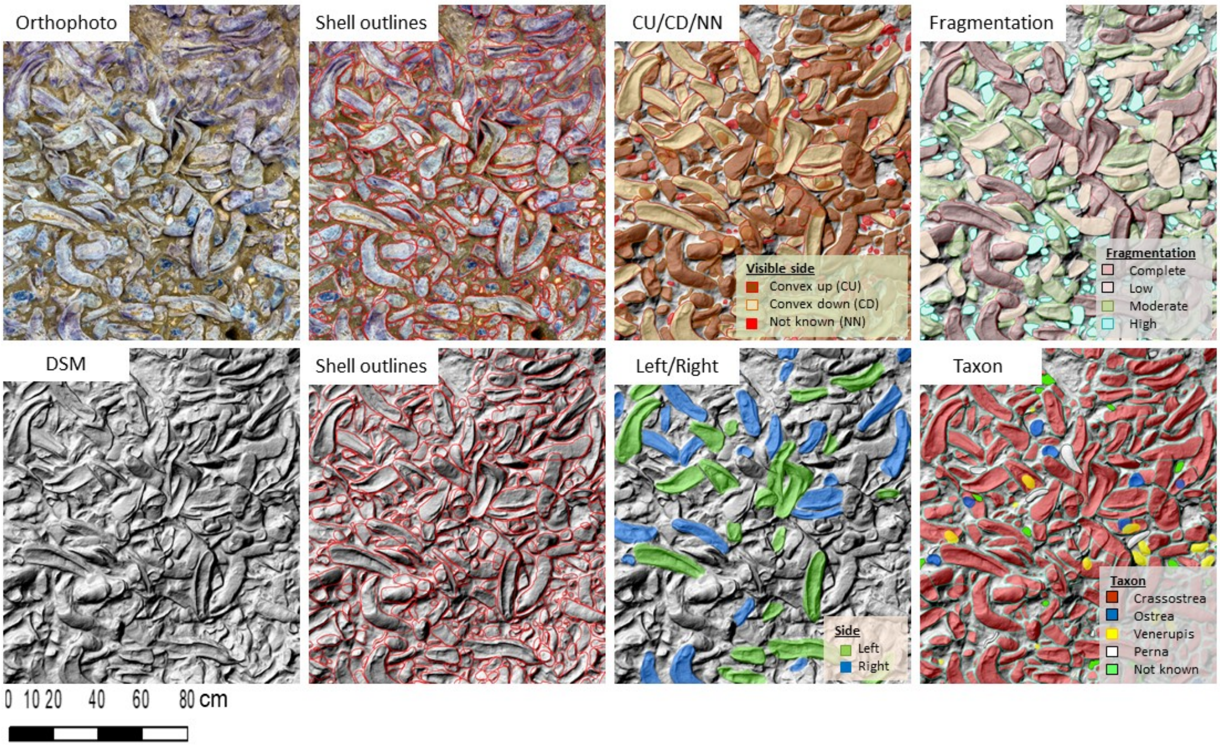

Figure 21: Examples of the reference data: orthophoto and digital surface model (DSM) are used to define shell outlines manually. Together with various attributes, such as visible side (convex up/down), side (left/right), degree of fragmentation and taxon ID, these data are stored in GIS database.

The derived data (e.g. attributive data) enables different spatial data queries such as encrustation by oysters, taphonomic map, distribution of left and right shells, distribution of convex up and convex down shells, distance maps or other specific thematic maps for geological purposes. The GIS database also allows you to define additional attributes if required, such as geological features: abrasion or bioerosion (0–no, 1-present a bit, 2–strong), covered by sediment (yes/no), encrustration by barnacles or another oyster (yes/no), see Figure 20 and Table 4.

4.2. Individual shell detection results

The method proposed was applied on entire oyster reef data set which is composed of 81 tiles with each tile having an area of 6 m^2. The point cloud size inside the tiles varies between the range from about 2 million points up to 17 million points. There were more scan points within the reef borders than on its edges. Therefore, the results are visualized and analyzed, and it is observed that tiles with less points are the outer tiles on the reef borders with the less shells or the open and plain sand areas, i.e. the tile area is not entirely covered by shells. The inner reef area is completely covered with shells and comprises 49 tiles, corresponding to 294 m^2 of TLS scanned area. However, the extraction of the shells was done completely automatically including the inner reef area and also an extended area to the total area of the reef that is covered with shells, 367 m^2. The extraction results are compared against the references of 13 different data tiles, consisting of 78 m^2 of oyster reef area in total. Accurate detection of individual shells using an automatic method is an important input for further steps in oyster reef data analysis.

4.2.1. Surface openness

Figure 22A shows the processed results of one tile adjacent to the north of the center tile (see Figure 13) as an example of the applied method: true positive (TP) pixels are colored in blue; false negative (FN) pixels are colored in dark yellow; false positive (FP) are presented with red color; and true negative (TN) features are in gray. Results are evaluated against the manual reference data (Figure 22B), where the results are assessed for more than 10,000 specimens by comparison with the manually determined shell polygons within the central area of the reef (Figure 13). The surface matching validation method uses completeness (reddish background in Supplemental Table S1[7]), correctness (bluish background in Supplemental Table S1 [see footnote 7]), and quality assessment (greenish background in Supplemental Table S1 [see footnote 7]). Quality assessment method proposed by Heipke et al. (1997) takes into account Quality ∈ [0; 1] and uses following formula

$$Quality = \frac{area\ of\ matched\ extraction}{area\ of\ extracted\ data + area\ of\ unmatched\ reference} = \frac{\mathrm{TP}}{\mathrm{TP} + \mathrm{FP} + \mathrm{FN}} \quad (22)$$

where TP – true positive (the matched extracted data), FP – false positive (the unmatched extracted data), and FN – false negative (the unmatched reference data).

Those values are depicted on one example within Figure 22. For the given scenario, the detection accuracy, based on validated surface matching and visual inspection of obtained results, reveals the feasibility of the proposed methodology.

The result shown in Figure 22 is an optimized result based on test runs using different kernel sizes: k = 1 (3 × 3 mm), k = 3 (7 × 7 mm), k = 5 (11 × 11 mm), and up to k = 27 (55 × 55 mm). The test runs showed that completeness and quality decreased from k = 1 to k = 3 and start increasing from k = 3 up to k = 25. Correctness is maximal at k = 3, but quality is minimal. The quality results show independence from majority filters, indicated by only minor changes (Figure 23 and Supplemental Table S1 [see footnote 7]). Therefore, parameters k = 25 and m = 3 (majority filter size 3) are chosen as the best parameters for the automatic surface detection of shells. In addition to the surface matching, the total number of detected objects was examined. Thus, the number of detected objects was validated by means of the following parameters:

(1) the best parameters estimated for surface matching, k = 25 and m = 3, and
(2) another pair of parameters were determined to be optimum for the number of detected objects, k = 7 and m = 6.

[7] Supplemental Material includes Supplemental Tables S1 and S2).

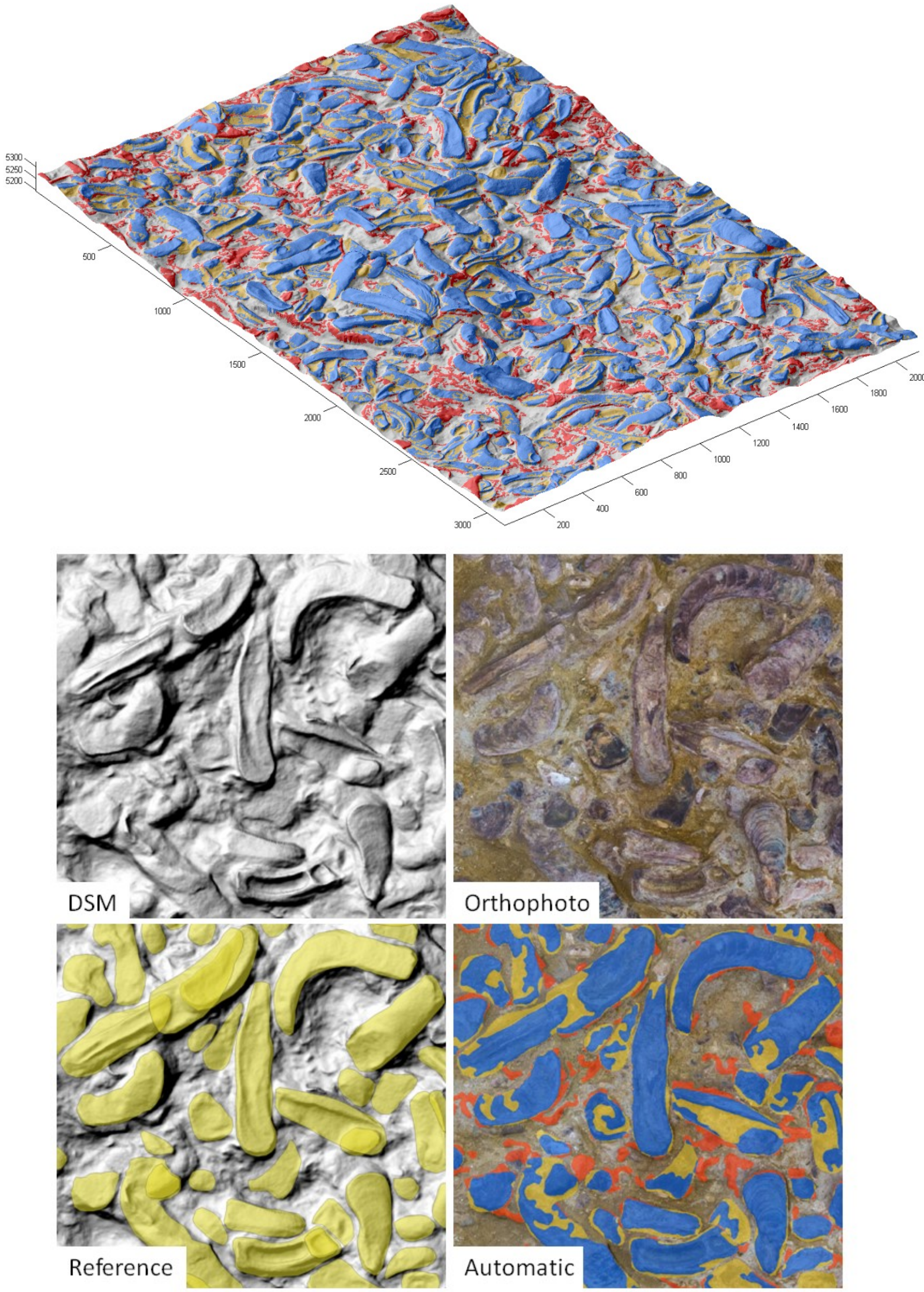

Figure 22: (A) The tile north of the center tile (see Figure 13). Quality of extraction: shaded model overlapped with automatic detection (blue—true positive [TP]; dark yellow—false negative [FN]; red—false positive [FP]; gray—true negative [TN] cells). (B) Detail from the reef showing data used for reference data (digital surface model [DSM] and orthophoto) and visualization of automatic extraction.

Surfaces of the shells were detected effectively for 69% of the data based on surface matching using k = 25 and m = 3 (Figure 24, boldface in Table 5 and Supplemental Table S1 [see footnote 7]) and for 50.25% of the data based on the detected number of objects. Overall, an accuracy of over 98% was achieved in detecting the number of objects by the use of another pair of parameters, k = 7 and m = 6 (Supplemental Table S2); but then surface matching completeness decreased slightly to 67%. According to the reference data (13 tiles), the number of shells (excluding highly fragmented shells smaller than 17 cm^2) ranges from 322 to 466 shells per tile with a mean of 387. Within those tiles, the number of automatically detected shells (based on k = 25 and m = 3) ranges from 170 to 210 shells per tile with a mean of 195. On the basis of k = 7 and m = 6, shells range from 310 to 410 with a mean of 381.

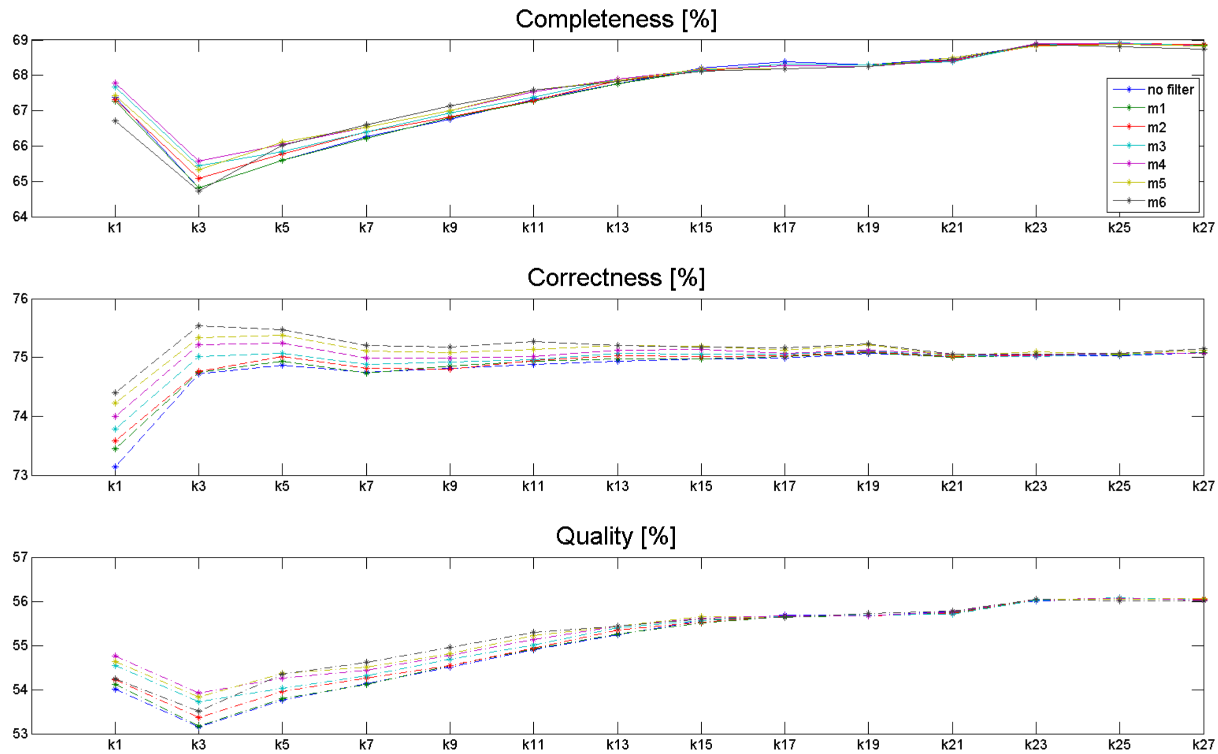

Figure 23: Quality assessment of reference tiles, based on different kernel sizes and filter values (data tabulated in Supplemental Table S1 [see footnote 7]).

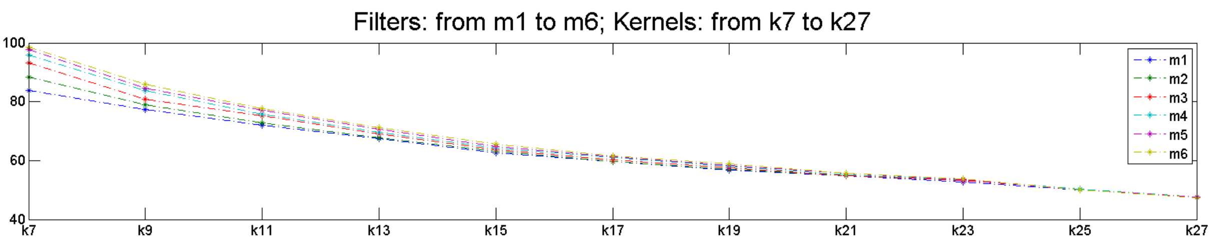

Figure 24: Quality assessment of reference tiles based on automatic object detection (includes different kernel sizes and filter values; the data are tabulated in Supplemental Table S2 [see footnote 7]).

4.2.2. Shell number estimation

Estimating the accuracy of the total shell number in the reef is important to determine if the automatic shell detection is suitable as an input for paleontological analysis and interpretation**.** Here, automatic shell detection together with the reference data were used for the first time in estimating the total number of shells on the reef. A total of 10,284 shells served as reference data (corresponds to 13 tiles or 78 m^2). In the reference data, the number of individual shells larger than 17 cm^2 was 6148. If overlapping shells are counted as one shell (as they typically appear in the automatic procedure), the number was reduced to 5035, the factor 1/1.23. The number of automatically detected objects over the region of the reference data was 4958 when the optimal numbers for object detection (k = 7, m = 6; boldface result in Table 5) were used. The inner reef area is completely covered with shells and comprises 49 tiles, corresponding to 294 m^2. The outer tiles are not entirely covered by shells, since shells are only found at an area below 6 m^2, i.e., the area of tile.

Table 5: Quality assessment – pairs of the best chosen parameters to identify and enumerate shells (Note: Kernel sizes k = 7, k = 25 and majority filter sizes m = 3, m = 6 – Please see text for boldface explanation).

Statistics		Parameters	***m* = 3**	***m* = 6**
Extracted	***k* = 7**	Completeness	66.40	**66.61**
		Correctness	74.88	75.21
		Quality	54.31	54.61
		Number of objects	4693 (93.21%)	**4958 (98.47%)**
	***k* = 25**	Completeness	**68.92**	68.81
		Correctness	75.06	75.07
		Quality	56.08	56.02
		Number of objects	**2530** (**50.25%**)	2523 (50.11%)
Reference		Complete shells larger than 17 cm^2: 5035		

The number of automatically detected shells larger than 17 cm^2 in the inner reef area is 18,264. Multiplied by a factor of 1.23 to account for overlapping shells, this leads to a number of 22,432 shells. In comparison, multiplying the number of manually delineated shells in the 13 reference tiles (6148) by 49/13 would correspond to 23,173 shells. Thus, the automatically detected number of shells is 97% of what is computed from the reference data and the area ratio, which compares well with the 98% (see above; Table 5 boldface result). Extending this estimation from the 49 tiles (294 m^2) to the total area of the reef that is covered with shells, 367 m^2, the estimated number of shells, based on the automatic detection and the factor 1.23 to account for overlaps, is 28,002—that is, the estimated number of shells larger than 17 cm^2 for the entire reef area. When the ratio of all shells to large shells in the reference area, 10,284/6148, is applied, the estimated total number of shells is 46,840. This number includes complete but also fragmented specimens.

4.3. 3D orientations of oysters

Based on the manually determined shell polygons, yaw, pitch, and roll angles for sample data set of 1904 shells were computed. The yaw angles represent a broad scatter in all directions, with a mean of 168.8°, and std. dev. 104°. The distribution in the interval [0°, 360°] has mean and std.dev. 180° and 104°, respectively. The distribution of the yaw angles is plotted in ascending order in Figures 26, 27, 28, 30, and 31. Figures evidently document the distribution closeness to the uniform distribution and, therefore, a highly random orientation pattern. The other two angles, pitch and roll, display distinctly less scattering. For the pitch angle (ϕ), a minimum value of − 32.8° and a maximum of 30.6° were observed (Table 6), with a mean of 1.11° (std. 9°). The roll angles ρ display a wider variation from − 65.7° to 67.5° with a mean of 0.74° (std. 15.4°). Distinct tails are formed in the distribution curves for pitch and roll angles, indicating the presence of few strongly tilted shells (Figure 34).

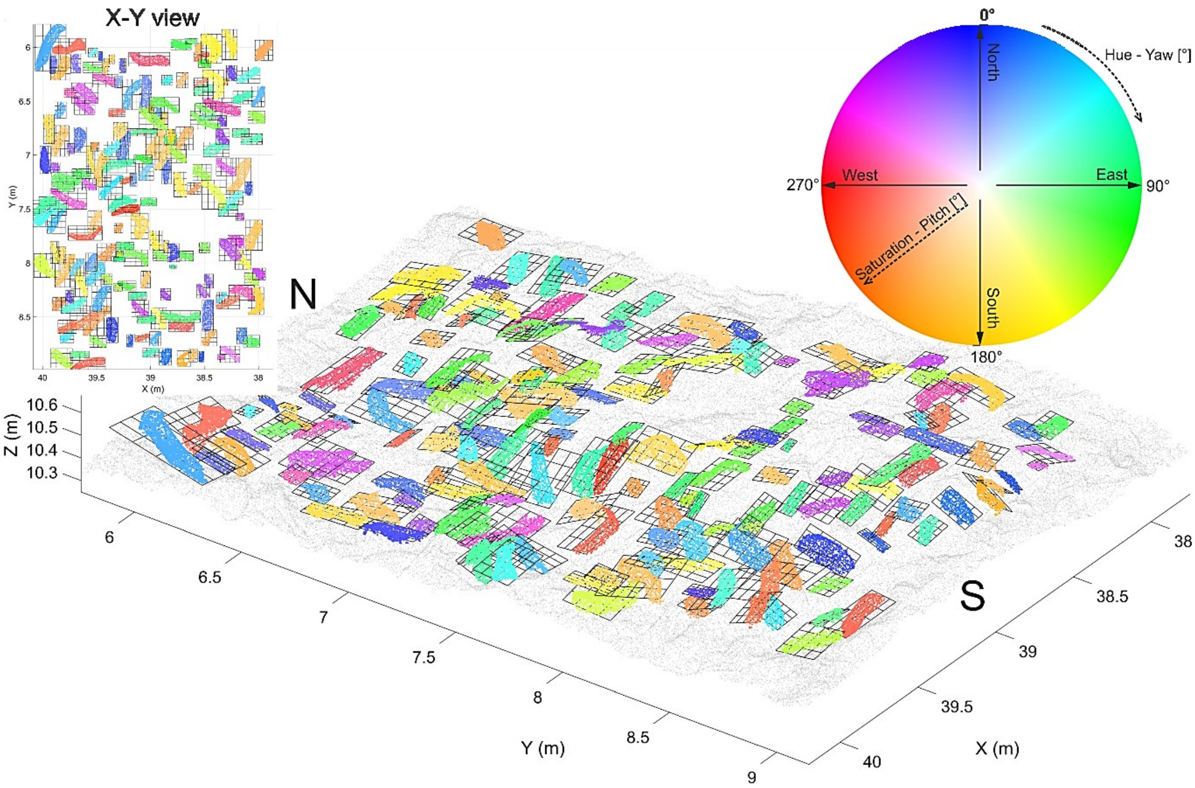

Figure 25: Orientation map of one tile size 3 × 2 m, comprising 177 shells. Color wheel coding depends on the angles. Hue encodes orientation angle yaw and saturation encodes pitch angle, while roll angle is not visualized. The color is darker on the places, where the pitch (tilt) is larger or lighter if the shell is approximately horizontal.

An intuitive option to visualize such 3D-orientation data is applying the color codes of a color wheel (Figures 19 and 25). Hue encodes the orientation angle yaw and saturation encodes pitch, while roll is not visualized. The color is darker on those places, where the pitch (tilt) is larger, and lighter if the shell is approximately horizontal. The color wheel ranges from 0°–360°. A yaw angle γ ranging from 0° to 90° is coded with blue to green colors (Figure 25). A yaw angle γ between 90° and 180° is visualized in green-to-yellow color; from 180° to 270°, the color code stretches from yellow to red, and for yaw from 270° to 360°, the color will range from red to blue. The color coded, automatically derived results for all 13 tiles with manually defined shells is shown in Figure 29. Illustration of each angle in a separate map with its own color bar is shown in Figures 30, 31.

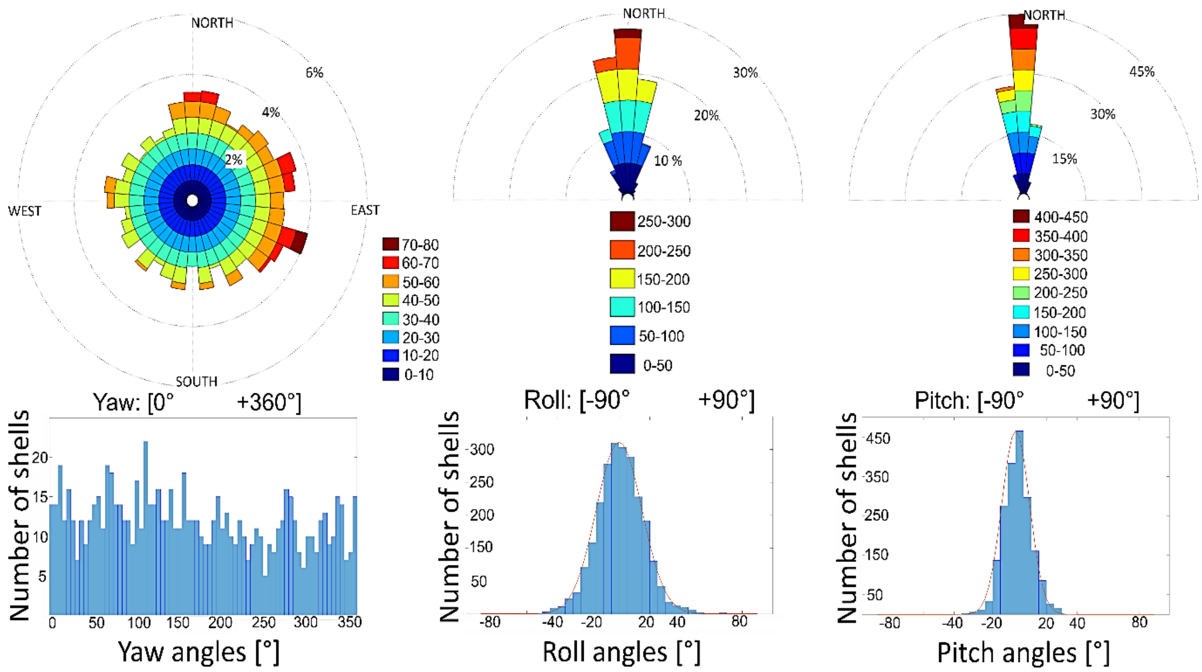

Figure 26: Rose diagrams and histograms based on γ, ϕ, and ρ angles of 1904 shells (bar width = 5°).

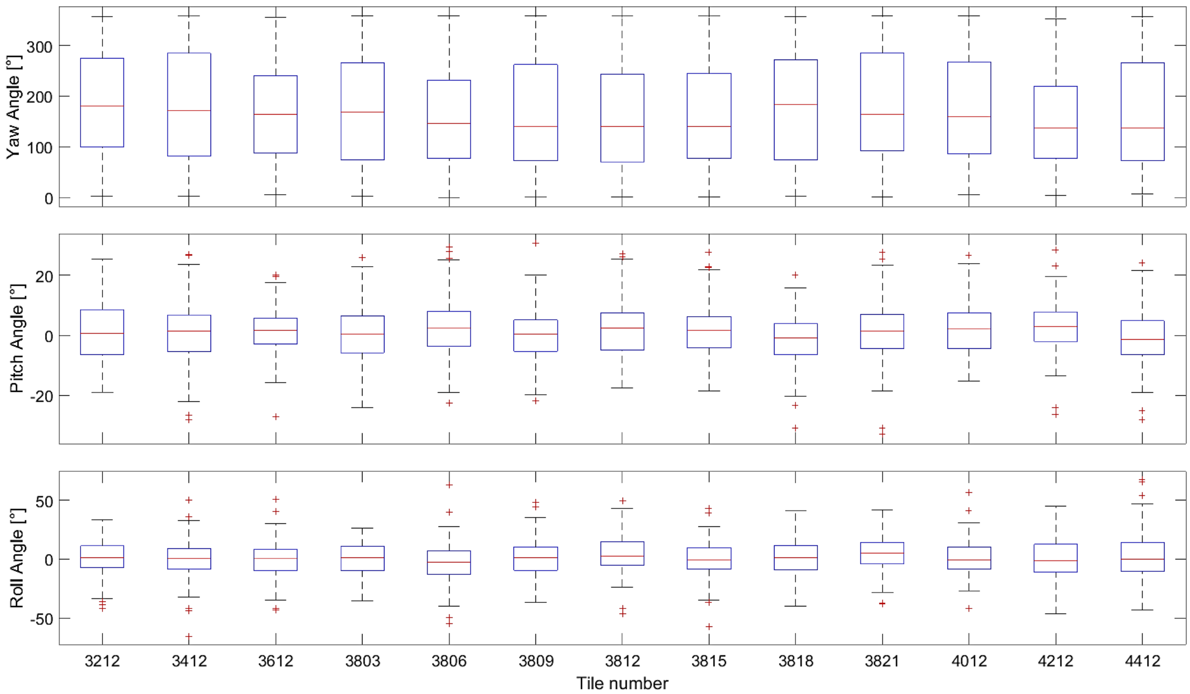

Figure 27: Tilewise distribution of yaw, pitch, and roll angles ranges in box plots.

Student t test values are given in Table 6. Using the one-sample t test, it is evaluated if mean roll and pitch for each tile are equal to the overall mean. p value of the test, returned as a scalar value in the range [0,1], presents the probability of accepting or rejecting the null hypothesis. The null hypothesis (h = 0) is accepted if the p is larger than 0.05. This is the case for 10 tiles for the roll angle and 11 tiles for the pitch angle. This points that there is no significant mean difference between the compared tiles, while for tiles 3806, 3812, and 3821 (see tile map on Figure 29) of the roll angle, the null hypothesis is rejected (h = 1). The same is observed for the tiles 3812 and 4212 of the pitch angle. As the mean roll (0.74°) and the mean pitch (1.11°) values do not deviate significantly from 0°, the null hypothesis has to be rejected at the confidence level 5%.

Table 6: Student *t*-test values (roll, pitch) for all shells and each tile. t is the test statistic. Roll [°] gives the average roll value. Pitch [°] gives the average pitch value. p-value of the test, returned as a scalar value in the range [0,1], presents the probability of accepting (p>0.05, h=0) or rejecting (p≤0.05, h=1) the null hypothesis.

Tile Number	Shells	t-roll	Roll [°] mean	Roll h (p)	t-pitch	Pitch [°] mean	Pitch h (p)
all	n=1904	2.09	0.74	1 (0.04)	5.39	1.11	1 (0)
3212	n=151	-1.01	0.38	0 (0.76)	1.95	1.51	0 (0.62)
3412	n=181	-3.26	-0.41	0 (0.32)	-3.08	0.48	0 (0.38)
3612	n=155	-3.08	-0.35	0 (0.34)	2.41	1.61	0 (0.42)
3803	n=183	-2.22	-0.04	0 (0.46)	-3.27	0.44	0 (0.31)
3806	n=177	-10.56	-2.99	1 (0.002)	5.93	2.33	0 (0.09)
3809	n=142	2.23	1.52	0 (0.55)	-2.72	0.55	0 (0.44)
3812	n=103	9.91	4.24	1 (0.03)	3.08	1.75	0 (0.47)
3815	n=153	-1.84	0.44	0 (0.79)	0.95	1.31	0 (0.77)
3818	n=137	-1.65	0.16	0 (0.64)	-11.30	-1.22	1 (0.00)
3821	n=164	11.35	4.74	1 (0.00)	0.51	1.22	0 (0.89)
4012	n=125	1.08	1.12	0 (0.76)	4.86	2.11	0 (0.21)
4212	n=125	0.21	0.81	0 (0.96)	8.75	2.92	1 (0.02)
4412	n=108	4.53	2.34	0 (0.40)	-8.10	-0.56	0 (0.06)

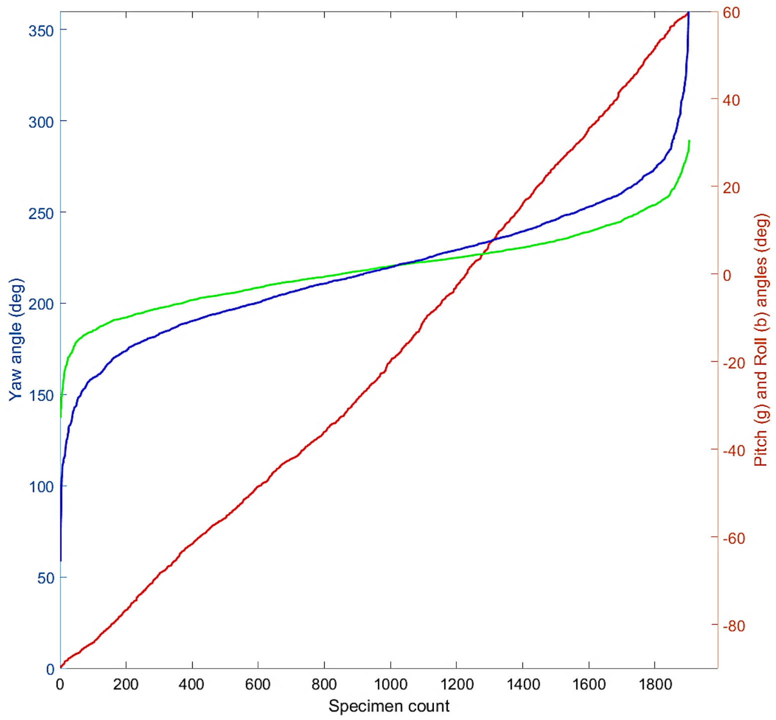

Figure 28: Yaw, pitch, and roll angles of 1904 oyster shells sorted in ascending order for each angle.

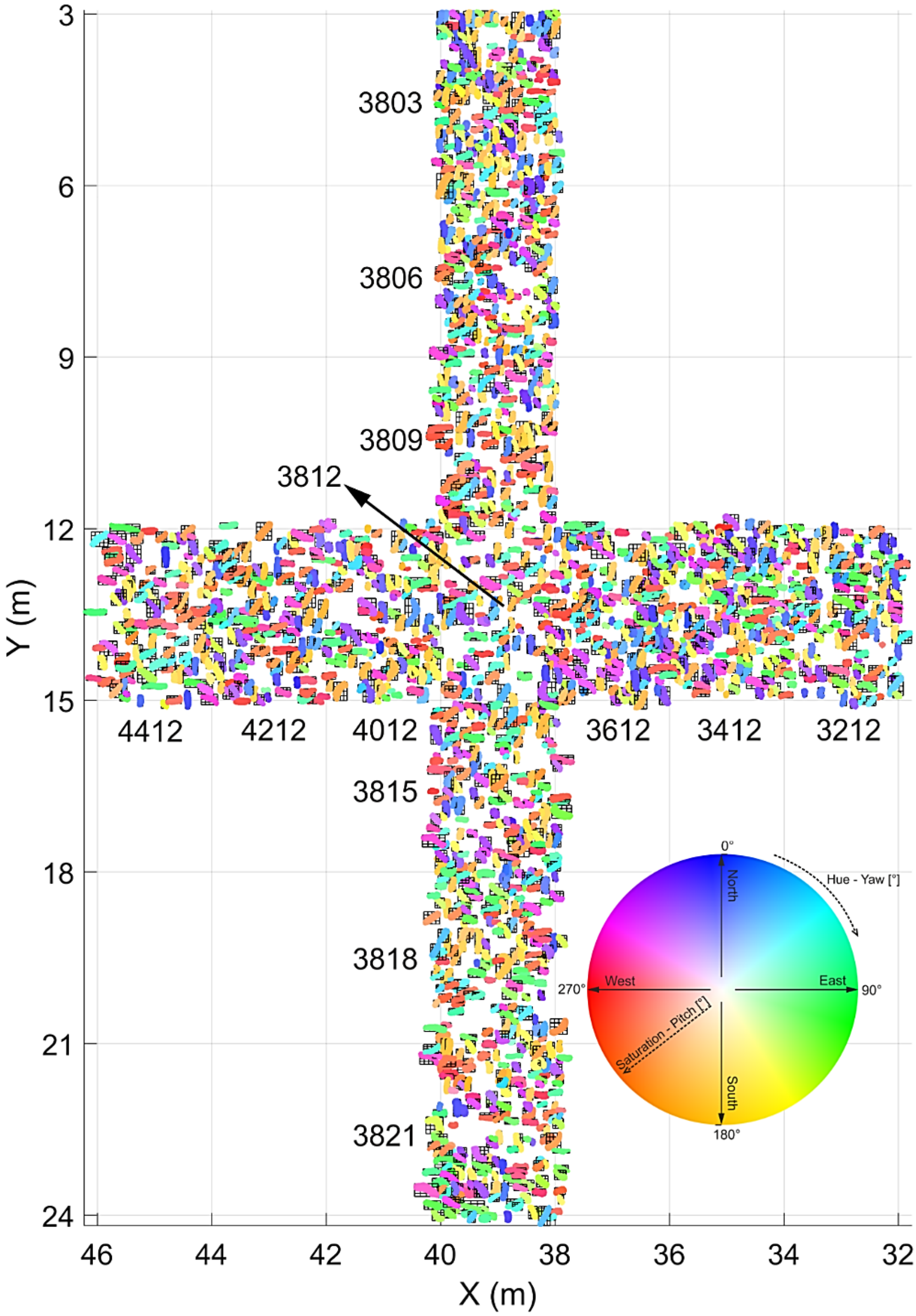

Figure 29: Shell orientation map for an N–S and a W–E transect with 1904 shells over 13 tiles (the same color wheel coding, as shown in Figure 25)

The Kolmogorov–Smirnov test is used to study if an empirical distribution follows an expected (i.e., predefined) distribution in the interval [0°, 360°]. The cumulative distribution is generated from ascending sorted yaw angles (values from 0 to 360). The cumulative distribution as a curve which is always increasing by 1/1904, for each yaw value, and the differences (Dn) between the values of the cumulative distribution function (cdf) and the reference. If the sample data are uniformly distributed, these differences should be zero. Dn is the largest value and in our case is

0.05. If the data are uniformly distributed, then the critical value Dn,α should be larger than Dn. From the Kolmogorov–Smirnov table, it is obvious that Dn,α = D1904,0.05 = 1.36/ sqrt(1904) = 0.031. Since Dn = 0.05 > 0.031 = Dn,α, we conclude that the data do not follow a uniform distribution.

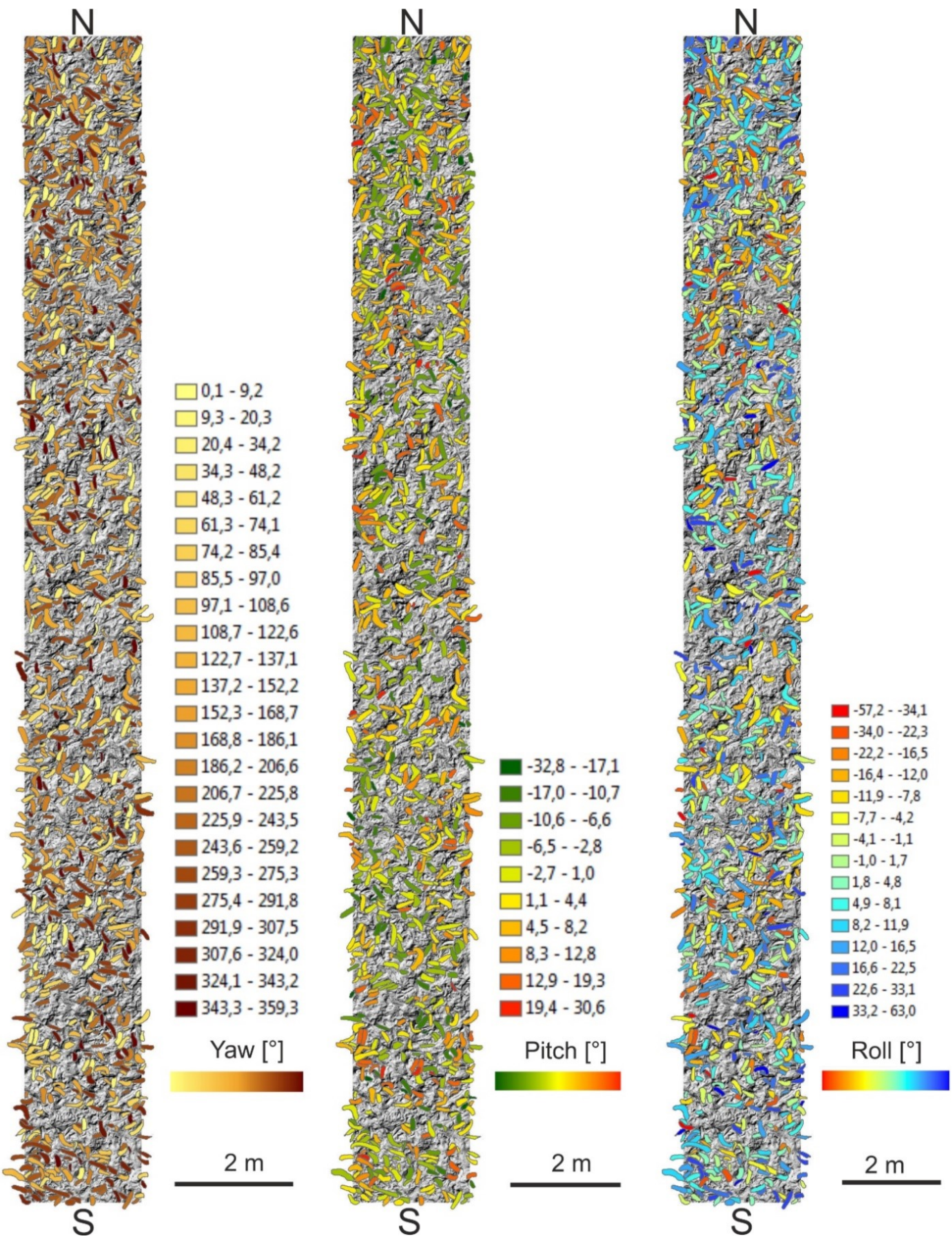

Figure 30: N–S transect distribution of yaw, pitch and roll angles.

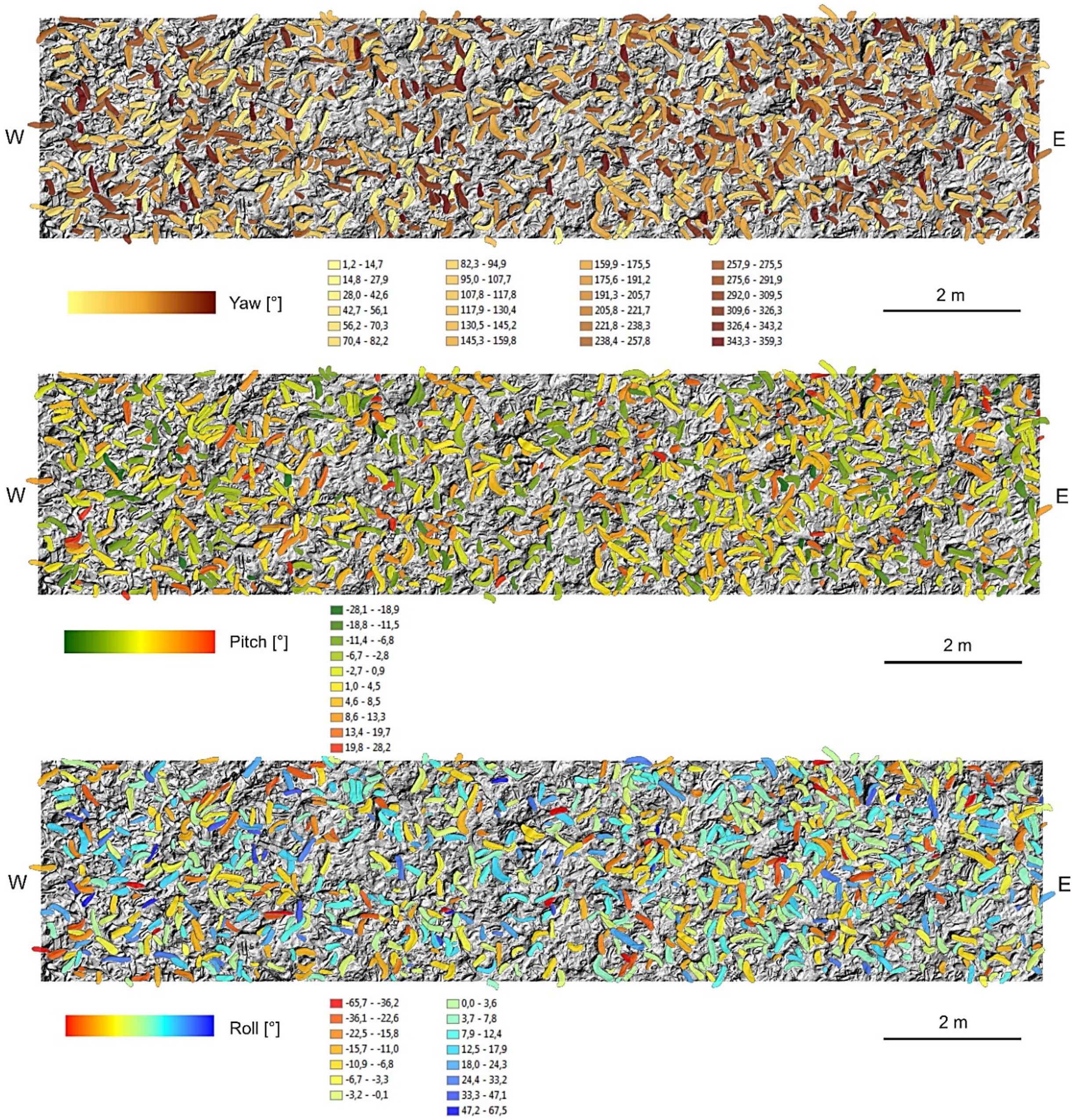

Figure 31: W–E transect distribution of yaw, pitch, and roll angles.

To quantify the effect of post-sedimentary displacement by faults on shell orientation, we analyzed the relation between strongly tilted shells close to the fault lines (Figure 34): shells shown in blue present roll angle above 31.5° and yellow shells present pitch angle tilt above 18.4°. We show the difference between fault and shell azimuth versus nearest distance of the shell to the fault line for the shells with pitch angle tilt above 18.4° (Figure 32A) and for the shells with roll angle tilt above 31.5° (Figure 32B). Figures 33 and 34 illustrate the individual shells on the reef bed within the multi-buffers surrounding the fault lines. They are in close distance to the fault lines or on it. The close distance is described via multi-buffer distances: blue: 0.1 m, pink: 0.2 m, and green: 0.3 m (Figures 33 and 34). The accumulative values (buffer wise) are displayed in Table 7. Quantification parameters were the nearest distance of individual shells from the fault line and the shell angles ($\phi > 18.4°$ or $\rho > 31.5°$). Table 7 shows that the accumulative number of the oyster shells with outlying orientation pitch angles has differences up to 2.2% points compared to that of all the shells in the tile. For outlying roll angles, the corresponding accumulative distance ratios vary more, being up to 10.0% points for 0.10 m buffer and then decreasing to 2.2% points for the 0.30 m buffer. In terms of oyster shell numbers, these differences are one shell for the pitch angle and five shells for the roll angle. These numbers indicate that the fault line vicinity does not seem to have an effect to the high outlying pitch angle values. A similar assumption can be made about the shells with high outlying roll angle values even while they are not as strongly correlated. This interpretation holds true, because tectonic activity postdates sedimentation distinctly.

Table 7: Buffer Zones: Accumulative ratio of individual oyster shells within the buffer zones of the nearest fault line (see also Figure 32). Please note that the two first buffers are not visualized on Figure 32.

Buffer distance	**Oyster shells with Pitch angle ϕ > 18.4° (N = 47)**	**Oyster shells with Roll angle ρ > 31.5° (N = 58)**	**All shells (1904) – outliers (99)**
0.01 m	20.4	17.7	21.4
0.05 m	34.4	28.1	36.9
0.10 m	48.4	40.6	50.6
0.20 m	73.1	67.7	72.5
0.30 m	88.2	84.4	86.6

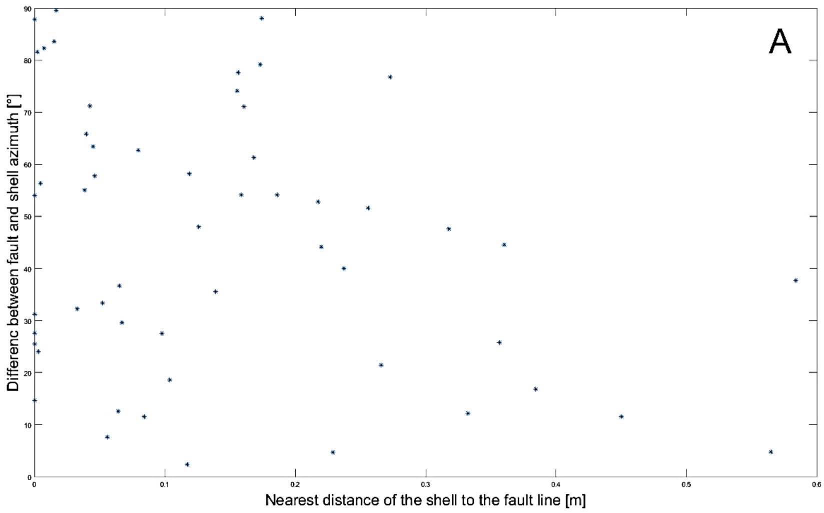

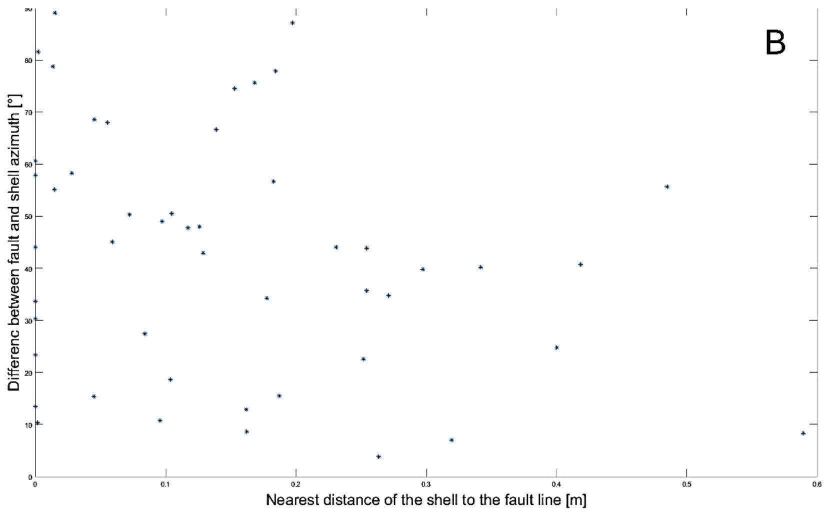

Figure 32: A Shells with pitch angle tilt above 18.4°; B shells with roll angle tilt above 31.5°.

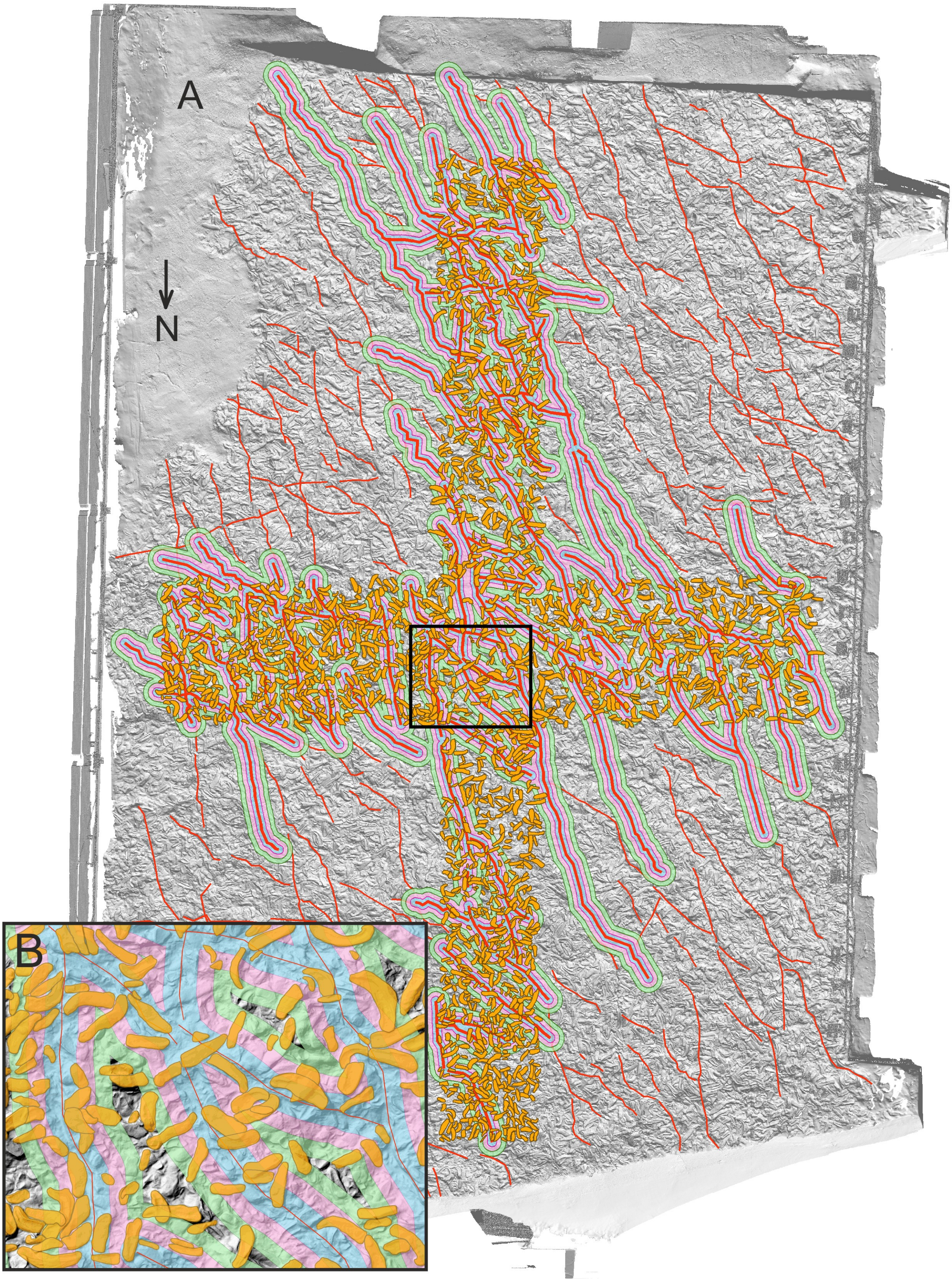

Figure 33: Individual shells within the multi-buffers surrounding the fault lines (red); buffer distances: blue: 0.1 m, pink: 0.2 m, green: 0.3 m. B Represents a magnification of a rectangle with a black outline in A.

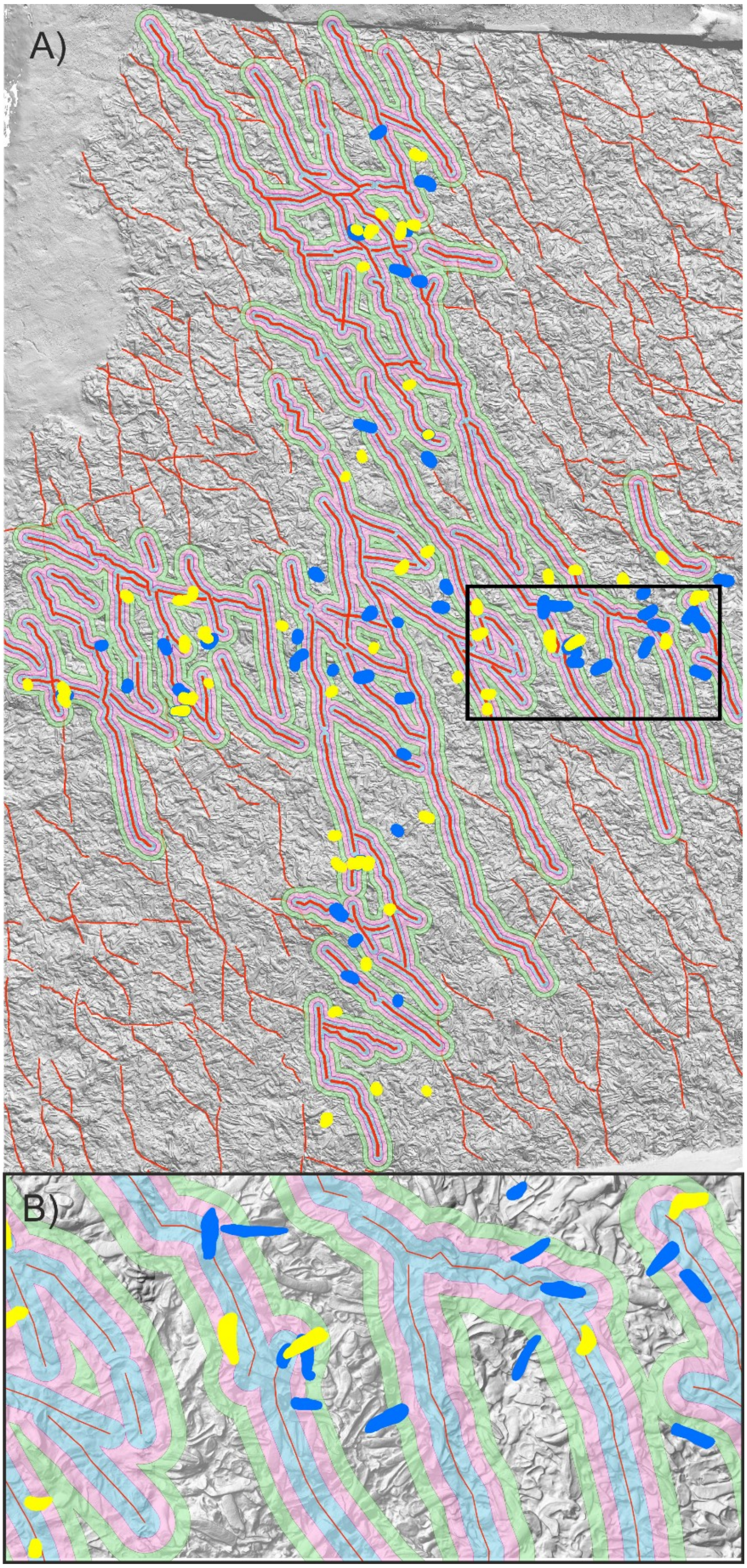

Figure 34: Shaded DSM overlapped with fault lines and strongly tilted shells: blue shells present roll angle tilt above 31.5° and yellow shells present pitch angle tilt above 18.4°. B Represents a magnification of a rectangle with a black outline in A.

4.4. Oyster age estimation using central line length, volume calculations and shell density

In this research, the age of *Magallana gryphoides* specimens from Stetten, Austria, was estimated, providing a basis for future studies on this species. The central line lengths (as they are derived from the point cloud data) were used as the input to analyse the growth of *Magallana gryphoides* shells. The relationship between the volume and the length of high resolution 3D oyster models was used to determine the age of *Magallana* shells. The shell volume calculation was performed using an algorithm for fast and accurate computation of polyhedral mass properties (Mirtich, 1996; section 3.1.7.1.) for completely excavated shells. For the shells laying on the reef with visible convex up or convex down side, von Bertalanffy equation was applied instead Mirtich´ algorithm. Oyster shell central line extraction algorithm (section 3.4.) was used to estimate the central line length. Shell density is determined by image analysis of left and right shell layers of the longitudinal section through *Magallana gryphoides* from the oyster reef site (see section 4.4.2.5). The results of performed algorithms provided the first age estimation in paleontological research for specimens of *Magallana reef* in Stetten, Austria. The age of analyzed oysters was ranging between 3 and 6 years (for statistical distribution, see chapter Results, section 4.4.2.4). The maximal age of 1121 analyzed oysters from the reef was 16 years.

4.4.1. Central line length calculations and evaluation

Three-dimensional (3D) shell central lines are derived in objective and automated manner using 3D point cloud data. The length and orientation estimation of particular oyster shells are determined by using corresponding 3D central line. An example of 3D central line results are shown in Figure 35. The described method first approximates a 2D central line and then also 3D central line (section 3.4.). It produces a graph with many path options within a shell due to diverse shell shapes. The longest path information is stored in a database for 10.284 specimens, because this information was used to support length estimation of *Magallana* and other species. However, the evaluation is done for the sample data set, the lengths of the 1121 complete *Magallana* shells. Fragments are not considered herein, as they are not informative for length/age calculations.

In 3D, the situation becomes more difficult because of the wavy, rough and complex shell surface. It is common that *Magallana* provides habitat for other species, hence it happens that for instance specimens of *Ostrea* were attached to *Magallana* shells (when alive), or *Venerupis* shells lie inside the interior part of *Magallana* (after death) (Figure 37). Therefore, 3D information is added to 2D line and 3D length is calculated (Figure 36).

Two-dimensional and three-dimensional lengths of 1121 shells are compared in order to visualize possible differences between 2D and 3D lengths. Differences (residuals) support automatic discovering of strongly curved shells and potential encrustation of *Magallana* by *Ostrea*, *Venerupis* or any other type of shells or even fragments.

The length differences (Figure 36, Table 8) can be interpreted as consequence of many height surface variations. It appears that the differences are mainly under 10-20% of total shell length which most likely represents a group of oysters with no overlap (or no encrustation) or not strongly curved shells. Those shells are lying on the uppermost surface of the reef bed or are surrounded with sand. Interpretation of residuals over 20% is interesting as these shells may potentially overlap with another shell, barnacles, and fragments such as shown in 3D visualized cases in Figure 37, or the strongly curved case in Figure 39. In order to be on the safe side, a constraint is applied: if a residual is significantly large and there is no overlap and no strong curve along the surface, the distance from points of 3D central line to the shell plane is checked. If there is an unexpected or sudden jump in point height, then those points are removed, and the 3D length is recalculated. Such cases may appear due to many natural overhangs because of the shell local positions; or for the reason that irregularly shaped outlines were nearly cutting shell surrounding beside the shell edge sharply. In order to explore multiple overlaps with more detail, we visualized the relationship between absolute residuals (3D-2D length) and existing number of overlap levels (from 0 to 3) for each shell (Figures 37 and 38).

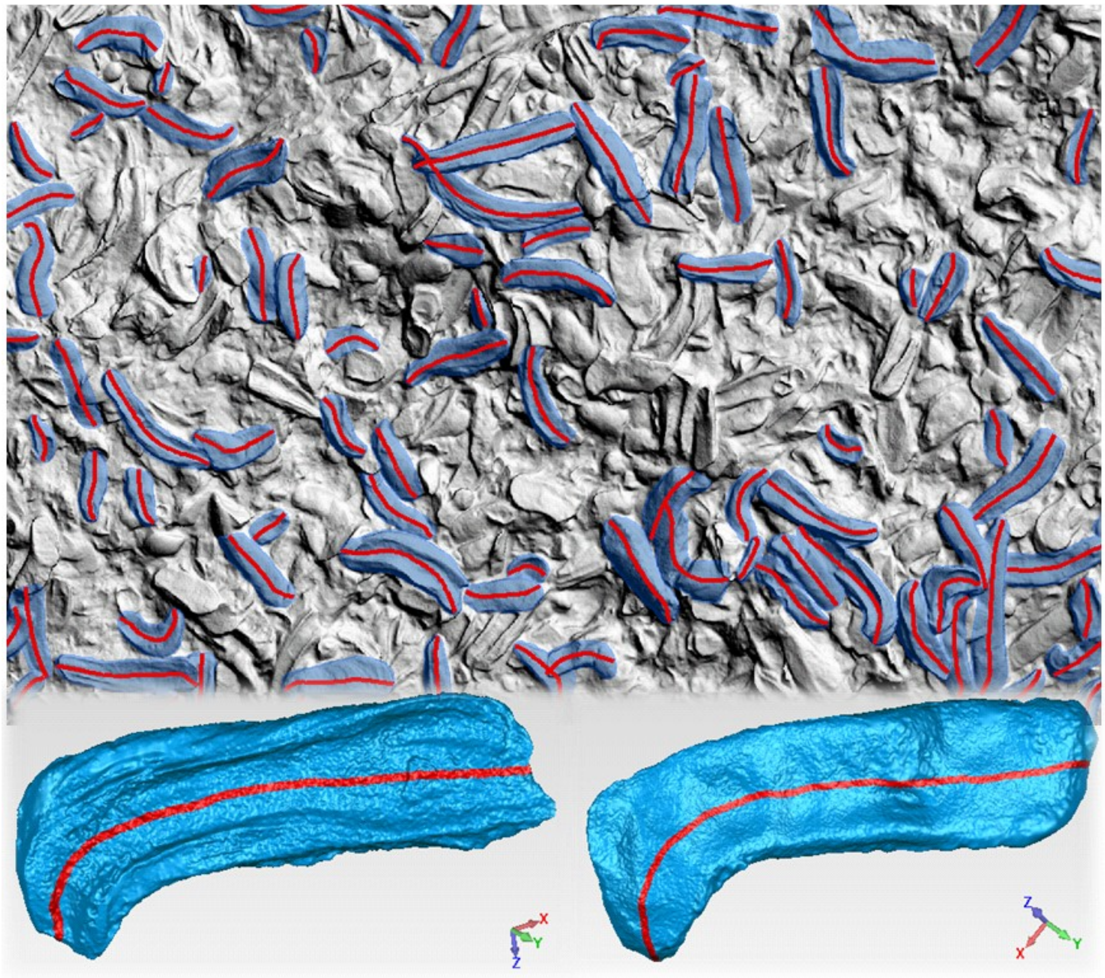

Figure 35: Top row: Shaded DSM (2 m by 3 m) overlapped with extracted 2D lines (red) of complete *Magallana gryphoides* oysters (blue); Bottom row: visualization of fitted 3D central line on shell pair mesh model (convex down left shell and convex up right shell). Figure is originally published in Djuricic et al. (2016d).

The overlap levels of individual shells were available in the reference database. Among the large number of diverse cases, there are some particular shell characteristics such as by being long and thin, or short and wide, or long and wide, etc. Consequently, the ratio between area of the projected shell surface and the 3D-2D residuals was analyzed. The aim was to find a correlation between large residuals (> 0.05 m) and small areas as a confirmation of height surface variations.

We focused mainly on large residuals, which allowed detecting the presence of encrustation or overlap and cases of strongly curved shells (Figure 38 and 39). Please note that encrustation is the case when another specimen is attached to the oyster (mainly exterior part of valve) in order to use it as a shelter for living on it. Overlap is the case when the shell imbricates nearby shell or lay over it (see Figure 37).

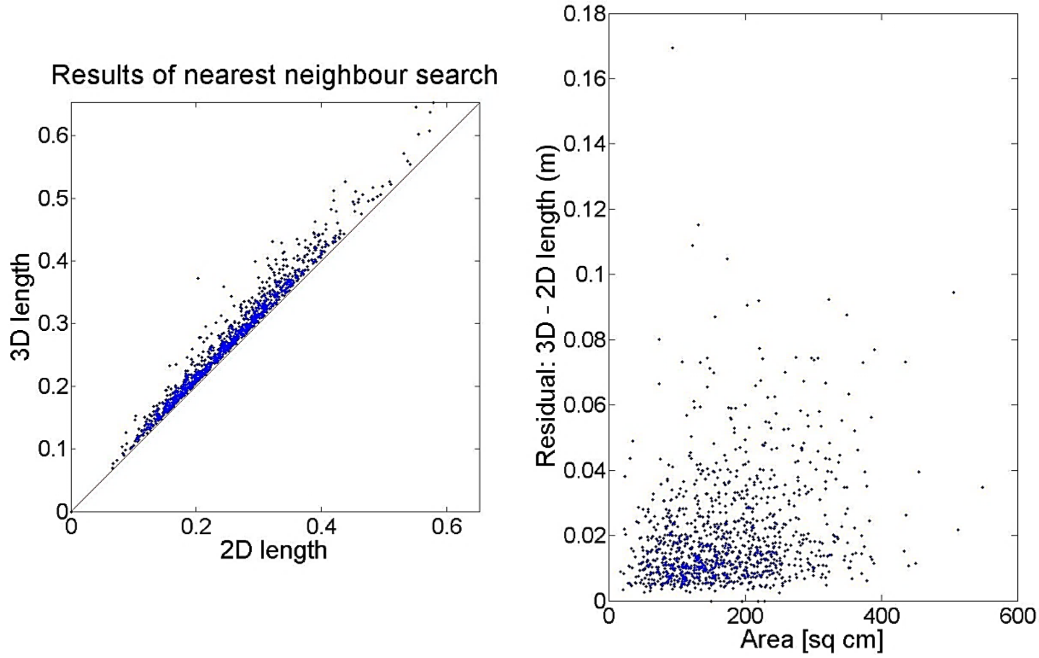

Figure 36: Left: Differences between 2D and 3D lengths; Right: residual vs. area of projected shell surface.

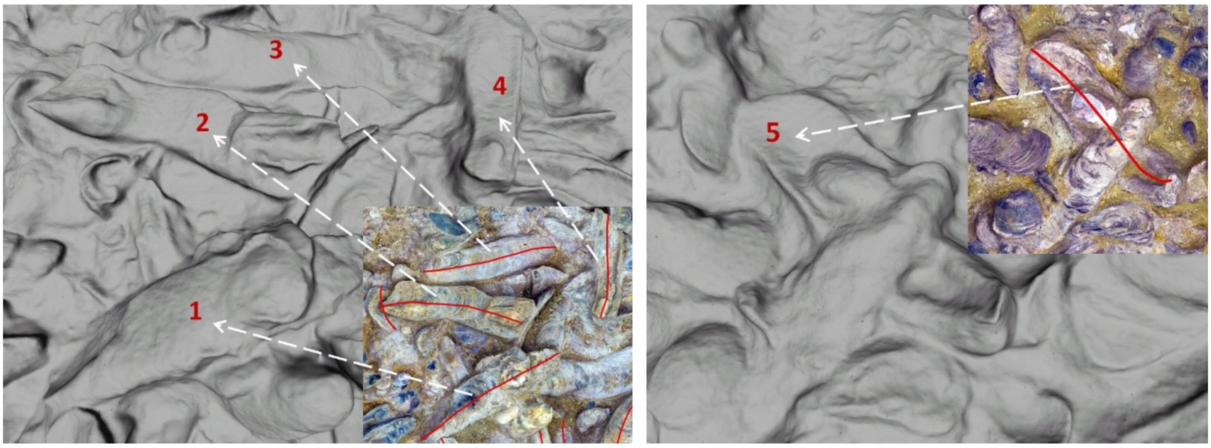

Figure 37: Visual inspection of overlap and encrustation cases (mesh model and orthophoto). 1, 3 and 4 are different encrustation cases, while 2 and 5 present overlap cases.

One of the most noticeable distinct differences between 2D and 3D length is the large residual of about 16 cm (Figure 38) where the level of overlap is equal 0. Since there is no encrustation to cause surface variation, such case is interpreted as special type of shell with strong curved interior part of the surface. Projected 2D border line of this case and central line are much smaller than 3D approximation. Example of automatically discovered curved shell is visualized in Fig. 39.

Table 8: Example comparison of 2D vs. 3D lengths from Figure 37.

	Shells	1	2	3	4	5
Extracted	2D length [m]	0.388	0.328	0.320	0.263	0.328
	3D length [m]	0.445	0.343	0.333	0.287	0.395
Ref.	2D length [m]	0.392	0.346	0.321	0.246	0.304

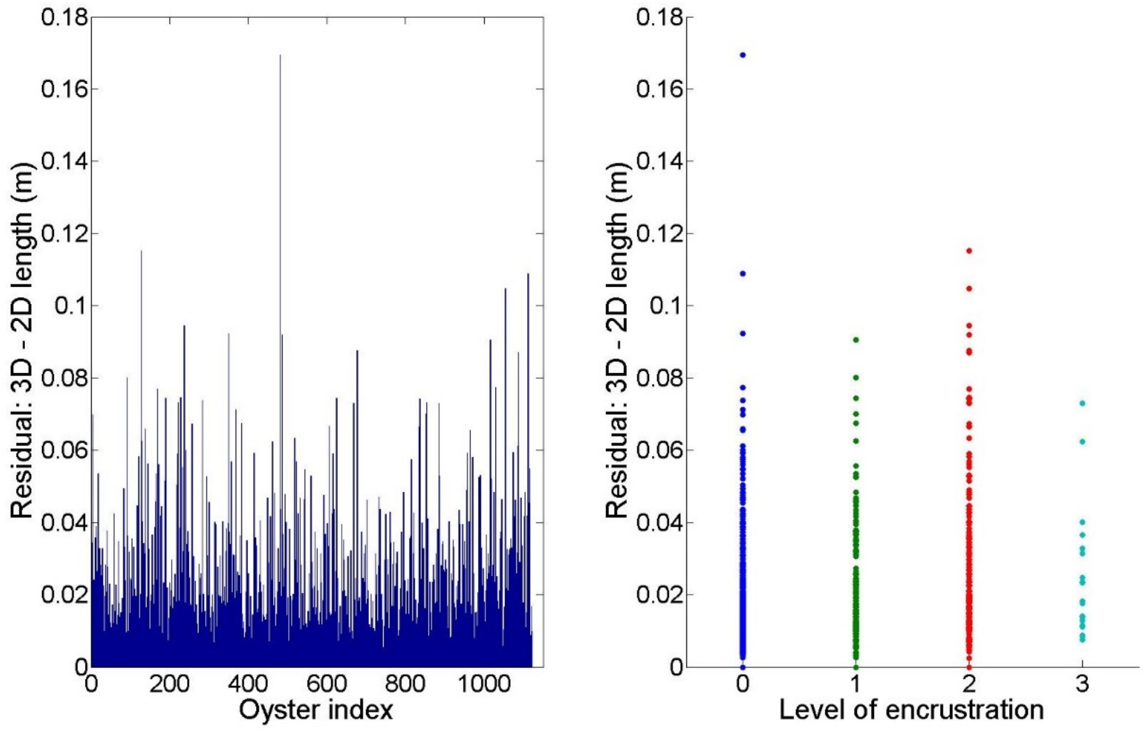

Figure 38: Left: histogram of absolute residuals between 2D and 3D lengths; Right: number of overlaps for each shell among 1121 *Magallana* oysters.

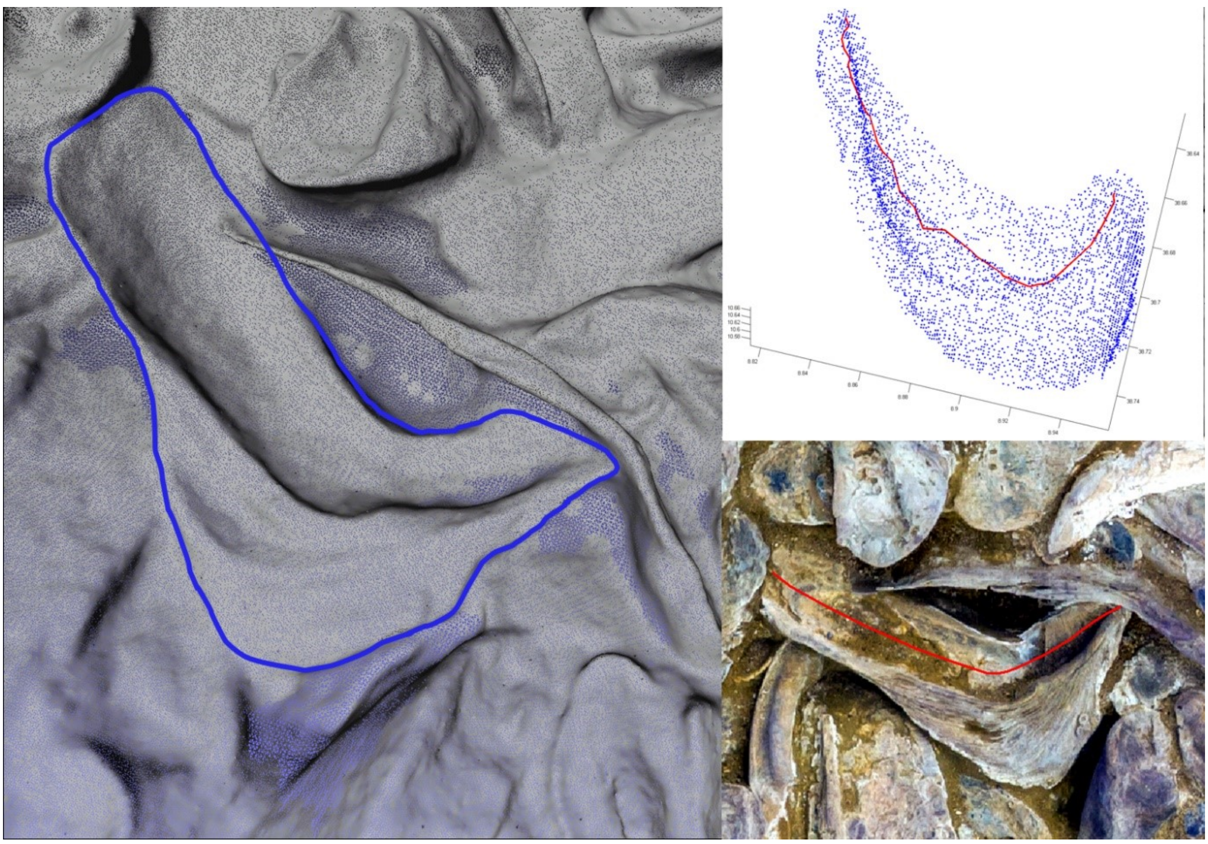

Figure 39: Curved shell mesh model (left); 3D central line and orthophoto (right).

Based on the presented method and results, two hypotheses are validated for evaluation of expectation of potentially strongly curved or (multiple) overlapped shells in dataset:

- Curved specimens are detectable if their residual is larger than 20% of the length and level of overlap is 0.
- The ratio between the level number of specimen and residuals has an impact on encrustation or overlap identification.

Based on comparison between automatically calculated length and 500 references (Table 9), an overestimated result of 101.5% is obtained. Accordingly, the total sum of extracted lengths is equivalent; they are well matching with each other.

Further, in order to check the accuracy of centering, an accumulative, buffer wise approach is applied. We took 6 buffers of 0.5 cm around reference central line and checked their intersection with the extracted line. This approach enables an accurate comparison by taking a total sum of the closest distances from extracted lines to the references (blue, Figure 41).

Table 9: Length differences of 500 shells: reference vs. automatic extraction.

Statistics	Min	Max	Sum [m]	Mean	Std.
Extracted	0.085	0.574	134.235	0.268	0.085
Reference	0.084	0.577	132.253	0.264	0.084

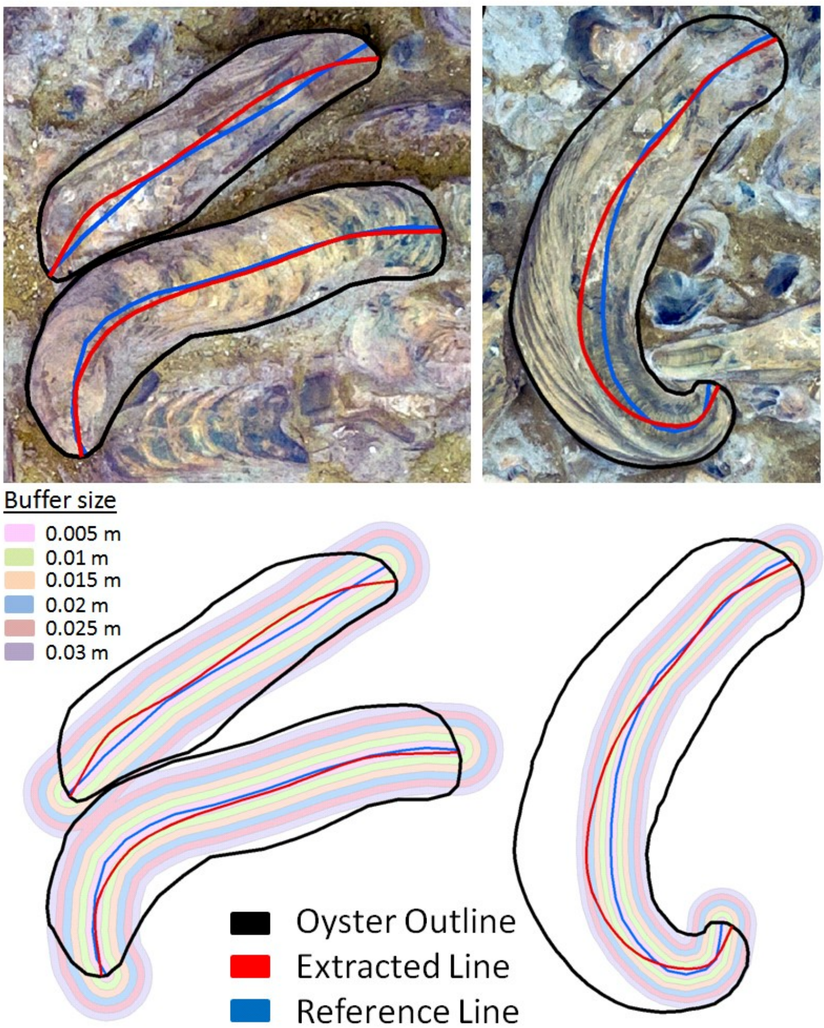

Figure 40: Buffer zones growing around reference central line (blue) and visualized extracted line (red), see also Fig.41.

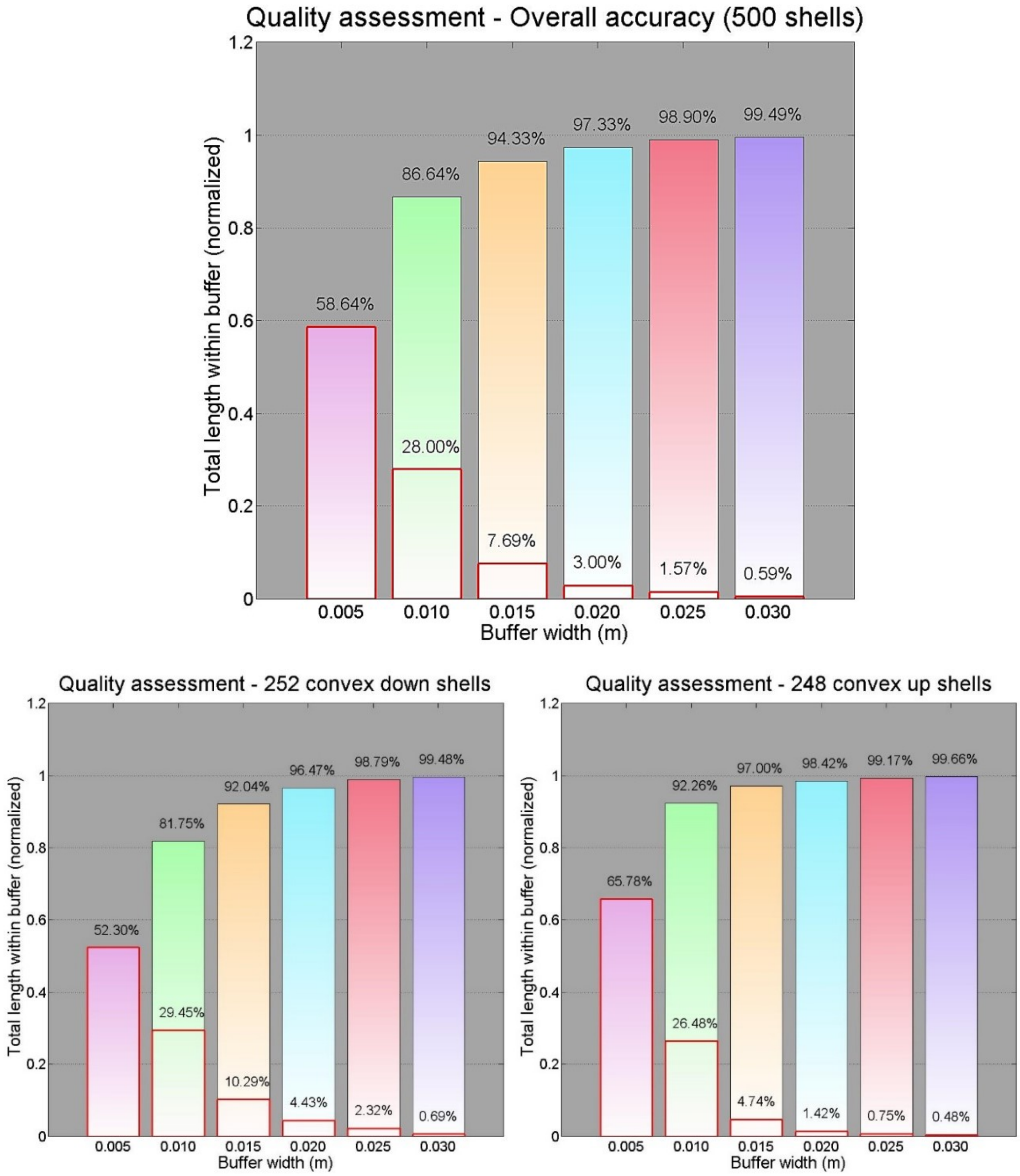

Figure 41: Quality assessment – overall, convex down, convex up accuracy of accumulative (filled bar) and buffer wise (red bar outline) extracted line distribution, see also Fig. 40.

Based on quality assessment, 86% of extracted line lengths are within first two buffers. Beside extracted segments under 0.01 m distance from reference central line, the overall accuracy gives information that all segments are within 0.03 m. Proportion of the length inside the closest buffers to reference line is high, about 58% first and 28% second buffer. In addition, central line extraction of 252 convex down and 248 convex up shells was separately evaluated. Obtained results show that accuracy assessment decreases in case of convex down extractions due to complexity of interior parts of the shell structure.

4.4.2. The volume of oysters

This section presents the outcomes from method`s section 3.5.2. It includes the correlation between shell lengths and areas (4.4.2.1.). Section 4.4.2.2. shows length–frequency and size-frequency data related to length-at-age relationships and size distribution patterns. Section 4.4.2.3. presents the length-at-age relationships for establishing of age classes. In section 4.4.2.4., oyster shell densities are derived from a ratio between chalky and foliate layers in shells. Finally, section 4.4.2.5. presents a summary about the annual carbonite production calculations based on the total shell volume computation. The calculations were carried out for 1121 shells on the reef using density per cubic centimetre. Sections 4.4.2.2., 4.4.2.3., 4.4.2.4. and 4.4.2.5. are mainly led by Mathias Harzhauser based on outcomes from data derived in section 4.4.1.

4.4.2.1. Volume computations of individual shells

The volume of individual shells was computed based on empirical measurements of nine shells using the algorithm of Mirtich (1996), see Figure 42. The volume values are ranging from 108 to 1215 cm^3, see Table 10. The relation between central line length and shell volume is shown on Figure 43. In this figure, there are two shell pairs and their valves are linked; all shells are marked with corresponding side L-left shell, R-right shell.

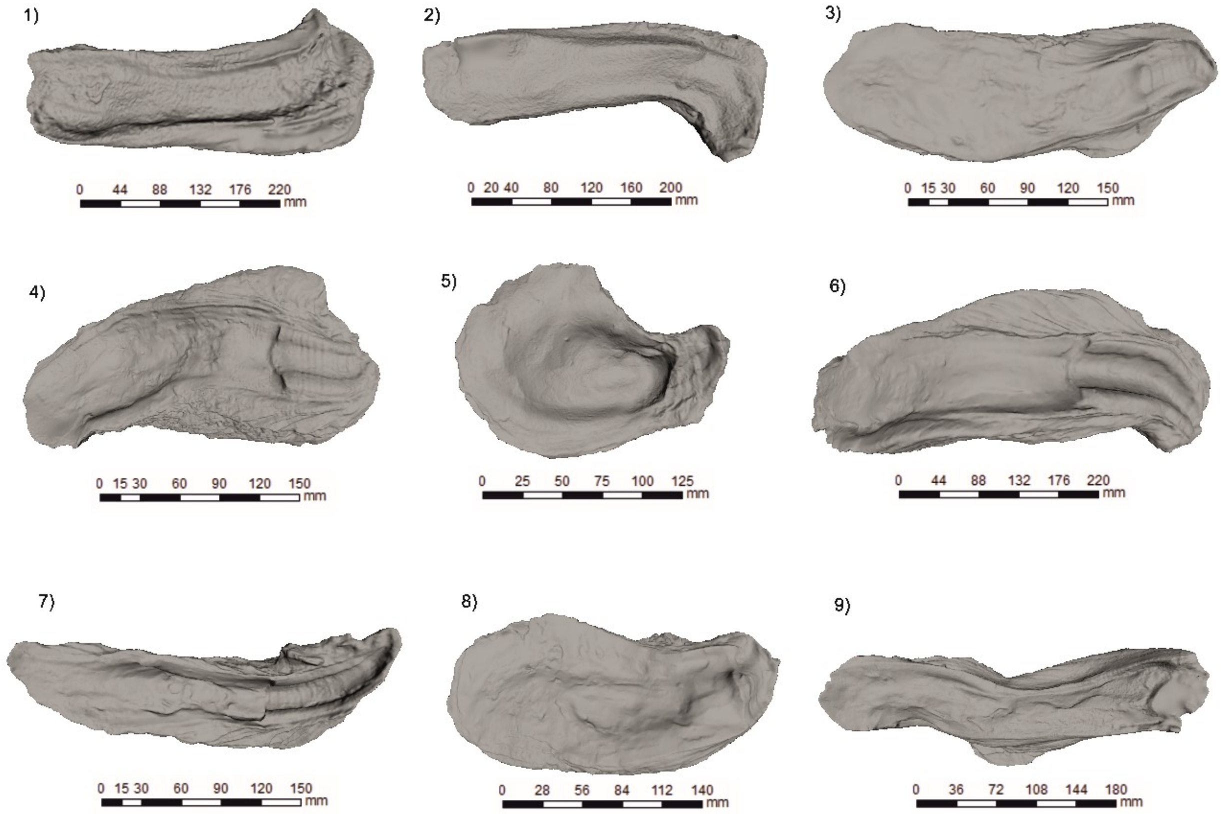

Figure 42: Models of nine shells based on high-resolution laser scanning data of shells from the collections of the Natural History Museum. These specimens document the broad range of morphologies and were used for volume calculations.

Table 10: Volume calculations of nine shells from Figure 42.

ID	Volume [cm³]	Center line length [cm]	Side (Left/Right)
1	1 069,26	39,0	L
2	1.215, 97	40,2	R
3	333,76	25,4	R
4	462,07	26,3	L
5	108,68	14,1	L
6	816,84	40,6	L
7	258,76	27,9	L
8	237,48	21,8	R
9	509,25	32,7	R

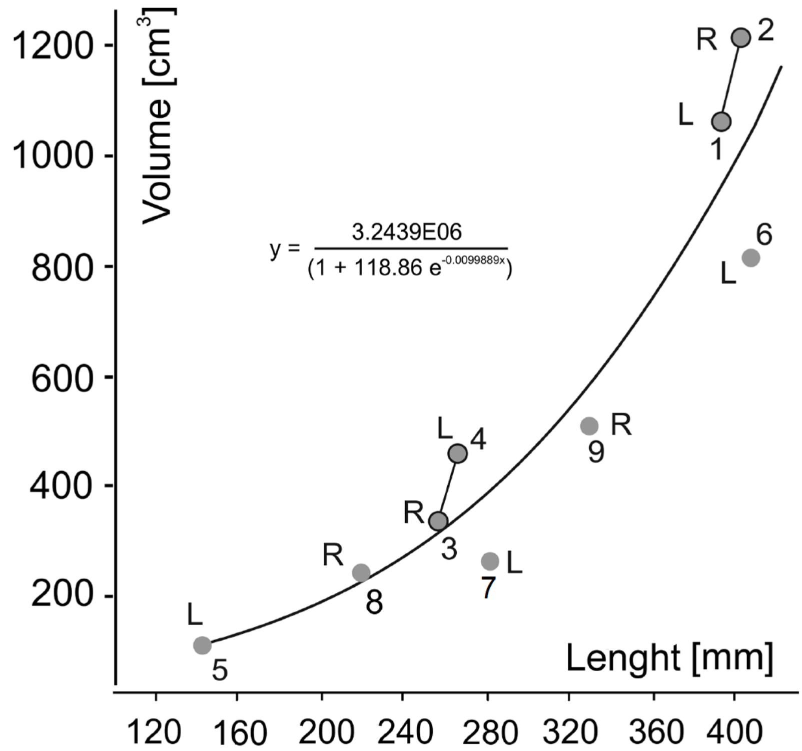

Figure 43: Logistic function showing the relation between central line length and shell volume based on empirical measurements of nine shells (dots); L-left shell, R-right shell; shell pairs are linked; numbers correspond to specimens illustrated in Figure 42. Figure is originally published in Harzhauser et al. (2015).

4.4.2.2. Size–frequency data

The central line lengths of 1121 complete *Magallana* shells, rounded to the nearest mm, range from 48 to 602 mm with a mean of 237 mm (σ = 89 mm) (Figure 44a). The data distribution displays a positive skewness of 0.52 and the Shapiro–Wilk test excludes normal distribution for raw data and log10-transformed measurements. Area data range from 1708 to 56 755 mm^2 with a mean of 16 983 mm^2 (σ = 8414 mm^2) (Figure 44b). These data show also a positive skewness (0.83) and normal distribution is rejected by the Shapiro–Wilk test.

Based on the manual outlines, the exposed shell area can be deduced directly. Area data are slightly underestimated because shells are not always exposed parallel to the bedding plane but may be somewhat oblique. Despite the fact that area data are somewhat biased by oblique shells, the correlation between central line lengths and areas is highly significant (raw data: r = 0.92, p<0.001; log10-transformed: r =0.93, p<0.001) (Figure 45).

The size–frequency data refer to length and shell area. Figure 44 shows the size distribution, size–frequency diagrams, for central line length and area data with cohorts (dashed lines) as detected by mixture analysis. Fragments distribution (n =7047) is separated from the size distribution pattern of complete shells (n= 1121) (Figure 44c). Figure 45 shows a significant correlation between length and area of complete shells in regression analysis.

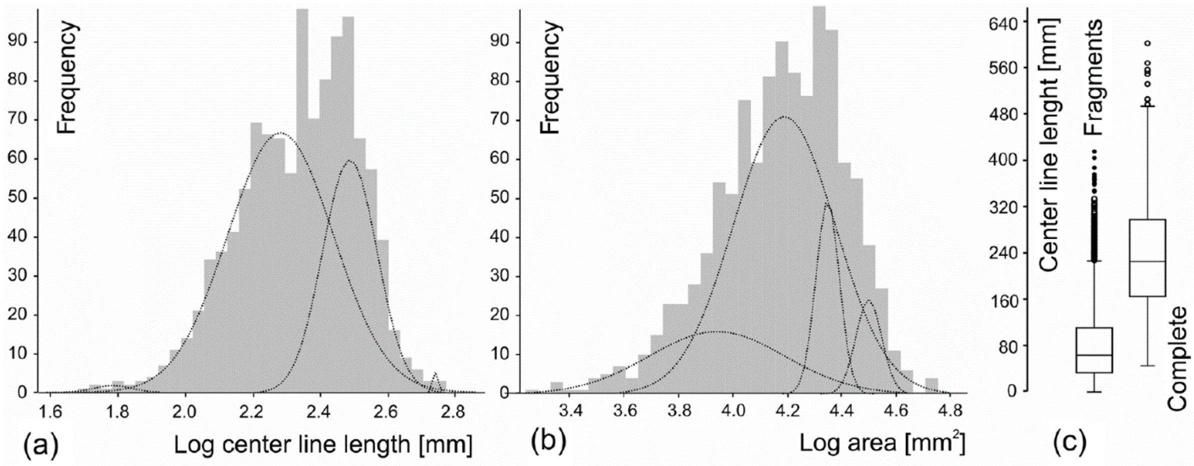

Figure 44: Size–frequency diagrams for central line length and area data (log transformed) with cohorts (dashed lines) as detected by mixture analysis (a, b). Box-plot illustrating the strongly right-skewed distribution for fragments (n =7047) and a clear separation from the size distribution pattern of complete shells (n= 1121) (c). Figure is originally published in Harzhauser et al. (2015).

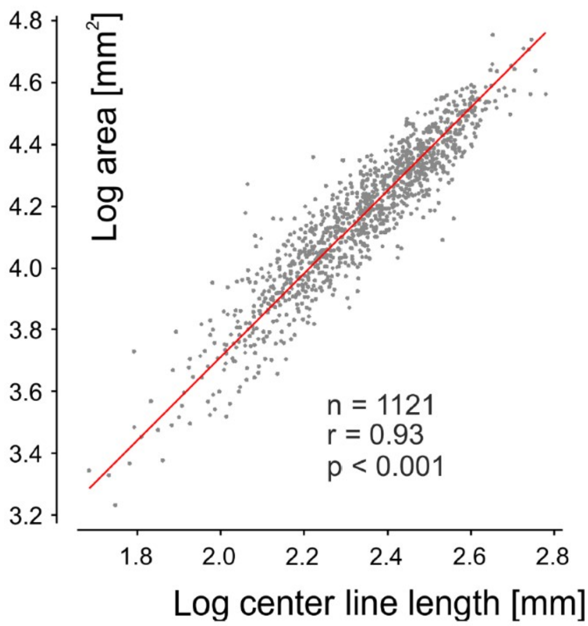

Figure 45: Regression analysis revealing a significant correlation between length and area of complete shells. Figure is originally published in Harzhauser et al. (2015).

4.4.2.3. *Length–frequency data*

Four distinct cohorts (dashed lines in Figure 44) are detected by mixture analysis. For extant *Magallana* reefs, the analysis of the cohorts is routinely performed using Bhattacharya's model or the EM-Algorithm of Dempster et al. (1977), which tries to detect normal distributions within the length–frequency data. Consequently, in order to test for cohort mixing, lengths of *M. gryphoides* were subjected to mixture analysis, a maximum-likelihood method for estimating the parameters of two or more univariate normal distributions, based on a pooled univariate sample (Hammer, 2015). Statistical analyses were performed in PAST versions 2.17c and 3.06 (Hammer et al., 2001). Akaike's information criterion (AIC) was used to test the goodness of fit of the maximum likelihood estimates to the length–frequency data.

In log10-transformed length frequency diagrams, the maximum likelihood based analysis reveals lowest AIC values for four or five cohorts. Similarly, log-transformed area data have lowest AIC values if four or five cohorts are detected. The assumption of more groups does not lower the AIC, or the computed cohorts comprise unrealistic narrow cohort ranges, which are nested within larger ones.

4.4.2.4. *Age classes*

Based on the assumption that the size–frequency groups represent age classes it is apparent to establish length-at-age relationships. Applying the von Bertalanffy equation to the length data reveals a strongly right-skewed distribution with 50% of the shells ranging between 3 and 6 years (Figure 46). The frequency of specimens between 6 and 9 years decreases rapidly and the contribution by shells older than 9 years is subordinate although outliers with up to 16 years occur. Again the non-normal distribution of the von Bertalanffy growth model data suggests cohort mixing and the mixture analysis assumes at least four significant cohorts with low AIC value. Due to the rareness of large and aged shells, the fourth cohort displays a rather low amplitude and we assume that at least two natural cohorts may be amalgamated in this group. This suggests that more or less continuous recruitment accentuated by very successful settlement peaks every 2 or 3 years.

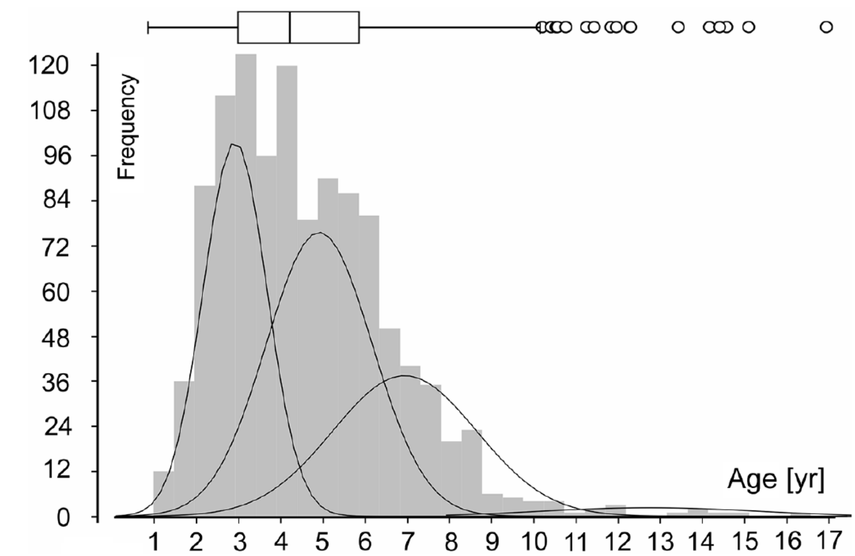

Figure 46: Age–frequency data and box-plot of the shells based on center length data transformed with the von Bertalanffy growth equation. Four cohorts are detected by mixture analysis. Figure is originally published in Harzhauser et al. (2015).

4.4.2.5. *Shell density*

The shell density in *Magallana* species was estimated by taking the ratio between chalky and foliate oyster shell layers (Figure 47). The average density estimate was calculated to be about 1.82 g cm^{-3} for one valve of *Magallana* shell.

The image analysis of the cross-section documents proportions of 64 chalky to 36% foliate layers for the right shell and of 61 to 39% for the left shell. This is determined automatically according to ratio between dark and gray pixels in the cross-section. The density of the chalky layer when wet ranges around 1.15–1.32 g cm^{-3} (Chinzei, 1995) and the density of the foliate layer ranges around 2.2–2.5 g cm^{-3} (Chinzei, 1995; Yoon et al., 2003) and has a clear upper limit by the density of calcite (2.7 g cm^{-3}). Using 1.2 for the chalky layer and 2.2 g cm^{-3} for the foliate layer as rough estimates, mean density results in 1.84 and 1.81 g cm^{-3} for the right and left valves, respectively. Shell density in *Magallan*a species is independent of age and size (Lombardi et al., 2013) and therefore the density estimates are applied to the entire data set.

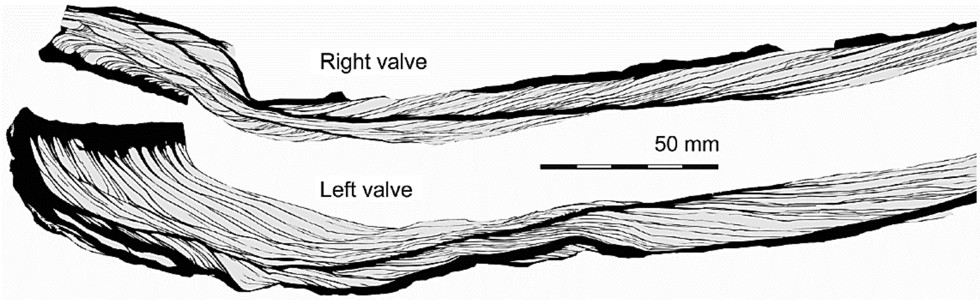

Figure 47: Longitudinal section through *M. gryphoides* from the oyster reef site showing the high amount of chalky layers (gray) and the low amount of foliate layers (black). Figure is originally published in Harzhauser et al. (2015).

4.4.2.6. *Volume and carbonate mass computations for shells on the reef*

Information about the annual carbonate production per shell per year is derived based on a volume and shell density estimate (the density of about 1.82 g cm^{-3} is estimated for *Magallana gryphoides*).

Applying the equation (8) to all shells results in a total volume of 393 273 cm^3 with a mean shell volume of 350.8 cm^3 (σ =313.7). These values do not change significantly if a non-linear Gompertz growth model is assumed as frequently done for *Crassostrea*[8] (Lopes et al., 2013; Ginger et al., 2013). The respective equation

$$\vartheta = 1.978E08_{e} - 9.1404e^{0.0013762\,x}, (23)$$

results in a total volume of 398 474 cm^3. Applying the average shell gravity of 1.82 gcm^{-3}, which is estimated in section 4.4.2.4., results in a total carbonate mass of ~715 kg (logistic) to ~725 kg (Gompertz) for dataset of 1121 shells. Thus, based on the age models of the shells, the annual carbonate production per shell was calculated, which ranges from 74 (σ = 2.9) (Gompertz) to 83 gyr^{-1} (σ = 2.8) (logistic), accounting for ~150 gyr^{-1} per living oyster individual (i.e., two valves).

The most populated areas within the shell bed had more than 100 individuals per m^2. On average, shell density is 129 shells (~64 individuals) per m^2 (including also moderately fragmented

[8] *Crassostrea gryphoides* (Schlotheim 1813) has been moved to the genus *Magallana*.

shells). This would point to a hypothetic annual carbonate production of up to 15 kgm^{-2} with the oyster reef. Although this calculation is just a very rough estimate, it indicates that the carbonate production is in the range of fast growing coral reefs with productions of 6–10 kgm^{-2} yr^{-1} (Montaggioni, 2005; Jones et al., 2015). A major difference, however, is the rapid shell loss in *Magallana*[8] reefs, which prevents the formation of rigid and stable structures comparable to coral reefs.

5 Discussion

5.1. General discussion

The main goal of the research project is to demonstrate an interdisciplinary method to digitize, detect shape, estimate size, and calculate 3D-orientations of elongated objects (fossilized oyster shells) from a densely packed shell bed based on approaches developed in photogrammetry. This overall goal was divided in separate research questions. For each it was necessary to select and develop an appropriate approach to reach the defined goal. The following sections will go through each pair-wise Photogrammetry – Geology question presented in the Introduction and discuss how the selected approaches succeeded in answering the research questions.

The selected order is used for going through the questions not based on published works, but based on possible automatization of the processes and derivation of information. Therefore, extraction of individual oysters is prioritized, because as soon as we have adequate shell outline, then we can use it for the work on estimation of shell size, distribution, orientation or encrustation.

5.2. Discussion on the research questions

- Q Photo – Can we extract individual oysters from point clouds automatically, and with which quality?

We developed a method to identify and enumerate convex parts of the shells automatically. The method is based on geometric feature extraction, morphological operations (Heijmans, 1994), and connected component analysis. This was possible as the entire site has been surveyed by terrestrial laser scanning and digital imagery, providing point cloud data of one billion points with an average resolution of 1 mm and orthophoto with resolution of 0.5 mm. Then, an experiment on automatic analysis of high-resolution laser scanning data was performed, in which geomorphometric derivatives were calculated, such as openness (convexity/concavity). The performed quality assessment resulted in 69% successful detections based on shell surface matching and over 98% based on number of detected objects. The manually derived reference data were used to crosscheck and validate these results. In order to provide reference data, the following parameters had to be extracted: distinguishment of different taxa, fragmentation stage, shell sides, presence of other patterns on the oyster shells such as abrasion and bioerosion, and recognition of settlement on oyster shells of barnacles and other specimen.

Earlier literature and our studies have shown that the openness feature works very well in describing the oyster reef surface and supports visualization of the oyster reef terrain (Yokoyama et al., 2002; Doneus, 2013). In our studies, convex-up surfaces (negative openness) provide information about the respective exterior parts of the shells, which are more dominant on the reef than interior parts, convex-down surfaces (positive openness). However, after applying the negative openness feature, the method worked insufficiently for convex-down oriented shells, because the interior parts of those shells may have concave geometries. Hence, convex-down shells were partly detected via a border band (Figure 4, Article III), while information from the interior part was missing. Therefore, mathematical morphological operations such as flood-fill and majority filter improved the completeness of the results and helped to better structure connected components. Thereby, the outlines of the oyster shells were smoothed, noise was minimized, and small remaining gaps were filled exactly inside the concave shells and not in the other concave parts of the surrounding terrain. This approach proved to be effective, since concave (i.e., convex-down) shells have noticeably narrow convex borders that form mostly closed components (approximately elliptical rings).

Kernel-size optimization has a large influence on the results. Hence, here is the fact which should be considered when choosing the best approach to select the kernel value based on the studies. For example, loss of information might occur if the kernel size is enlarging, because increasing the neighborhood size corresponds to the scale of surface roughness. The value of the kernel size should not be too large (e.g., not larger than the width of the shell), if the aim is to capture details on the reef, such as low or moderate fragmentation of specimens.

Separation of overlapping parts still remains a work in progress due to the shell border interruptions between underlying shells and due to many irregular protruding parts. A possible approach to handle this non-trivial difficulty in future work is to investigate usage of more features, such as radiometrically corrected intensity data. Solving the problem of overlapping shell parts should improve 69% of shell surface matching to become more successful, over 85%.

- Q Geology – What is the specimen distribution (age, size, species, etc.)?

Our study aimed at high-resolution digital documentation of the world's largest known fossil oyster reef, comprising thousands of shells of *Magallana gryphoides*. This question initiated research needs such as data acquisition and processing to maximize scanning efficiency of the very complex surface. Additional challenges in data collection were caused by low visibility, tilted geometry of the site, and restricted access to the surface. By using a sophisticated configuration of TLS, image acquisition, and processing, 83 individual scan positions were acquired, together with 300 images, and 40 measured ground control points (GCPs). GCP information was used to make transforms from the acquisition coordinate system into a local analysis coordinate system, as well as in to UTM.

To make the captured surface understandable and accessible to the scientific community, various visualization techniques have been applied including 3D triangulated surfaces, shaded digital surface models, and color-coded relief models. The importance of making the data of the reef surface openly available for the scientific community is to approach the dataset from a different perspective to those who collected it. The benefits of open oyster reef data are replicability, reproducibility, and reusability used for paleontological, geological or sedimentological analysis. There are multiple reasons for these analysis: to identify something what was not researched before and to create new values of it. We showed that digitized reef data can be used for monitoring network of fault lines and their spatial relations with individual shells. This is an ideal example of how data that is collected for a given purpose, such as individual object detection, can be reused in creative ways for novel purposes.

For automated analysis of the oysters on the reef, the detection of individual objects is necessary. For this, the goal of applying openness feature was achieved in practice by using a method implemented in scientific software OPALS. It provided a raster map of local viewsheds (i.e. openness) based on a DTM grid model which was not enought itself for shell delineation but it had to be processed further on based on morphological operations and connected component analysis. For the purpose of evaluation of our method, the automatically detected shells were comapared against corresponding reference data. Reference data for object delineation was obtained manually for 10,284 objects. The majority of objects represent *Magallana gryphoides*, which is also the largest species found on the oyster reef. The brownish and massive calcitic oyster shells are represented exclusively by disarticulated single valves. These particular species have specific importance as evidence of reef formation in an Early Miocene estuary of the Paratethys Sea. Expert knowledge is used to detect and outline the individual shell correctly and to determine its parameters—species; level of overlap; shell side (left, right, unknown); orientation (convex side up/down, not known); fragmentation (complete, low, moderate, high); and tile number. These parapmeters are standard, but it is difficult to obtain them on the field due large number of shells and limit access to protected site. Digitization of the validation data was performed manually in ArcGIS, producing vector data stored as shape files. The fastest digitization was achieved with the shaded relief of the DSM as the bottom layer, a semi-transparent orthophoto superimposed onto it, and the previously digitized outlines on the top most layer. A similar presentation of a fossilized reef has not been done before and the benefits of the digitalizations are multiple, e.g. possibility to do reanalysis, experts can extract data faster than on the site manually, data sharing, data visualizations, etc.

A near normal distribution of shell sizes and the balanced ratio between left and right valves reflected the original age structure of the oyster biostrome. The near normal distribution was not expected, but it might be explain by limited growth for bivalves living in the intertidal zone (Strayer et al., 1996). Their vertical growth is limited, and larvae have little possibility to settle in the densely packed structure. The near equal contribution by left and right valves points to the preservation of the primary composition and contradicts the hypothesis of hydrodynamic sorting and selective transport introduced in work of Harzhauser et al. (2015). The data collection technique possibly affects this result, because the data is collected remotely and contactless, which in practice means that only shells with visible interior side on orthophoto and DSM are examined and sorted as left or right valves. Shells with visible exterior side, i.e. convex up position, are not possible to be examined for their side without removing them first from the site to turn them around. This would be however very laborious and destructive to the reef bed.

Original hypothesis was based on the study of Kidwell and Bosence (1991) who interpreted that water energy was high enough to favor the preservation in stable position such as convex-up position. This hypothesis was confirmed since the significant dominance of convex-up positions is present in most tiles. In addition, the stable convex-up position increases significantly with shell density. This may indicate that high water energy led to a denser accumulation and simultaneously turned over convex-down shells into the stable position. The distribution of fragmentation, in contrast, is less homogeneous, southern and central tiles contain high fragmented shells while north, west and east tiles have fewer fragments. Overall, only 25% of the shells display no or only low damage and fragmentation. Another 20% are moderately well preserved, and the majority (55%) comprise highly fragmented specimens. The largest recognized complete specimen is 60.1 cm in length. The mean central line length is 23.7 cm (σ = 9 cm). This implicates that *Magallana gryphoides* is the fastest growing and largest *Magallana* known so far, it is exceptionally large species.

- Q Photo – How to characterize and extract orientation of specimen?

High resolution digitized data makes it possible to present the reef in a standardized coordinate systems which allows new possibilities in making GIS based analyses (spatial distributions, fault/shell relations, etc.). The selection of LACS helped in characterizing the specimen orientation analysis, because it presents reference coordinate system and it was used as well as the individual shell coordinate system to set the orientation of an oyster shell. The orientation was specified using standard aerial photogrammetry principle angles and used further in determining the rotations of complex objects. Those principal rotations are known as yaw, pitch, and roll angle and they were the most practical way to describe the orientation of a 3D oyster in any orientation. A mathematical method was developed to distinguish individual shell rotation angles assuming that the beginning and the ending of a shell were known. This developed method had acceptable performance and other methods were not looked into. However, the beginning/end information were extracted manually for convex-up and –down shells, because the automation was not technically possible with the present data for convex-up shells, only for convex-down shells where interior side of a shell was clearly visible. The automation should be studied further based on a geometry of a shell outline or their lateral margins and contextual knowledge about the hinge position (beginning of a shell) or muscle footprint (ending of a shell). Textured point clouds might be helpful for muscle footprints.

- Q Geology – Was it a storm or a tsunami that triggered shell bed formation?

The shell bed is an event deposit resulting from a high-energy process of short duration. This implies that the shell bed might have been formed after a storm or a tsunami. The hypothesis is made based on the information on tsunami event frequency on a geological scale. About 500,000 tsunamis may be expected globally per 1 million years based on calculations of Scheffers and Kelletat (2003). Moreover, the reef was located on a seismically active area during the late Early Miocene and earthquakes could have likely triggered high-energy hydrodynamic events frequently.

The differentiation between tsunami-generated deposits and storm deposits is difficult. Nearly all sedimentary signatures reported in the literature to characterize tsunami-generated deposits are opposed by contradicting cases. This casts doubt on simple models. Morton et al. (2007), Engel and Brückner (2011), Goff et al. (2012) and Shanmugam (2012) provide extensive reviews and examples on the subject. Studies on coastal tsunami versus storm deposits of Bourgeois (2009) suggest that wedge-like bed-load dominated deposits are more typical for storms, whereas sheet-like, suspended-load dominated deposits point to tsunamis.

The oyster shells in the event-bed lack a significant orientation of the yaw angles. This suggests a complete loss of potential current patterns related to the storm or tsunami event that formed the shell bed during a longer phase of exposure. Based on the large data set on the orientation, the reported weak preponderance of W-E orientations was shown to be statistically insignificant. The random distribution of the pitch and roll angles clearly excludes any imbrication fabrics, which could have been related to tsunami- or storm generated surge currents. Therefore, based on the analyzed data, the event cannot be clearly associated with a tsunami or an exceptional storm. Although the high-energy event might be expected to have had a directional force, no distinct main orientation pattern is preserved in the shell bed. Most of the analyzed 6 m^2 tiles suggest significant orientations of the shells, which often are in conflict with predominant orientations in neighboring tiles. We concluded that such patterns result from “forced alignments” of elongate shells due to their spatial density, occasional movement by waves or currents, and due to bioturbation by vertebrates. In particular, the attempt to use shell beds as indicators for tsunami may be difficult due to severe post-event modifications of the primary patterns. Similarly, reconstructions of paleo-currents based on single-area data sets are very dangerous.

- Q Photo – How can we detect encrustation of shells?

Our method to develop to detect central lines of oyster shells was used for various shapes and sizes with LiDAR-obtained 3D point cloud data. The accurate computation of the central line of each oyster of the reef included two-dimensional and three-dimensional central line. Their lengths are compared in order to visualize possible differences between 2D and 3D lengths. Differences (residuals) support automatic discovering of strongly curved shells and potential encrustation of *Magallana* by *Ostrea*, *Venerupis* or any other type of shells or even fragments.

The relationship between residuals of 2D and 3D central line lengths and number of shell overlap levels were examined. Significant deviations of 2D/3D ratio work as a good quality estimator. Some key findings are emphasized herein:

i) certain central line properties such as residuals (3D-2D length) have direct relationship with the encrustation estimates;

ii) the ratio between the level number of specimen (multiple overlap) and residuals of the central line lenghts have an impact on encrustation identification;

iii) normalized residuals under 20% of lengths and over 20% differences indicate possibility of multiple overlaps or strong curvatures.

The central line length differences are interpreted as a consequence of many height surface variations. The shells with differences under 20% are a group of oysters with no encrustation (i.e. overlap) which are laying on the uppermost surface of the reef bed or are surrounded by sand. The shells with differences over 20% are typically overlapped with another shell, barnacles, and fragments, or they present shells with strong curvature.

The algorithm developed in oyster reef study points out multiple overlaps and strongly curved shells in order to identify them. The obtained information is sufficient to support paleontological experts during interpretation and to document the presence of encrustation on the oyster shells. The method is not a general, it needs specific adjusting when applying in other cases (with prerequisites such as 2D and 3D lengths of object and possible information about level of overlap).

- Q Geology – Which visible patterns in the shell bed occurred pre- and which during post-event?

Patterns which are observed on the shell surface are a consequence of other species settlement, predators, hydrodynamics, weathering or the strongly wave-exposed shells. Bioturbation in shallow marine settings is a common phenomenon from animals such as rays, turtles and teleost fishes. Many other taxa are found within the reef beside dead *Magallana* shells, because different habitats are mixed due to different ecological requirements of the species. For example, on the inner surface of *Magallana* shells settlement of *Ostrea* took place after the death of the *Magallana* specimens. In total, 55% of data consists highly fragmented specimens. The tested methodology helped in determination of fragment sizes and stage. Then, it was interpreted that the main cause for fragmentation was a predatory and being exposed to water energy breakage while shells were alive. During the excavation of the reef, artificial fragmentation did not occur, therefore shells and fragments remained in their original position. A near normal distribution of shell sizes and the balanced ratio between left and right valves still reflects the original age structure of the oyster reef. The convex-up (CU) valve position predominates along the N–S transect, CU shells occur up to twice as often as the convex-down shells (with a slight decreasing trend).

The shells are now catalogued and located from the DSM and orthophoto data, and further stored in a database. This allows paleontologists to interpret the patterns on the reef without needing to visit the site itself. They are able to make spatial queries and visualize them on the distance map or other specific thematic map for paleontological purposes. Visual inspection of the site from digital data is an advantage comparing to traditional measurements on the oyster reef that are limited by X, Y, and Z.

6 Conclusions and Future Research

The workflow developed for the data collection was successful. The entire site was surveyed by terrestrial laser scanning and digital imagery at resolutions of 1 mm and 0.5 mm, which formed the basis for analysis in further steps. However, intensity values acquired with terrestrial laser scanning were only used in scan registration and they were not exploited, corrected or systematically investigated in further steps. The quality of intensity values could be helpful in future studies since these information support the visual analysis of a point cloud, and have thus potential for more sophisticated applications such as classifying objects by their surface material properties (Pfeifer et al., 2007; Pesci and Teza, 2008; Burton et al., 2011; Kaasalainen et al., 2011).

The method developed to extract oysters automatically from the reef performed with sufficient accuracy to make an objective estimation of the object number on the reef. It would still require additional work to improve the completeness results of oyster shell surface extraction. The obtained results were promising at the level of 69% in shell surface matching, but the level of 85% or more should be reached for more operative use. The method developed to detect oyster shell orientations worked on acceptable level when the beginning of shell growth (position of the hinge) and the ending of shell (position of the muscle) were predefined. However, our results were not able to support the hypothesis if the shell bed was formed because of a storm or a tsunami, because the preponderance of W-E orientations was weak and no clear directional domination was detected. The method developed to detect shell encrustation gave promising results which help in determining the separation between pre- and post-event patterns. The method works if the information on multiple overlap is available and if the residual between the 2D and the 3D central line lengths is significant (about 20% of shell length).

The method based on openness feature and used in outlining the oyster shells from their background was found to be promising, but it still leaves room for improvement regarding the completeness and the correctness of the results to be suitable for operative usage. Especially difficult case was one where the method was used in detecting objects with smooth continuous borders but without interior gaps. Finding such objects might be possible in future by testing new combinations of additional features/attributes like by involving intensity information. For the purposes of the thesis, manually delineated oyster shell outlines were used instead as an alternative to the automatically detected outlines to allow development of further analysis tools, such as central line estimation of shells and their length. The manual outlines were also used in extracting points to calculate the 3D-rotations of individual oyster shells. Development of these tools were successful and they helped to rise new research questions. For instance, the oyster shell length information can be combined with volume calculation to estimate the oyster shell ages. Furthermore, knowledge on individual oyster shell rotations were used in combination with the fault lines locations (Molnár et al., 2015) in order to establish a relationship between the fault lines and shells with emphasized rotation angles. These combined information allow to document better shell related anomalies and possible postsedimentary vertical displacement related to the faults.

Overall, the following successful parts of the research done for this thesis are summarized here:

- The main novelty in this thesis is the usage of remote mapping techniques in providing high-resolution digital documentation of complex geometrical surface.
- Terrestrial laser scanning is tested and documented for the first time on this extent as a method to handle large paleontological datasets. The future aim would be to replace manual in-situ surveys and enable the palaeontologist to benefit of using novel representations based on the digitally documented data.
- The research work created a dataset of a single Miocene shell bed with 10,283 manually outlined objects and presented it in a standardized GIS framework. The dataset enables making different spatial data queries such as taphonomic maps, distribution of left and right shells, and distribution of convex up and convex down shells, distance maps, and other specifically attributed thematic maps for geological purposes. The dataset also allows to work with other descriptive attributes like geological features including abrasion or bioerosion, sediment coverage (yes/no), and encrustration by barnacles or another oyster (yes/no). The fully digital representation of the reef also helps to preserve it as new attributes can be extracted directly from the dataset without disturbing the reef itself.
- New automatized methods were developed to estimate parameters such as shell length, area and volume in order to derive age structure, carbonate production and shell loss rate. Accurate collection of these features would not be feasible without the reef digitation.
- A method to detect oyster shells from their background with 69% success ratio that was based on shell surface matching. Over 98% of the detected objects were correct as verified with a manual quality assessment.
- A study that demonstrated the possibility to automatically extract 3D central lines from the variable shapes of fossilized oyster shells. The 3D central line lengths support the automatic determination of shell sizes.
- How the 3D-rotation angles of individual oyster shells can be used in combination with their location to find similarly aligned orientation patterns which help in interpreting the reef dynamics.
- Digitization of the reef helps to promote the results by making them more intuitive and easier for the public to approach and to interact. The geotainment-park in Stetten and the Museum of the Natural History visitors benefit from the opportunity to search, zoom

and study a virtual oyster reef by making spatial data queries that visualize different spatial layers.

- As summary, the main benefits of this thesis are the new research methods and questions found during the research project, as well as the material and presentations for edutainment geopark that are made openly available at PANGAEA (includes digital surface model, orthophotos and corresponding hillshade data — Djuricic et al., 2016b).

Successful parts of the research opened new possibilities for further development. For example, the central line research work can be extended to obtain point sets in the vicinity of the central line and use their properties to describe relations between the point sets as statistical distributions. The point-based neighbourhood information can be extracted from surrounding points by calculating several geometrical features (planarity, sphericity, etc.) from them. The neighbourhood information dependency on the neighborhood size is expected to be correlated with the oyster shell surface roughness, which is a significant marker for analyzing bioerosion and abrasion on the world's largest fossil oyster reef.

At present, the whole oyster reef information is not presented on interactive maps. The future aim is to extend the spatial and non-spatial attributes available for all tiles through GIS database. The GIS database is an ideal candidate for interpretative mapping and outlining of small objects such as fossil shells as it integrates different map layers which contain different information about the mapped area. Addition of new attributes and their relationships to the database will be followed by creation of new thematic maps that increase possibilities to extract additional information from the world's largest fossil oyster reef.

One such possibility is pairing of oyster shells which requires studying properties that would match the left-sided shells with the right-sided ones. Further studies should aim to develop potential methods that match and link spatially separated oyster halves together. One potential approach would be to check if the oyster half surface properties have enough feature correspondences along their central line profiles. A successful method capable of matching object pieces over distance would provide important support in making spatial interpretations and objects visualizations for several disciplines, including geology, palaeontology, and biology.

In retrospect, it can be concluded that terrestrial laser scanning is an appropriate tool to document complex geological structures like the world's largest fossil oyster reef investigated here. This conclusion is based on considering how well the research questions and the aims of the project Smart-Geology were answered during the project. The laser scanning data were supported with photos that were also acquired to generate high-resolution orthophoto. The photograph content was helpful and necessary for the manual interpretation and validation of shell delineation, oyster shell side determination, and in detecting encrustation and other features of the shell bed. Image information was also used in generating the textured 3D models of the reef for visualization purposes (Harzhauser et al., 2015, 2016; Djuricic et al., 2016a).

While the imaging information was helpful, the main source of information in the research project were the automatically derived features that relied on the geometric content of objects. These could only be provided with terrestrial laser scanning. This thesis applied for the first time terrestrial laser scanning for monitoring a fossilized oyster reef with an unprecedented accuracy of one-millimeter resolution for paleontological research. The complex surface structure of the oyster reef and the self-similarity between the objects on it rendered the automatic bundle block adjustment methods infeasible. Individual oyster shells were detected by segmenting the 3D point cloud data into meaningful regions that represented particular shell borders. Automation of the procedure reached an accuracy of 69% of the manually acquired reference data.

To obtain shell length, new method was developed to derive 3D central lines of various oyster shapes and sizes. More than 86% of automatically extracted central lines were displaced less than 1 cm from manually drawn reference lines. Central line lengths and accurate volume calculations were used in establishing a relationship to determine oyster age classes. This helped in estimating the annual carbonate production per shell that was indicated the fastest growing and largest oyster species known so far. To interpret transport direction or presence of imbrication, a new method was created to calculate rotation angles (roll, pitch, and yaw) of oysters represented as 3D point cloud in a Cartesian coordinate system. Additionally, the influence of fault lines present in the reef were tested on strongly tilted oyster shells for the first time.

A very important outcome of this project and PhD thesis is the digital documentation of the shell bed in high resolution (Djuricic et al., 2016b), which should be used to test future approaches from photogrammetry community or may help paleontologists for the new interpretations. The accurate documentation of the structural information allowed to create the first GIS database for the protected natural heritage site and enables to design novel thematic maps that link individual shells with their spatial and descriptive attributes without disturbing the site.

Acknowledgements

This thesis presents the research I have conducted at the Research Groups Photogrammetry and Remote Sensing, Department of Geodesy and Geoinformation (GEO), Faculty of Mathematics and Geoinformation, Technische Universität Wien (TU Wien) in cooperation with Natural History Museum Vienna (NHM), Geological-Paleontological Department. I am grateful for the funding provided by Austrian Science Fund (FWF project no. P 25883-N29 "Smart-Geology für das größte fossile Austernriff der Welt").

I would first like to thank my thesis supervisors Professor Norbert Pfeifer at TU Wien and Mathias Harzhauser at NHM Vienna for giving me the chance to be under their guidance through five years of research. Norbert's office door was always open whenever I had a question about my research or writing without making an appointment in advance. He was always reading the first version of my text and cut forty per cent out of it without losing anything important. Actually, he managed to make it more technical and provide valuable feedback. I am glad he did it. He gave me the right instruction about the PhD goals. I would like extend my gratitude to the supervisor Mathias who gave me dynamical and straightforward tasks, so we published the first two papers in almost no time. He was the project leader. Without his expertise and deep knowledge I would not have been able to choose the right direction for investigations. I was processing data, designing visualizations and put in narrative part, but then he brought his academic style of writing into it and all his storytelling abilities made the work scientifically valuable. I want to thank him for involving me in media performances at TV and Radio as well as nominating and believing in me during *Carl von Schreibers Forschungspreis* price presentation. If you are ever lucky enough to be able to work with him, take the chance! His stories and humour are unforgettable.

Doing science is harder than I thought, especially writing text in academic technical style instead of my prosaic writing. Not to mention all those following review rounds that I could not have ever imagined! Therefore, true friendships which you make during this long journey are what help you to go on, with its all ups and downs. Thank you Slavica and Kristina for cheering me up all the time!

I would like to thank Sajid Ghuffar whom I first met, when I moved to Vienna during MSc thesis research. Our friendship continued also during PhD studies; he was in the first semester my office mate and he stood by me during every struggle and all my successes. Sajid motivated me to go for scientific journey, although I was more communication and marketing oriented person. Further on, I want to thank Andreas, my office mate during first 3 years of PhD, who was taking care always to answer all kind of mathematical, MATLAB coding or related questions, and had time for good, humorous daily stories! Thank you for friendship but also for practical advices and quick solutions. I want to thank Milutin who was my University assistant already at University of Belgrade during my BSc studies and then a colleague at TU Wien during my PhD studies. He was organizing around 5 lectures at Geoinformatics department which I attended in Belgrade, but then a few years later when he started research in the photogrammetry group at TU Vienna. I, as a younger colleague, was amazed with his new position and I was looking at him as a role model and science-ambassador.

I am very grateful to following people who have participated in my PhD life:

A special thank you goes to my two professors from Belgrade Dragan Mihajlović and Željko Cvijetinović: for writing the reference letters, but also for introducing me to the subjects of photogrammetry and LiDAR way back in 2010 while I studied for my MSc. Who knows what I might have ended up doing if I was not been attending those early introduction lectures.

Peter Dorninger, who really puts a lot of effort and dedication into everything he does. He organized unique field campaign for the project and we have participated in interesting conferences together, and talked about international projects. Beside to this all, he has a very kind personality and a great sense of humour.

Balázs Székely gives inspiration, ideas, and in one word - he is a scientific coach, number 1. He made me to dream about becoming a good hard working scientist. I was privileged to sit at his former working table and to have with him many interesting discussions before or after eight o'clock in the evening.

Professor Josef Jansa was my first contact with IPF/GEO Institute in 2012. Thanks to his support I have received the prestige Austrian OeAD scholarship, which was significant for my Master thesis research and helped me to gain important knowledge about point cloud processing and to get into contact with experienced researchers from the field and with the future PhD supervisor.

Oleg Mandic is a great palaeontologist who provided scientific discussions and feedback in our native language about life, structure, and parameters of sea shells. He was kindly explaining to me basics of the paleo world and supporting my investigations.

Stefano Elefante is a computer scientist who decided to show me that there is a life in Vienna beside PhD, there is a Milonga event every week. I started dancing Tango. We created officially Argentine Tango group at TU Wien in 2015, and organized the first Milonga at TU Ball in Hofburg palace in 2017. The cooperation continued also in 2018 and 2019. I worked as a moderator every year during the Milonga openings.

My fellow doctoral students: Livia, Di, Michael, Nan, Tran, Duy, Natalia, Karolina, Sasha, Elisabet and Mladen.

The staff of GEO for the last minute favours: Hans, Elmar and Felix.

Students whom I supervised during "Seminar der Geowissenschaften" and summer jobs: Madalina Iasmina, Nilüfer Cipa, Sharif Hasan, and Francisco Arroyo Pinilla.

Guest students at Viennese Universities which I supervised via OeAD programs: Tijana, Nikola, Milos, Maja O., Hristina, Maja Dj., Jelena B., Jelena S., Marko L., Marko M.; they have improved my skills how to be a supervisor and make good grant hunters.

Professor Masato Katoh for support during short-term research mobility at Shinshu University in Japan.

To all other family members, friends and colleagues who have given me some feedback here and there, and apologies for not mentioning you all, but I have to stop somewhere.

I am thankful to my sister Maja who has provided me moral and emotional support in my life and has visited me nearly in every city where I have worked abroad. I want to thank to my mother Ljiljana and father Ratko who taught me discipline, manners, respect, and so much more that has helped me succeed in life. I am also grateful to my husband Eetu for supporting me along the way and to our daughter Lea for daily dose of happiness and love.

References

Abellan, A., Derron, M. H., Jaboyedoff, M., 2016. Use of 3D Point Clouds in Geohazards. Special Issue: Current Challenges and Future Trends, Remote Sensing 8, 130.

Allen, Y.C., Wilson, C.A., Roberts, H.H., Supan, J., 2005. High resolution mapping and classification of oyster habitats in nearshore Louisiana using side scan sonar: Estuaries, 28, 435–446.

Amenta, N., Choi, S., Kolluri, R. K., 2001a. The power crust, unions of balls, and the medial axis transform. Computational Geometry, 19(2), 127–153.

Amenta, N., Choi, S., Kolluri, R. K., 2001b. The power crust. In Proceedings of the sixth ACM symposium on Solid modeling and applications, 249-266. ACM.

Arav, R., Niv, D., Filin, S., Rilov, G., 2014. Intertidal habitat characterization of rocky shores using terrestrial laser scans: Vienna, Proceedings, International Workshop on Remote Sensing and GIS for Monitoring of Habitat Quality, September 2014, 48–51.

Au, O. K. C., Tai, C. L., Chu, H. K., Cohen-Or, D., Lee, T. Y., 2008. Skeleton extraction by mesh contraction. In ACM Transactions on Graphics (TOG), 27(3), 44.

Baewert, H., Bimböse, M., Rascher, E., Schmidt, K-H., Morche, D., 2014. Roughness determination of coarse grained alpine river bed surfaces using terrestrial laser scanning data: Zeitschrift für Geomorphologie, Supplementary Issues, 58(1), 81–95.

Bahr, L. M., Lanier, W. P., 1981. The ecology of intertidal oyster reefs of the South Atlantic coast: a community profile (No. 81/15). US Fish and Wildlife Service.

Barbarella, M., Fiani, M., Lugli, A., 2015. Landslide monitoring using multitemporal terrestrial laser scanning for ground displacement analysis. Geomatics, Natural Hazards and Risk, 6(5-7), 398-418.

Barber, C. B., Dobkin, D. P., Huhdanpää, H., 1996. The quickhull algorithm for convex hulls. ACM Transactions on Mathematical Software (TOMS), 22(4), 469-483.

Bellian, J.A., Kerans, C., Jennette, D.C., 2005. Digital outcrop models: Applications of terrestrial scanning lidar technology in stratigraphic modeling: Journal of Sedimentary Research, 75, 166–176.

Bertin, S., Friedrich, H., Delmas, P., 2016. A merging solution for close-range DEMs to optimize surface coverage and measurement resolution: Photogrammetric Engineering & Remote Sensing, 82, 31–40.

Blum, H., 1967. “A Transformation for Extracting New Descriptors of Shape,” Models for the Perception of Speech and Visual Form, Proc. Symp., 362-380.

Boucot, A.J., Brace, W., DeMar, R., 1958. Distribution of brachiopod and pelecypod shells by currents. Journal of Sedimentary Research, 28(3), 321–332.

Bourgeois, J., 2009. Geologic effects and records of tsunamis. In: Robinson, A.R., Bernard, E.N. (Eds.), The Sea, 15, Tsunamis. Harvard University Press, 53–91.

Boykov, Y. Y., Jolly, M. P., 2001, Interactive graph cuts for optimal boundary & region segmentation of objects in ND images: Proceedings, Eighth IEEE International Conference on Computer Vision, ICCV 2001: IEEE, 1, 105–112.

Brasington, J., Vericat, D., Rychkov, I., 2012. Modeling river bed morphology, roughness, and surface sedimentology using high resolution terrestrial laser scanning: Water Resources Research, 48, W11519.

Brenchley, P.J., Newall, G., 1970. Flume experiments on the orientation and transport of models and shell valves. Palaeogeography, Palaeoclimatology, Palaeoecology, 7(3), 185–220.

Brodu, N., Lague, D., 2012. 3D terrestrial lidar data classification of complex natural scenes using a multi-scale dimensionality criterion: Applications in geomorphology, ISPRS Journal of Photogrammetry and Remote Sensing, 88, 121–134.

Buckley, S. J., Howell, J. A., Enge, H. D., Kurz, T. H., 2008. Terrestrial laser scanning in geology: Data acquisition, processing and accuracy considerations: Journal of the Geological Society of London, 165, 625–638.

Buckley, S. J., Enge, H. D., Carlsson, C., Howell, J. A., 2010. Terrestrial laser scanning for use in virtual outcrop geology: The Photogrammetric Record, 25, 225–239.

Bucksch, A., Fleck, S., 2011. Automated detection of branch dimensions in woody skeletons of fruit tree canopies. Photogrammetric engineering & remote sensing, 77(3), 229-240.

Bucksch, A., Lindenbergh, R. C., Menenti, M., 2009. SkelTre-fast skeletonisation for imperfect point cloud data of botanic trees. Eurographics, 13-20.

Bucksch, A., Lindenbergh, R., 2008. CAMPINO—A skeletonization method for point cloud processing. ISPRS journal of photogrammetry and remote sensing, 63(1), 115-127.

Burton, D., Dunlap, D.B., Wood, L.J., Flaig, P. P., 2011. Lidar intensity as a remote sensor of rock properties: Journal of Sedimentary Research, 81, 339–347.

Cai, H., Rasdorf, W., 2008. Modeling Road Central lines and Predicting Lengths in 3-D Using LIDAR Point Cloud and Planimetric Road Central line Data. Computer-Aided Civil and Infrastructure Engineering, 23(3), 157-173.

Cao, J., Tagliasacchi, A., Olson, M., Zhang, H., Su, Z., 2010. Point cloud skeletons via laplacian based contraction. In Shape Modeling International Conference (SMI), 187-197. IEEE.

Cao, T., Xiao, A., Wu, L., Mao, L., 2017. Automatic fracture detection based on Terrestrial Laser Scanning data: a new method and case study. Computers & Geosciences, 106, 209-216.

Caumon, G., Collon-Drouaillet, P., De Veslud, C. L. C., Viseur, S., Sausse, J., 2009, Surface-based 3D modeling of geological structures: Mathematical Geosciences, 41(8), 927–945.

Chan, T. F., Vese, L. A., 2001. Active contours without edges, IEEE Transactions on Image Processing, 10(2), 266–277.

Cornea, N. D., Silver, D., Min, P., 2005a. Curve-skeleton applications. In Visualization, 2005. VIS 05. IEEE, 95-102.

Cornea, N. D., Silver, D., Yuan, X., Balasubramanian, R., 2005b. Computing hierarchical curve-skeletons of 3D objects. The Visual Computer, 21(11), 945-955.

Delaunay, B., 1934: Sur la sphère vide, Izvestia Akademii Nauk SSSR, Otdelenie Matematicheskikh i Estestvennykh Nauk, 7, 793-800.

Dewez, T. J., Girardeau-Montaut, D., Allanic, C., Rohmer, J., 2016. Facets: a cloudcompare plugin to extract geological planes from unstructured 3d point clouds. International Archives of the Photogrammetry, Remote Sensing & Spatial Information Sciences, 41.

Dey, T. K., Zhao, W., 2004. Approximate medial axis as a voronoi subcomplex. Computer-Aided Design, 36(2), 195-202.

Di Salvo, F., Brutto, M. L., 2014. Full-waveform terrestrial laser scanning for extracting a high-resolution 3D topographic model: A case study on an area of archaeological significance: European Journal of Remote Sensing, 307–332.

Dijkstra, E. W., 1959. A note on two problems in connexion with graphs. Numerische Mathematik 1, 269–271.

Dittrich, A., Weinmann, M., Hinz, S., 2017. Analytical and numerical investigations on the accuracy and robustness of geometric features extracted from 3D point cloud data. ISPRS Journal of Photogrammetry and Remote Sensing, 126, 195-208.

Djuricic, A., Dorninger, P., Nothegger, C., Harzhauser, M., Székely, B., Rasztovits, S., Mandic, O., Molnár, G., Pfeifer, N., 2016a. High-resolution 3D surface modeling of a fossil oyster reef. Geosphere Journal, 12(5), 1457-1477.

Djuricic, A., Dorninger, P., Nothegger, C., Harzhauser, M., Székely, B., Rasztovits, S., Mandic, O., Molnár, G., Pfeifer, N., 2016b. Digital surface model, hillshade and orthophoto of the world's largest fossil oyster reef, links to GeoTIFFs. doi:10.1594/PANGAEA.863615.

Djuricic, A., Nothegger, C., Székely, B., Pfeifer, N., Harzhauser, M., Dorninger, P., Mandic, O., 2016c. GIS database for the World's largest fossil oyster reef. The 19th AGILE International Conference on Geographic Information Science, 14-17th June, Helsinki, Finland.

Djuricic, A., Puttonen, E., Harzhauser, M., Mandic, O., Székely, B., Pfeifer, N., 2016d. 3D central line extraction of fossil oyster shells. ISPRS Annals of the Photogrammetry, Remote Sensing and Spatial Information Sciences, 3, 121–128.

Doneus, M., 2013. Openness as visualization technique for interpretative mapping of airborne lidar derived digital terrain models: Remote Sensing, 5, 6427–6442.

Dorninger, P., Nothegger, C., 2009. Automated processing of terrestrial mid-range laser scanner data for restoration documentation at millimeter scale: Vienna, Austria, Proceedings, 14th International Congress Cultural Heritage and New Technologies, 602–609.

Doucette, P., Agouris, P., Stefanidis, A., 2004. Automated road extraction from high resolution multispectral imagery. Photogrammetric Engineering & Remote Sensing, 70(12), 1405-1416.

Duda, R. O., Hart, P. E., 1972. Use of the Hough transformation to detect lines and curves in pictures: Communications of the ACM, 15, 11–15.

Dunca, E., Mutvei, H., Göransson, P., Mörth, C.M., Schöne, B.R., Whitehouse, M.J., Baden, S.P., 2009. Using ocean quahog (Arctica islandica) shells to reconstruct palaeoenvironment in Öresund, Kattegat and Skagerrak, Sweden. International Journal of Earth Sciences, 98(1), 3–17.

Edelsbrunner, H., Mücke, E. P., 1994. Three-dimensional alpha shapes: Transactions on Graphics (TOG), 13, 43–72.

El-Hedeny, M.M., 2005. Taphonomy and Paleoecology of the Middle Miocene oysters from Wadi Sudr, Gulf of Suez, Egypt. Revue de Paléobiologie, 24, 719–733.

Engel, M., Brückner, H., 2011. The identification of palaeo-tsunami deposits—a major challenge in coastal sedimentary research. Coastline Reports, 17, 65–80.

Fairley, I., Thomas, T., Phillips, M., Reeve, D., 2016. Terrestrial laser scanner techniques for enhancement in understanding of coastal environments. In Seafloor Mapping along Continental Shelves, 273-289. Springer, Cham.

FARO (2018) Manufacturer's Specification: http://www.faro.com/ (December 2018).

Feng, Q. H., Röshoff, K., 2004. In-situ mapping and documentation of rock faces using a full-coverage 3d laser scanning technique: International Journal of Rock Mechanics and Mining Sciences, 41, 139–144.

Fürsich, F.T., Oschmann W., 1993. Shell beds as tools in basin analysis: the Jurassic of Kachchh, western India. Journal of the Geological Society, London, 150, 169–185.

Gagvani, N., Silver, D., 2001. Animating volumetric models. Graphical Models, 63(6), 443-458.

Goff, J., Chague-Goff, C., Nichol, S., Jaffe, B., Dominey-Howes, D., 2012. Progress in palaeotsunami research. Sedimentary Geology, 243–244, 70–88.

Goodman, J. A., Purkis, S. J., Phinn, S. R., editors, 2013. Coral reef remote sensing: A guide for mapping, monitoring and management: Springer Netherlands.

Gorte, B., Pfeifer, N., 2004. Structuring laser-scanned trees using 3D mathematical morphology. International Archives of Photogrammetry and Remote Sensing, 35(B5), 929-933.

Grant, J., Emerson, W., Shumway, S.E., 1992. Orientation, passive transport, and sediment erosion features of the sea scallop Placopecten magellanicus in the benthic boundary layer. Canadian Journal of Zoology, 1993, 71(5), 953–959.

Greenspan, H., Laifenfeld, M., Einav, S., Barnea, O., 2001. Evaluation of central-line extraction algorithms in quantitative coronary angiography. Medical Imaging, IEEE Transactions on, 20(9), 928-941.

Gregory, M.R., 1991. New trace fossils from the Miocene of Northland, New Zealand: Rorschachichnus amoeba and Piscichnus waitemata. Ichnos 1, 195–205.

Grizzle, R.E., Ward, L.G., Adams, J.R., Dijkstra, S.J., Smith, B., 2005 Mapping and characterizing subtidal oyster reefs using acoustic techniques, underwater videography, and quadrat counts: American Fisheries Society Symposium, 41, 153–159.

Hackel, T., Wegner, J. D., Schindler, K., 2017. Joint classification and contour extraction of large 3D point clouds. ISPRS Journal of Photogrammetry and Remote Sensing, 130, 231-245.

Hakala, T., Suomalainen, J., Kaasalainen, S., Chen, Y., 2012. Full waveform hyperspectral LiDAR for terrestrial laser scanning: Optics Express, 20, 7119–7127.

Hamylton, S., Leon, J., Saunders, M., Woodroffe, C., 2014. Simulating reef response to sea-level rise at Lizard Island: A geospatial approach: Geomorphology, 222, 151–161.

Han, F., Tu, Z., Zhu, S. C., 2004, Range image segmentation by an effective jump-diffusion method: IEEE, Pattern Analysis and Machine Intelligence, 26, 1138–1153.

Harzhauser, M., Djuricic, A., Mandic, O., Dorninger, P., Nothegger, C., Székely, B., Puttonen, E., Molnár, G., Pfeifer, N., 2015. Disentangling the history of complex multi-phased shell beds based on the analysis of 3D point cloud data. Palaeogeography, Palaeoclimatology, Palaeoecology, 437, 165–180.

Harzhauser, M., Djuricic, A., Mandic, O., Neubauer, T. A., Zuschin, M. and Pfeifer, N., 2016. Age structure, carbonate production and shell loss rate in an Early Miocene reef of the giant oyster Crassostrea gryphoides. Biogeosciences, 13, 1223-1235.

Harzhauser, M., Sovis, W., Kroh, A., 2009. Das verschwundene Meer: Vienna, Naturhistorisches Museum, Wien, ISBN 978-3-902421-42-5, 1–48.

Heijmans, H. J., 1994. Morphological image operators: Advances in Electronics and Electron Physics, Boston, Academic Press, 50, Supplement 24.

Heipke, C., Mayer, H., Wiedemann, C., Jamet, O., 1997. Evaluation of automatic road extraction: International Archives of the Photogrammetry, Remote Sensing and Spatial Information Sciences, 32, 47–56.

Heritage, G. L., Milan, D. J., 2009. Terrestrial laser scanning of grain roughness in a gravel-bed river: Geomorphology, 113, 4–11.

Hladil, J., Cejchan, P., Gabasova, A., Tdeaborsky, Z., Hladikova, J., 1996. Sedimentology and orientation of tentaculite shells in turbidite lime mudstone to packstone; Lower Devonian, Barrandian, Bohemia. Journal of Sedimentary Research, 66, 888–899.

Hodge, R., Brasington, J., Richards, K., 2009a. In situ characterization of grain-scale fluvial morphology using Terrestrial Laser Scanning: Earth Surface Processes and Landforms, 34, no. 7, 954–968.

Hodge, R., Brasington, J., Richards, K., 2009b. Analysing laser-scanned digital terrain models of gravel bed surfaces: Linking morphology to sediment transport processes and hydraulics: Sedimentology, 56, 2024–2043.

Hofer, M., Odehnal, B., Pottmann, H., Steiner, T., Wallner, J., 2005. 3D shape recognition and reconstruction based on line element geometry, in Proceedings, Tenth IEEE International Conference on Computer Vision, Beijing, October 2005, 2, 1532–1538.

Hoffmeister, D., Tillya, N., Curdt, C., Aasen, H., Ntageretzis, K., Hadler, H., Bareth, G., 2012. Terrestrial laser scanning for coastal geomorphologic research in western Greece: ISPRS-International Archives of the Photogrammetry, Remote Sensing and Spatial Information Sciences, 1, 511–516.

Hofmann-Wellenhof, B., Legat, K., Wieser, M., 2011. Navigation: principles of positioning and guidance: Springer Science & Business Media, 290–293.

Hoppe, H., DeRose, T., Duchamp, T., McDonald, J., and Stuetzle, W., 1992. Surface reconstruction from unorganized points: ACM SIGGRAPH Computer Graphics, 26, 71–78.

Huang, J., Menq, C.-H., 2001. Automatic data segmentation for geometric feature extraction from unorganized 3-d coordinate points. Robotics and Automation, IEEE Transactions on, 17(3), 268–279.

Huang, H., Wu, S., Cohen-Or, D., Gong, M., Zhang, H., Li, G., and Chen, B., 2013. L1-medial skeleton of point cloud. ACM Trans. Graph., 32(4), 65.

Ioannou, Y., Taati, B., Harrap, R., Greenspan, M., 2012. Difference of normals as a multi-scale operator in unorganized point clouds. In 2012 Second International Conference on 3D Imaging, Modeling, Processing, Visualization & Transmission, 501-508. IEEE.

Jessell, M., 2011. Three-dimensional geological modeling of potential-field data: Computers & Geosciences, 27, 455–465.

Kaasalainen, S., Jaakkola, A., Kaasalainen, M., Krooks, A., and Kukko, A., 2011. Analysis of incidence angle and distance effects on TLS intensity: Search for correction methods: Remote Sensing, 3, 2207–2221.

Kamintzis, J. E., Jones, J. P. P., Irvine-Fynn, T. D. L., Holt, T. O., Bunting, P., Jennings, S. J. A., Hubbard, B., 2018. Assessing the applicability of terrestrial laser scanning for mapping englacial conduits. Journal of Glaciology, 64(243), 37-48.

Kasap, M., Magnenat-Thalmann, N., 2011. Skeleton-aware size variations in digital mannequins. The Visual Computer, 27(4), 263-274.

Kazhdan, M., Bolitho, M., Hoppe, H., 2006. Poisson surface reconstruction, in Proceedings, Fourth Eurographics Symposium on Geometry processing, 7, 61-70.

Kazhdan, M., Bolitho, M., Hoppe, H., 2006. Poisson surface reconstruction. In Proceedings of the fourth Eurographics symposium on Geometry processing, 7, 61-70.

Kidwell, S.M., 1986. Models for fossil concentrations: paleobiologic implications. Paleobiology 12, 6–24.

Kidwell, S.M., 1991. The stratigraphy of shell concentrations. Allison, P.A. and Briggs, D.E.G. (eds.) 1991. Taphonomy, Releasing the Data Locked in the Fossil Record. Plenum Press, New York, 211–290.

Kidwell, S. M., Bosence, D. W., Allison, P. A., Briggs, D. E. G., 1991. Taphonomy and time-averaging of marine shelly faunas. Taphonomy: releasing the data locked in the fossil record. Plenum, New York, 115-209.

Kraus, K., 2007. Photogrammetry — Geometry from Images and Laser Scans, 2nd ed.; De Gruyter: Berlin, Germany.

Krissian, K., Malandain, G., Ayache, N., Vaillant, R., Trousset, Y., 2000. Model-based detection of tubular structures in 3D images. Computer Vision and Image Understanding, 80(2), 130-171.

Kuhn, D., Prüfer, S., 2014. Coastal cliff monitoring and analysis of mass wasting processes with the application of terrestrial laser scanning: A case study of Rügen, Germany. Geomorphology, 213, 153-165.

Kurz, T. H., Buckley, S. J., Howell, J. A., 2013. Close-range hyperspectral imaging for geological field studies: Workflow and methods: International Journal of Remote Sensing, 34(5), 1798–1822.

Lahee, F.H., 1932. Bioherm and biostrome: geological notes. AAPG Bulletin, 16, 484.

Lam, L., Lee, S. W., Suen, C. Y., 1992. Thinning methodologies-a comprehensive survey. IEEE Transactions on Pattern Analysis and Machine Intelligence, 14(9), 869-885.

Lancaster, P., Salkauskas, K., 1981. Surfaces generated by moving least squares methods.

Latal, C., Piller, W. E., Harzhauser, M., 2006. Shifts in oxygen and carbon isotope signals in marine molluscs from the Central Paratethys (Europe) around the Lower/Middle Miocene transition: Palaeogeography, Palaeoclimatology, Palaeoecology, 231, 347–360.

Lazar, B., Gračan, R., Katić, J., Zavodnik, D., Jaklin, A., Tvrtković, N., 2011. Loggerhead sea turtles (Caretta caretta) as bioturbators in neritic habitats: an insight through the analysis of benthic molluscs in the diet. Marine Ecology, 32, 65–74.

Lejart, M., Hily, C., 2011. Differential response of benthic macrofauna to the formation of novel oyster reefs (Crassostrea gigas, Thunberg) on soft and rocky substrate in the intertidal of the Bay of Brest, France. Journal of Sea Research, 65, 84–93.

Lin, C. H., Chen, J. Y., Su, P. L., Chen, C. H., 2014, Eigen-feature analysis of weighted covariance matrices for LiDAR point cloud classification: ISPRS Journal of Photogrammetry and Remote Sensing, 94, 70–79.

Livny, Y., Yan, F., Olson, M., Chen, B., Zhang, H., El-Sana, J., 2010. Automatic reconstruction of tree skeletal structures from point clouds. ACM Transactions on Graphics, 29(6), 151.

Longoni, L., Papini, M., Brambilla, D., Barazzetti, L., Roncoroni, F., Scaioni, M., Ivanov, V. I., 2016. Monitoring riverbank erosion in mountain catchments using terrestrial laser scanning. Remote Sensing, 8(3), 241.

Luhmann, T., Robson, S., Kyle, S., Boehm, J., 2014. Close-range photogrammetry and 3D imaging: Walter de Gruyter, 339-342.

Lukeneder, S., Lukeneder, A., Weber G.W., 2014. Computed reconstruction of spatial ammonoid-shell orientation captured from digitized grinding and landmark data. Computers & Geosciences, 64, 104-114.

Mallet, J. L., 1989. Discrete smooth interpolation [TOG]: ACM Transactions on Graphics, 8, 121–144.

Mandic, O., Harzhauser, M., Roetzel, R., 2004. Taphonomy and sequence stratigraphy of spectacular shell accumulation from the type stratum of the Central Paratethys stage Eggenburgian (Lower Miocene, NE Austria). Courier des Forschungsinstituts Senckenberg, 246, 69–88.

Mandlburger, G., Otepka, J., Karel, W., Wagner, W., Pfeifer, N., 2009. Orientation and processing of airborne laser scanning data (OPALS)—Concept and first results of a comprehensive ALS software: International Archives of Photogrammetry, Remote Sensing and Spatial Information Sciences, 38, 55–60.

Marshall, D., Lukacs, G., Martin, R., 2001. Robust segmentation of primitives from range data in the presence of geometric degeneracy: Pattern Analysis and Machine Intelligence, IEEE, 23, 304–314.

Martin, R.E. 1999. Taphonomy: A process approach: Cambridge University Press, 508.

Mayer, H., Laptev, I., Baumgartner, A., 1998. Multi-scale and snakes for automatic road extraction. In Computer Vision—ECCV'98, 720-733. Springer Berlin Heidelberg.

Mayrhofer, S., Lukeneder, A., Krystyn, L., 2016. Taphonomy and palaeoecology of Late Triassic (Carnian) ammonoid concentrations from the Taurus Mountains, Turkey. Lethaia, 50, 87–104.

Mederos, B., Amenta, N., Velho, L., & De Figueiredo, L. H., 2005. Surface Reconstruction for Noisy Point Clouds. In Symposium on Geometry Processing, 53-62.

Merigot, Q., Ovsjanikov, M., Guibas, L., 2011. Voronoi-based curvature and feature estimation from point clouds: IEEE Transactions on Visualization and Computer Graphics, 17(6), 743–756.

Miao, Z., Shi, W., Zhang, H., Wang, X., 2013. Road central line extraction from high-resolution imagery based on shape features and multivariate adaptive regression splines. Geoscience and Remote Sensing Letters, IEEE, 10(3), 583-587.

Milan, D.J., Heritage, G.L., Hetherington, D., 2007. Application of a 3D Laser Scanner in the Assessment of Erosion and Deposition Volumes and Channel Change in a Proglacial River. Earth Surfaces Processes and Landforms, 32, 1657–1674.

Millane, R. P., Weir, M.I., Smart, G.M., 2006. Automated analysis of imbrication and flow direction in alluvial sediments using laser-scan data. Journal of Sedimentary Research, 76(8), 1049–1055.

Milenković, M., Pfeifer, N., Glira, P., 2015. Applying terrestrial laser scanning for soil surface roughness assessment: Remote Sensing, 7, 2007–2045.

Molnár, G., Székely, B., Harzhauser, M., Djuricic, A., Mandic, O., Dorninger, P., Nothegger, C., Exner, U., Pfeifer, N., 2015. Semi-automated fault system extraction and displacement analysis of an excavated oyster reef using high-resolution laser scanned data. EGU General Assembly Conference Abstracts, 17, abstract 11417.

Morton, R.A., Gelfenbaum, G., Jaffe, B.E., 2007. Physical criteria for distinguishing sandy tsunami and storm deposits using modern examples. Sedimentary Geology, 200, 184–207.

Nagle, J.S., 1967. Wave and current orientation of shells. Journal of Sedimentary Research, 37(4), 1124-1138.

Niblack, C. W., Gibbons, P. B., Capson, D. W., 1992. Generating skeletons and central lines from the distance transform. CVGIP: Graphical Models and Image Processing, 54(5), 420-437.

Nield, J. M., King, J., Wiggs, G. F., Leyland, J., Bryant, R. G., Chiverrell, R. C., Washington, R., 2013, Estimating aerodynamic roughness over complex surface terrain: Journal of Geophysical Research: Atmospheres, 118, 12–948.

Nothegger, C., 2011. Improving completeness of geometric models from terrestrial laser scanning data: Geoinformatics FCE CTU, 6, 233–240.

Nothegger, C., Dorninger, P., 2007. Automated modeling of surface detail from point clouds of historical objects: Talk: International Symposium of CIPA, 21st CIPA Symposium, Anticipating the Future of the Cultural Past: The International Archives of Photogrammetry, Remote Sensing and Spatial Information Sciences, XXXVI-5/C53, Athens, October 2007, ISSN: 1682-1750; 538 – 543.

Nothegger, C., Dorninger, P., 2009. 3D filtering of high-resolution terrestrial laser scanner point clouds for cultural heritage documentation: Photogrammetrie-Fernerkundung-Geoinformation, 2009(1), 53–63.

Olsen, M. J., Wartman, J., McAlister, M., Mahmoudabadi, H., O'Banion, M. S., Dunham, L., Cunningham, K., 2015. To fill or not to fill: sensitivity analysis of the influence of resolution and hole filling on point cloud surface modeling and individual rockfall event detection. Remote Sensing, 7(9), 12103-12134.

Otepka, J., Ghuffar, S., Waldhauser, C., Hochreiter, R., Pfeifer, N., 2013. Georeferenced point clouds: A survey of features and point cloud management: ISPRS International Journal of Geo-Information, 2, 1038–1065.

Palágyi, K., Balogh, E., Kuba, A., Halmai, C., Erdőhelyi, B., Sorantin, E., Hausegger, K., 2001. A sequential 3D thinning algorithm and its medical applications. In Information Processing in Medical Imaging. Springer Berlin Heidelberg, 409-415.

Palágyi, K., Kuba, A., 1998. A 3D 6-subiteration thinning algorithm for extracting medial lines. Pattern Recognition Letters, 19(7), 613-627.

Pearson, N.J., Gingras, M.K., Armitage, I.A., Pemberton, S.G., 2007. Significance of Atlantic sturgeon feeding excavations, Mary's Point, Bay of Fundy, New Brunswick, Canada. Palaios 22, 457–464.

Pervesler, P., Roetzel, R., Uchman, A., 2011. Ichnology of shallow sublittoral siliciclastics of the Burgschleinitz Formation (Lower Miocene, Eggenburgian) in the Alpine-Carpathian Foredeep (NE Austria). Austrian Journal of Earth Science, 104, 81–96.

Pesci, A., Teza, G., 2008. Effects of surface irregularities on intensity data from laser scanning: An experimental approach: Annals of Geophysics, 51, no. 5/6, 839–848.

Pfeifer, N., Dorninger, P., Haring, A., Fan, H., 2007. Investigating terrestrial laser scanning intensity data: Quality and functional relations, in Gruen, A., and Kahmen, H., eds., International Conference on Optical 3-D Measurement Techniques, 328–337.

Pfeifer, N., Roncat, A., Stötter, J., Becht, M., 2011. Laser scanning applications in geomorphology: Zeitschrift für Geomorphologie, 55, 105-126.

PhotoScan, 2018, Software, http://www.agisoft.com/ (December, 2018).

Pottmann, H., Hofer, M., Odehnal, B., and Wallner, J., 2004. Line geometry for 3D shape understanding and reconstruction, in Pajdla, T., and Matas, J., eds., ECCV 2004, Eighth European Conference on Computer Vision: Prague, Czech Republic, Lecture Notes in Computer Science, 3021, 297–309.

Pottmann, H., Leopoldseder, S., Wallner, J., and Peternell, M., 2002. Recognition and reconstruction of special surfaces from point clouds: International Archives of Photogrammetry Remote Sensing and Spatial Information Sciences, 34, 271–276.

Powell, E.N., Kraeuter, J.N., Ashton-Alcox, K.A., 2006. How long does oyster shell last on an oyster reef? Estuarine, Coastal and Shelf Science, 69, 531–542.

Puttonen, E., Hakala, T., Nevalainen, O., Kaasalainen, S., Krooks, A., Karjalainen, M., Anttila, K., 2015. Artificial target detection with a hyperspectral LiDAR over 26-h measurement: Redondo Beach California, Optical Engineering, 54(1), 013105.

Raumonen, P., Kaasalainen, M., Åkerblom, M., Kaasalainen, S., Kaartinen, H., Vastaranta, M., Holopainen, M., Disney, M., Lewis, P., 2013. Fast automatic precision tree models from terrestrial laser scanner data. Remote Sensing, 5(2), 491-520.

Ridge, J.T., Rodriguez, A.B., Fodrie, F.J., Lindquist, N.L., Brodeur, M.C., Coleman, S.E., Grabowski, J.H., Theuerkauf, E.J., 2015. Maximizing oyster-reef growth supports green infrastructure with accelerating sea-level rise. Scientific Reports, 5, 14785.

Ridge, J. T., Rodriguez, A. B., and Fodrie, F. J., 2017. Evidence of exceptional oyster-reef resilience to fluctuations in sea level. Ecology and Evolution, 7(23), 10409-10420.

Roberts, E.M., Tapanila, L., and Mijal, B., 2008. Taphonomy and sedimentology of storm-generated continental shell beds: a case example from the Cretaceous Western Interior Basin. Journal of Geology, 116, 462–479.

Rodriguez, A.B., Fodrie, F.J., Ridge, J.T., Lindquist, N.L., Theuerkauf, E.J., Coleman, S.E., Grabowski, J.H., Brodeur, M.C., Gittman, R.K., Keller, D.A., Kenworthy, M.D., 2014, Oyster reefs can outpace sea-level rise: Nature Climate Change, 4, 493–497.

Rusu, R. B., Marton, Z. C., Blodow, N., Beetz, M., 2008. Persistent point feature histograms for 3D point clouds. In Proc 10th Int Conf Intel Autonomous Syst (IAS-10), Baden-Baden, Germany, 119-128.

Salvi, D., Mariottini, P., 2016. Molecular taxonomy in 2D: a novel ITS2 rRNA sequence-structure approach guides the description of the oysters' subfamily Saccostreinae and the genus Magallana (Bivalvia: Ostreidae). Zoological Journal of the Linnean Society, 179(2): 263–276.

Samson, P., Mallet, J. L., 1997. Curvature analysis of triangulated surfaces in structural geology: Mathematical Geology, 29, 391–412.

Sankey, J. B., Eitel, J. U. H., Glenn, N. F., Germino, M. J., Vierling, L. A., 2011. Quantifying relationships of burning, roughness, and potential dust emission with laser altimetry of soil surfaces at submeter scales: Geomorphology, 135, 181–190.

Schaap, M., Metz, C. T., van Walsum, T., van der Giessen, A. G., Weustink, A. C., Mollet, N. R., Niessen, W. J., 2009. Standardized evaluation methodology and reference database for evaluating coronary artery central line extraction algorithms. Medical Image Analysis, 13(5), 701-714.

Scheffers, A., Kelletat, D., 2003. Sedimentologic and geomorphologic tsunami imprints worldwide—a review. Earth Science Reviews, 63, 83–92

Schlotheim, E. F., 1813, Beiträge zur Naturgeschichte der Versteinerungen in geognostischer 30 Hinsicht, in Leonhard, C. C., ed., Leonhard's Taschenbuch für die gesammte Mineralogie mit Hinsicht auf die neuesten Entdeckungen, Series 1, 7: Frankfurt a. M., Johann Christian Hermann, 1–134.

Schnabel, R., Wahl, R., Klein, R., 2007. Efficient RANSAC for point-cloud shape detection, in Computer Graphics Forum, Blackwell Publishing Ltd., 26, 214-226.

Shanmugam, G., 2012. Process-sedimentological challenges in distinguishing paleotsunami deposits. Natural Hazards, 63, 5–30.

Smith, M., Vericat, D., Gibbins, C., 2012. Through-Water Terrestrial Laser Scanning of Gravel Beds at the Patch Scale. Earth Surface Processes and Landforms, 37, 411–421.

Soudarissanane, S., Lindenbergh, R., Menenti, M., Teunissen, P., 2011. Scanning geometry: Influencing factor on the quality of terrestrial laser scanning points: ISPRS Journal of Photogrammetry and Remote Sensing, 66, 399.

Soudarissanane, S.S., 2016. The geometry of terrestrial laser scanning; identification of errors, modeling and mitigation of scanning geometry. PhD Thesis at TU Delft, Nederlands.

Sovis, W., and Schmid, B., 1998, eds. Das Karpat des Korneuburger Beckens, Teil 1: Beiträge zur Paläontologie, 23, 1–413.

Sovis, W., Schmid, B., 2002, eds. Das Karpat des Korneuburger Beckens, Teil 2.

Strayer, D.L., Powell, J., Ambrose, P., Smith, L.C., Pace, M.L., and Fischer, D.T., 1996. Arrival, spread, and early dynamics of a zebra mussel (Dreissena polymorpha) population in the Hudson River estuary. Canadian Journal of Fisheries and Aquatic Sciences, 53, 1143–1149.

Remondino, F., Stylianidis, E., 2016. 3D recording, documentation and management of cultural heritage, 2. Whittles Publishing.

Tagliasacchi, A., Zhang, H., Cohen-Or, D., 2009. Curve skeleton extraction from incomplete point cloud. ACM Transactions on Graphics, 28(3), 7.

Tao, C., Li, R., Chapman, M. A., 1998. Automatic reconstruction of road centrallines from mobile mapping image sequences. Photogrammetric Engineering and Remote Sensing, 64(7), 709-716.

Tarolli, P., Arrowsmith, J. R., Vivonic, E. R., 2009. Understanding earth surface processes from remotely sensed digital terrain models: Geomorphology, 113, 1-3.

Telling, J., Lyda, A., Hartzell, P., Glennie, C., 2017. Review of Earth science research using terrestrial laser scanning. Earth-Science Reviews, 169, 35-68.

Thomsen, M.S., Silliman, B.R., McGlathery, K.J., 2007. Spatial variation in recruitment of native and invasive sessile species onto oyster reefs in a temperate soft-bottom lagoon. Estuarine, Coastal and Shelf Science, 72, 89–101.

Trewin, N. H., and Welsh, W., 1976. Formation and composition of a graded estuarine shell bed. Palaeogeography, Palaeoclimatology, Palaeoecology, 19(3), 219-230.

van der Zee, E.M., van der Heide, T., Donadi, S., Eklöf, J.S., Eriksson, B.K., Olff, H., van der Veer, H.W., and Piersma, T., 2012. Spatially extended habitat modification by intertidal reef-building bivalves has implications for consumer-resource interactions. Ecosystems, 15, 664–673.

Versteegh, E.A., Vonhof, H.B., Troelstra, S.R., Kroon, D., 2011. Can shells of freshwater mussels (Unionidae) be used to estimate low summer discharge of rivers and associated droughts? International Journal of Earth Sciences, 100(6), 1423–1432.

Voronoi, G., 1908. Nouvelles applications des paramètres continus à la théorie des formes quadratiques. Deuxième mémoire. Recherches sur les parallélloèdres primitifs, J. Reine Angew. Math., 133, 97–178.

Vosselman, G., Gorte, B. G., Sithole, G., Rabbani, T., 2004. Recognising structure in laser scanner point clouds. International archives of photogrammetry, remote sensing and spatial information sciences, 46(8), 33-38.

Walker, K. R., R. K. Bambach., 1971. The significance of fossil assemblages from fine-grained sediments: time-averaged communities. Geological Society of America Abstracts with Program 3, 783-784.

Wang, C.K., Wu, F.C., Huang, G.H., Lee, C.Y., 2011. Mesoscale terrestrial laser scanning of fluvial gravel surfaces. Geoscience and Remote Sensing Letters, IEEE, 8(6): 1075–1079.

Wang, Y., Liang, X., Flener, C., Kukko, A., Kaartinen, H., Kurkela, M., M. Vaaja, H. Hyyppä, Alho, P., 2013. 3D modeling of coarse fluvial sediments based on mobile laser scanning data: Remote Sensing, 5, 4571–4592.

Yokoyama, R., Shirasawa, M., Pike, R. J, 2002. Visualizing topography by openness: A new application of image processing to digital elevation models: Photogrammetric Engineering and Remote Sensing, 68, 257–266.

Zachos, J., Pagani, M., Sloan, L., Thomas, E., and Billups, K., 2001. Trends, rhythms, and aberrations in global climate: 65 Ma to present: Science, 292, 686–693.

Zakšek, K., Oštir, K., Kokalj, Ž, 2011. Sky-view factor as a relief visualization technique: Remote Sensing, 3, 398–415.

Zuschin, M., Harzhauser, M., Mandic, O., 2005. Influence of size-sorting on diversity estimates from tempestitic shell beds in the middle Miocene of Austria. Palaios 20: 142–158.

Zuschin, M., Harzhauser, M., Hengst, B., Mandic, O., Roetzel, R., 2014. Long-term ecosystem stability in an Early Miocene estuary: Geology, 42, 7–10.

Supplemental Material

Table S1. Quality assessment – surface matching [%]

Table S2. Quality assessment – number of detected objects (top: number of objects, below: percentage of detected objects in comparison to reference data, only shown for subset from *k* = 7 to *k* = 27 and from *m* = 1 to *m* = 6 not producing overestimations).

Figure S 1: Shaded digital surface model of the oyster reef, 1 mm resolution.

Figure S 2: Orthophoto of the oyster reef, 0.5 mm resolution

Supplemental Material

Table S1. Quality assessment – surface matching [%]

Parameters		no filter	m = 1	m = 2	m = 3	m = 4	m = 5	m = 6
k = 1	Completeness	67.38	67.27	67.32	67.66	67.79	67.42	66.70
	Correctness	73.14	73.45	73.59	73.78	74.00	74.22	74.39
	Quality	54.02	54.11	54.22	54.55	54.75	54.63	54.25
k = 3	Completeness	64.81	64.82	65.09	65.44	65.57	65.33	64.73
	Correctness	74.72	74.75	74.77	75.01	75.22	75.34	75.54
	Quality	53.15	53.17	53.37	53.73	53.92	53.82	53.51
k = 5	Completeness	65.60	65.60	65.78	65.83	66.05	66.11	66.01
	Correctness	74.86	74.94	75.02	75.07	75.24	75.37	75.47
	Quality	53.76	53.80	53.96	54.02	54.25	54.37	54.35
k = 7	Completeness	66.26	66.23	66.40	66.40	66.53	66.53	66.61
	Correctness	74.74	74.74	74.81	74.88	74.99	75.11	75.21
	Quality	54.14	54.11	54.26	54.31	54.44	54.52	54.61
k = 9	Completeness	66.75	66.79	66.82	67.09	67.01	67.01	67.13
	Correctness	74.81	74.86	74.80	74.90	74.99	75.08	75.17
	Quality	54.51	54.55	54.54	54.77	54.77	54.82	54.95
k = 11	Completeness	67.30	67.27	67.29	67.39	67.54	67.58	67.59
	Correctness	74.89	74.94	74.95	74.96	75.02	75.14	75.26
	Quality	54.91	54.92	54.94	55.01	55.14	55.23	55.30
k = 13	Completeness	67.76	67.75	67.84	67.89	67.90	67.85	67.84
	Correctness	74.94	74.98	75.02	75.07	75.13	75.20	75.21
	Quality	55.24	55.26	55.34	55.40	55.44	55.44	55.44
k = 15	Completeness	68.21	68.13	68.12	68.13	68.16	68.18	68.11
	Correctness	74.98	74.97	75.02	75.06	75.14	75.19	75.18
	Quality	55.56	55.51	55.53	55.55	55.62	55.66	55.61
k = 17	Completeness	68.38	68.31	68.33	68.32	68.28	68.19	68.18
	Correctness	74.99	75.01	75.03	75.05	75.07	75.12	75.16
	Quality	55.68	55.65	55.67	55.67	55.66	55.63	55.64
k = 19	Completeness	68.29	68.29	68.29	68.29	68.25	68.25	68.25
	Correctness	75.07	75.08	75.09	75.11	75.13	75.21	75.23
	Quality	55.67	55.67	55.68	55.69	55.67	55.72	55.73
k = 21	Completeness	68.49	68.44	68.42	68.39	68.43	68.49	68.46
	Correctness	75.01	75.00	75.01	75.03	75.06	75.04	75.06
	Quality	55.77	55.73	55.72	55.71	55.75	55.78	55.77
k = 23	Completeness	68.85	68.85	68.85	68.87	68.90	68.82	68.87
	Correctness	75.04	75.04	75.05	75.02	75.03	75.10	75.06
	Quality	56.02	56.02	56.02	56.02	56.04	56.04	56.04
k = 25	Completeness	68.90	68.89	68.89	**68.92**	68.90	68.88	68.81
	Correctness	75.02	75.05	75.06	**75.06**	75.07	75.06	75.07
	Quality	56.04	56.05	56.06	**56.08**	56.07	56.05	56.02
k = 27	Completeness	68.87	68.86	68.87	68.84	68.84	68.83	68.75
	Correctness	75.08	75.08	75.08	75.07	75.07	75.12	75.14
	Quality	56.06	56.05	56.05	56.03	56.03	56.05	56.01

Table S2. Quality assessment – number of detected objects (top: number of objects, below: percentage of detected objects in comparison to reference data, only shown for subset from *k* = 7 to *k* = 27 and from *m* = 1 to *m* = 6 not producing overestimations).

Parameters:	no filter	m = 1	m = 2	m = 3	m = 4	m = 5	m = 6
k = 1	84926	22056	17164	13805	11634	10449	9818
k = 3	44442	6385	7209	7765	7782	7681	7620
k = 5	32764	4712	5135	5513	5719	5799	5886
k = 7	28080	4221	4451	4693	4832	4925	**4958**
k = 9	24734	3890	3973	4067	4213	4266	4325
k = 11	22685	3624	3672	3781	3814	3879	3915
k = 13	20917	3397	3409	3476	3498	3553	3584
k = 15	19332	3160	3177	3206	3230	3261	3298
k = 17	18278	3001	3002	3032	3068	3080	3095
k = 19	17463	2855	2876	2901	2925	2944	2962
k = 21	16664	2762	2757	2765	2774	2806	2800
k = 23	16120	2655	2676	2685	2694	2697	2713
k = 25	15154	2515	2527	2530	2537	2522	2523
k = 27	14371	2398	2398	2396	2398	2398	2383

Parameters:		m = 1	m = 2	m = 3	m = 4	m = 5	m = 6
k = 7		83,83	88,40	93,21	95,97	97,82	**98,47**
k = 9		77,26	78,91	80,77	83,67	84,73	85,90
k = 11		71,98	72,93	75,09	75,75	77,04	77,76
k = 13		67,47	67,71	69,04	69,47	70,57	71,18
k = 15		62,76	63,10	63,67	64,15	64,77	65,50
k = 17	[%]	59,60	59,62	60,22	60,93	61,17	61,47
k = 19		56,70	57,12	57,62	58,09	58,47	58,83
k = 21		54,86	54,76	54,92	55,09	55,73	55,61
k = 23		52,73	53,15	53,33	53,51	53,57	53,88
k = 25		49,95	50,19	**50,25**	50,39	50,09	50,11
k = 27		47,63	47,63	47,59	47,63	47,63	47,33

Supplemental Material

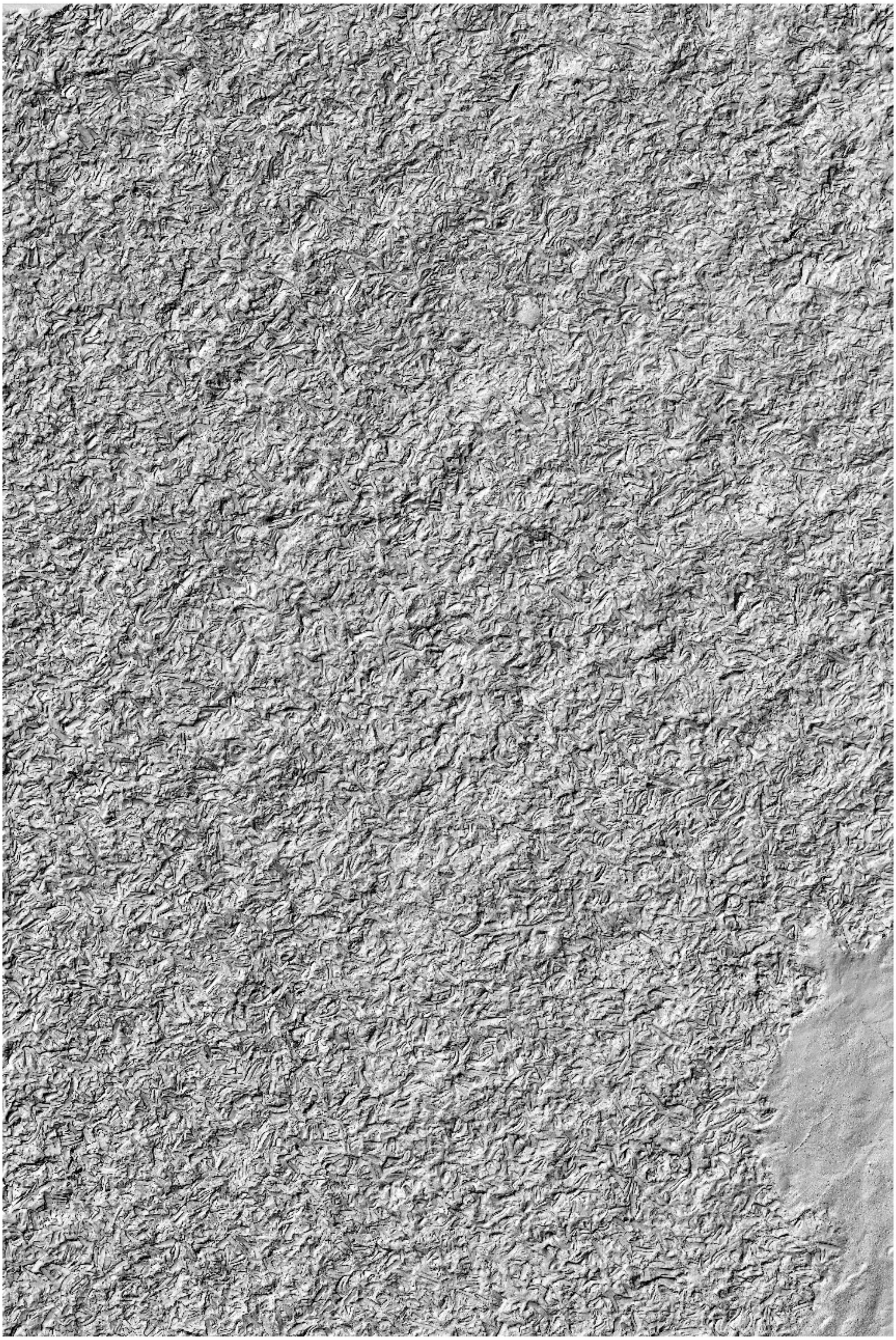

Figure S 1: Shaded digital surface model of the oyster reef, 1 mm resolution.

Figure S 2: Orthophoto of the oyster reef, 0.5 mm resolution

Curriculum Vitae

Ana Puttonen (Djuricic)

Nationality: Serbian
Phone: +436607218350 (AUT)
E-Mail: puttonen.ana@gmail.com
Family: Married, 1 child
Occupation: PhD researcher at TU Wien, Vienna, Austria

EDUCATION

01.2014 – 2019 **Faculty of Mathematics and Geoinformation, Department of Geodesy and Geoinformation (GEO), Research Group Photogrammetry, TU WIEN**

- PhD Topic: Automating analysis and processing of high resolution point clouds for the investigation of a paleontological oyster reef

09.2010– 12.2012 **Faculty of Civil Engineering, University of Belgrade, Serbia**

- MSc Geodesy and Geoinformatics (grade: 10.00/10.00), Topic: Extraction of Forest Roads from Full-waveform Airborne Laser Scanning Data

09.2007 – 07.2010 **Faculty of Civil Engineering, University of Belgrade, Serbia**

- BSc Geodesy and Geoinformatics (grade: 9.35/10.00), Topic: Spatial analysis of the biotope of the city of Belgrade using the ArcGIS software

WORK EXPERIENCE

10.2018 – 01.2019 **Visiting researcher**, Institute of Mountain Science, Shinshu University (Nagano), Japan

08.2018 – 01.2019 **Research scientist**, Finnish Geospatial Research Institute (FGI), Masala, Finland

03.2017 – 06.2018 **Maternity leave** in Austria

12.2013 – 02.2017 **Project assistant** at Natural History Museum Vienna, Austria

- **Austrian Science Fund (FWF)** - Project P 25883: Smart-Geology for the World's largest fossil oyster reef

01.2013 – 11.2013 **Visiting Scientist** at the Karlsruhe Institute of Technology (KIT)/University of Karlsruhe (TH), Institute for Photogrammetry and Remote Sensing (Karlsruhe, Germany)

- Research topic: Supporting UAVs in low visibility conditions by multiple-pulse laser scanning devices

07.2012 – 11.2012 **OeAD-Program** at TU WIEN

- Visiting scientist at the Institute of Photogrammetry and Remote Sensing (I.P.F.), Topic: Extraction of forest roads from airborne laser scanning data

01.2012 – 06.2012 **Internship - IAESTE Program** at the Federal Institute for Education, Science and Technology), Minas Gerais, Brazil

- Research topic: Monitoring temporal vegetation cover changes in the tropical south of Minas Gerais (Brazil) using Landsat satellite imagery and GIS (www.inpe.br)

09.2011 – 12.2011 **Oracle Academy**

- SQL programming, Grade: 96/100

07.2011 **Universidad Carlos III de Madrid,** Spain

- Summer courses about Aircraft Systems Technology at AirBUS Company

10.2010 **Università degli Studi di Napoli Federico II,** Italy

- Autumn courses at Faculty of Civil Engineering

08.2010 **Instituto Superior Técnico,** Portugal

- Summer courses in Lisboa about Energy, Sustainability and Transports

ADDITIONAL SKILLS

Teaching experience

- 5 semesters at TU Wien in Austria, supervision of MSc students during course: Seminar of Geosciences
- 1 semester at Shinshu University in Japan, course: Point cloud processing

Laboratory Practice:

- **Handling analysis methods and data in the field of:**
  - Airborne Laser Scanning (ALS) - LiDAR
  - Terrestrial Laser Scanning (TLS)
  - Orthophoto creation with digital cameras (aerial photos)
- **Design of experiments, method validation, process optimization**
- **Journal Referee** for: Photogrammetrie - Fernerkundung - Geoinformation (PFG); ISPRS Journal of Photogrammetry and Remote Sensing; Elsevier Journal of Estuarine, Coastal and Shelf Science; Palaeontologia Electronica.

SCHOLARSHIPS AND AWARDS

11.2018 **TU WIEN – "KUWI Scholarship"** for international research mobility in Japan

05.2018 **"MA7 Scholarship"** for completion of dissertation from Cultural Department of the City of Vienna

11.2016 **"Best App Award"** at the 21st Conference on Cultural Heritage and New Technologies (CHNT 21 - www.chnt.at), organized by Stadtarchäologie Wien, Austria

07.2016 **"Best Paper Award"** for Young Authors, Technical Commission V, 23rd ISPRS Congress in Prague, International Society for Photogrammetry and Remote Sensing (ISPRS)

06.2016 **"Best Poster Award"** at the 19th International Conference on Geographical Information Science, AGILE in Helsinki, Finland (AGILE - the Association of Geographic Information Laboratories in Europe)

01.2015 **"Grant - DOSITEJA"** from Foundation for Young Talents of the Republic of Serbia

12.2012 **"Best Master Thesis Award"** at Faculty of Civil Engineering, University of Belgrade, Serbia

2007 – 2014 **DAAD**-Scholarship (Germany), **OeAD** Scholarship (Austria), **ISPRS** Foundation Grant at the ISPRS Commission V Symposium (Italy), Scholarship of the Foundation **Studenica** - Republic of Serbia.